Winter 1-15-2021

Examining Early Interactions between Innate Airway Resident Immune Cells and Mtb-specific Factors during Pulmonary Infection with Mycobacterium tuberculosis

Micah D. Dunlap
Washington University in St. Louis

WASHINGTON UNIVERSITY IN ST. LOUIS

Division of Biology and Biomedical Sciences
Pathology and Immunology, Molecular Microbiology and Microbial Pathogenesis

Dissertation Examination Committee:

Shabaana A. Khader, Chair
Gaya Amarasinghe
Marco Colonna
Michael Holtzman
Andrew Kau
Gwendalyn Randolph

Examining Early Interactions between Innate Airway Resident Immune Cells and *Mtb*-specific Factors during Pulmonary Infection with *Mycobacterium tuberculosis*

by

Micah D. Dunlap

A dissertation presented to
The Graduate School
of Washington University in
in partial fulfillment of the
requirements for the degree
of Doctor of Philosophy

January 2021
St. Louis, Missouri

Table of Contents

List of Figures

Chapter 2: Identifying the critical role of CCR2^{+} Alveolar Macrophages in protective immunity during pulmonary TB infection

Chapter 3: What intrinsic and extrinsic factors are required for AM localization/migration and effector function within the lung?

Chapter 4: Examining the role of *Mtb*-specific lipid factors in modulating early lung immune interactions and long-term susceptibility

List of Tables

Chapter 1: Background and Introduction

Chapter 4: Examining the role of *Mtb*-specific lipid factors in modulating early lung immune interactions and long-term susceptibility

List of Abbreviations

2DG	2-deoxy-D-glucose
AEC	Airway epithelial cell
AM	Alveolar macrophage
ATB	Active tuberculosis
B6	C57Bl/6
BAL	Bronchoalveolar lavage
BCG	Bacille Calmette-Guerín
BMDM	Bone marrow derived macrophage
BMDC	Bone marrow derived dendritic cell
CCR	C-C chemokine receptor
CFU	Colony forming unit
CLR	C-type lectin receptor
CXCR	C-X-C motif chemokine receptor
DAT	Diacyl Trehalose
dLN	Draining lymph node
DR	Drug resistant
DS	Drug susceptible
FFPE	Formalin fixed paraffin embedded
G-CSF	Granulocyte colony stimulating factor
GM-CSF	Granulocyte-macrophage colony stimulating factor
H&E	Hematoxylin & Eosin
HK	Heat-killed
iNOS	inducible nitric oxide synthase
IFN	interferon
Ig	Immunoglobulin
IL	Interleukin
Iκκ2	IkB kinase (IKK) complex
LAM	Lipoarabinomannan
LC/MS	Lipid chromatography/mass spectrometry
LM	Lipomannan
LPS	Lipopolysaccharide
LTBI	Latent tuberculosis
ManLAM	Mannosylated lipoarabinomannan
mDC	Myeloid Dendritic Cell
MDM	Monocyte-derived macrophage
MDR	Multidrug resistant
MHC	Major histocompatibility complex
MOI	Multiplicity of infection
Mtb	Mycobacterium tuberculosis
NF-κB	Nuclear Factor kappa-light-chain-enhancer of activated B cell
NHP	Nonhuman primate
NO	Nitric oxide
PAMP	Pathogen-associated molecular pattern
PAT	Polyacyltrehalose
PDIM	Phthiocerol dimycocerosate

PIM	Phosphatidylinositol mannoside
PMN	Polymorphonuclear leukocyte
PRR	Pattern recognition receptor
RNS	Reactive nitrogen species
ROS	Reactive oxygen species
SNP	Single nucleotide polymorphism
SR	Scavenger receptor
TAG	Triacylglyceride
TB	Tuberculosis
TDM	Trehalose dimycolate (Dimycolyltrehalose)
Th	T helper
TLR	Toll-like receptor
TNF	Tumor necrosis factor
WT	Wildtype
XDR	Extensively drug resistant

Acknowledgments

I have had the immense privilege to work with some of the brightest minds in TB Immunology during my graduate studies. I want to thank Dr. Shabaana Khader for giving me the opportunity to join such a fantastic group of successful and motivated scientists. You have provided consistency and momentum throughout my time at WUSM, and I firmly believe that your mentorship has been instrumental to my success and development as a scientist. You have pushed me to be better, think bigger, and improve in every facet of my scientific career. Of the Khader lab, I want to specifically thank Dr. Shibali Das for being the best lab mate in the business. Our flawless collaboration as the "Dream Team" has been one of the keys to my productivity and development. Another special thanks to Dr. Shyamala Thirunavukkarasu; for thoroughly editing all my manuscripts and this very document, and also processing and analyzing the last-minute samples to make deadlines for this work. I also want to thank former members Dr. Nicole Howard, Dr. Kristin Griffiths Kallapur, and Dr. Oliver Prince; for being so patient, kind, and supportive at the beginning of my graduate studies, and for training me and helping me get these projects started.

I would not have gotten to this point if not for the teachers and coaches along the way who saw my spark. To coach Cecil Mock; thank you for believing in me, seeing and developing my hunger for excellence, and for pushing me to strengthen my mental resilience, work ethic, and general motivation. You are much of the reason I work and train the way I do to this today. To Elton Caviness and Emily Wray; thank you for being the enthusiastic scientific educators I needed when I was younger. You challenged me when others couldn't or wouldn't. You showed me how cool science really is, and you encouraged my curiosity by tirelessly answering my

questions and providing resources to help me understand how things worked. You recognized my potential and pushed me to achieve.

To my parents, Randy and Mechele Dunlap; thank you for instilling a love of learning and a thirst for knowledge from a very young age. You taught me to read, encouraged my curiosity, and always gave me what I needed to succeed. You sacrificed so much to get me to this point and helped me to achieve the American Dream. Thank you for teaching me to chase challenges, rise above obstacles, and relentlessly improve myself in all aspects of my life.

To my lovely wife, Philena; We met on March 9th, 2017, by far the most strange and influential day of my life; and it has only gotten weirder from there. You have seen me through almost every part of this journey, from that day just passing my qualifying exam, to early morning and weekend experiments, through paper drafts, edits, and revisions, to it all finally culminating here. Your constant encouragement during this process has been invaluable and you have truly made this experience infinitely better. I cannot thank you enough for all you have done for me. I am forever grateful for your unconditional love and support, as well as your enthusiasm and willingness to learn and grow with me all along this entire journey.

Micah D. Dunlap

Washington University

January 2021

ABSTRACT OF THE DISSERTATION

Examining Early Interactions between Innate Airway Resident Immune Cells and *Mtb*-specific Factors during Pulmonary Infection with *Mycobacterium tuberculosis*

by

Micah D. Dunlap

Doctor of Philosophy in Biology and Biomedical Sciences

Pathology and Immunology

Washington University in St. Louis, 2020

Professor Shabaana A. Khader, Chair

Mycobacterium tuberculosis (*Mtb*) is the leading cause of death by an infectious agent in the world today, infecting roughly one quarter of humans. Despite this, the mechanisms of early pathogenesis and host protective innate immune responses remain poorly understood and uncharacterized.

Lung resident Alveolar Macrophages (AMs) are the first host contact with *Mtb* bacilli after inhalation and are thus key mediators of the early pulmonary immune response. AMs are generally believed to reside entirely in the airway, but it was recently demonstrated that they have the capacity to egress and enter into granulomas during pulmonary infection with hypervirulent *Mtb*. Furthermore, we found that airway and non-airway AMs display distinct transcriptional profiles that suggest differential effector functions based on compartmental localization. The variety of effector function pathways expressed by non-airway AMs are primarily mediated by NF-κB signaling and are indicative of an M1 activation phenotype, which shifts the classic paradigm of AMs as permissive reservoirs for *Mtb* replication.

In the current work, we examine the host and *Mtb* factors/signals that modulate these compartmentally distinct AM effector functions and how these specific interactions determine protective or detrimental outcomes for the host. We examine the various functions that AMs contribute to the early immune response, focusing on migration from the airway, cellular interactions with epithelial or recruited immune cells, *Mtb* phagocytosis and killing, and inflammatory cytokine production. We also examine how specific *Mtb* cell wall lipid factors that mediate drug resistance and virulence can modulate these AM effector functions, thus skewing the host immune response.

Chapter 1: Background and Introduction

1.1 Global *Mtb* burden as a critical public health threat

Mycobacterium tuberculosis (*Mtb*), the causative agent of pulmonary tuberculosis (TB) infection, is one of the leading causes of death worldwide, infecting approximately one fourth of the world's human population and killing approximately 1.3 million people per year.[1] While this death toll is staggering, approximately 90-95% of infected people have latent disease (LTBI), and remain mostly asymptomatic with no clinical hallmarks of disease. However, approximately 5-10% of the estimated 2 billion humans infected with *Mtb* will develop active TB (ATB) during their lifetime. From 2000-2015, an estimated 33 million people died of TB with an estimated total global healthcare cost of $617B USD ($41.1B USD per year on average) for treatment and prevention per year.[1-3] While *Mtb* is endemic in the human population of many poor and middle income countries all over the world,[1] the main reservoir of *Mtb* is actually domesticated livestock and wild mammals.[4,5] It is estimated that ~50 million domestic livestock are infected with *Mtb*, costing the agriculture industry ~$3B USD per year.[6] *Mtb* bacteria are transmitted by aerosol, and the rapid dispersal of viable infectious bacilli from one mammalian host to multiple nearby can readily establish infection across populations of most mammalian species. The establishment of asymptomatic latent infection in the majority of infected hosts yields a vast pool of individuals at high risk of becoming contagious or immunocompromised, and chronic exposure of infected humans, livestock, or other mammals can heighten the risk of new infection or spontaneous reactivation of LTBI individuals. All these factors contribute to the persistence of this ancient disease, which has plagued modern *Homo sapiens* and our ancestors for over 9 millennia.[7,8] With all this in mind, it is no surprise that *Mtb* is regarded as the one of the most successful pathogens

in the world.

A significant contributor to the high global cost burden of *Mtb* treatment and prevention stems from the difficulty of treatment, where the standard of care for drug susceptible *Mtb* strains is a ~6 month course of a cocktail of three frontline antibiotics.[9,10] Emergence of multiple drug-resistant (MDR) and extensively drug-resistant (XDR) strains in 4% of new and 21% of recurrent cases drives treatment regimens that can persist for >20 months.[9,10]

These shocking figures demonstrate how widespread and pertinent this threat is to global public health and demonstrate the urgent need for research focused on addressing several gaps in our knowledge of TB pathogenesis and treatment. Global research efforts should focus on understanding *Mtb* pathogenesis, characterizing host immune correlates of protection,[11,12] developing better diagnostic tools, prophylactic and therapeutic treatment strategies and creating more effective vaccines. *Mycobacterium bovis* bacillus Calmette-Guérin (BCG) is currently the only licensed vaccine against TB, which was developed for human use in 1921.[13] While this century-old approach to vaccination is effective at preventing lethality in infants and adolescents, it is not effective at protecting against adult pulmonary ATB, highlighting a significant need for new treatment strategies. Current research efforts are being made to discover novel antibiotics or combinations of antibiotics that are less toxic and more effective than the current standard of care. However, it is also likely that major strides in novel vaccine development will provide a better option for global eradication of *Mtb*. Vaccination is a more attractive option because it is generally less costly and can be performed once or over a short span of time while providing long-term, broad protection with little risk of *Mtb* developing resistance.

Some of immune parameters that demarcate the differences between ATB and LTBI have just recently been elucidated,[11,12,14,15] which will provide insights to develop better diagnostic

and therapeutic tools. However, one of the greatest barriers to developing better vaccine treatments for TB is our poor understanding of the early host response mechanisms that mediate protective immunity against *Mtb* infection. Most current vaccine strategies in development are focused on targeting the recruitment and effector functions of helper $CD4^+$ T-cells[16-20] and thus driving the local formation of protective tertiary lymphoid follicles in the lung. These strategies focus on adaptive immune responses, which are generally thought to be the key driver of protection against *Mtb*. Unfortunately, pulmonary adaptive immune responses to *Mtb* are delayed compared to other infections,[21] due to delayed pulmonary dendritic cell (DC) migration and antigen presentation to $CD4^+$ T-cells in the lung draining lymph nodes (dLNs).[22] Because of this delay, adaptive immune responses often do not reach peak magnitude and efficaciousness until over a month after exposure.[23] As such, novel vaccine strategies should aim for hastening early protective immune responses and/or preventing establishment of infection. These protective early responses are likely initiated and driven by local pulmonary innate immune cells, and understanding their interactions and functions is the focus of my dissertation research presented here.

There is a growing body of evidence suggesting that early innate immune responses can *prevent the establishment of infection* prior to the induction of adaptive immunity, providing an attractive alternative to the current approach of controlling *Mtb* disease severity, spread, and treatment *after onset of symptoms* of ATB. A meta-analysis of 41 studies of human cohorts across the world found that approximately 50% of highly exposed household contacts of TB patients remaining uninfected long term with no evidence of adaptive immune activation,[24] and other studies have highlighted a key but understudied role of early innate responses in prevention of *Mtb* establishment and persistence in the lung. [25-28]

Furthermore, almost 100 years ago it was accidentally demonstrated that humans have a variable capacity for early clearance of *Mtb* by innate immunity alone.[29,30] This terrible incident demonstrated that human infants, which do not have robustly developed adaptive immune repertoires, have variable capacity to prevent *Mtb* infection, thus providing evidence for consequential interactions between *Mtb* and the innate immune system.

In 1929 and 1930 in the Lübeck General Hospital in Germany, 252 infants were orally administered the standard 3 doses of the standard live BCG vaccine, which was established as avirulent in humans and protective against lethal *Mtb* infection in infants and children.[29] Due to a tragic mistake, the laboratory stock of BCG used for the vaccination was accidentally contaminated with live, virulent *Mtb.* This meant that all 252 infants were administered live cultures of *M bovis* and *Mtb*, which led to TB disease related deaths of approximately one third of these infants, with another third displaying moderate to severe TB disease and the remaining third surprisingly showing mild symptoms or no TB disease.[25,30]

Together, these lines of evidence across many human cohorts demonstrate a critical role for pulmonary innate responses in mediating early *Mtb* clearance. These findings further suggest a differential ability of some individuals to entirely prevent the establishment of *Mtb* infection.[25] My thesis research focuses on these innate immune interactions with *Mtb*, and how these interactions can modulate short and long term disease outcomes.

1.2 Lung compartments play distinct roles during both homeostasis and infection

The lungs contain several distinct microenvironments, or compartments, that maintain distinct homeostatic functions and ontologically distinct cell types.[31,32] These compartments

provide specific immune niches which are associated with production of certain molecules and signals at homeostasis, such as the production of surfactants and mucous in the airway, or the expression of integrins in the vasculature. During infection-induced inflammation, the pulmonary immune response is also tailored to the specific microenvironments associated with each compartment, with inflammatory chemokines driving homing signals and migration of specific cell types, which will be discussed in a later section. Additionally, distinct microenvironments of each compartment can alter specific immune effector functions as cells home to the lungs from circulation and migrate between compartments, thus suggesting plasticity of function dependent on location/context.

The airway of the lung is the mucosal surface making direct contact with the outside environment via inhalation and is associated with respiratory gas exchange and the physical filtration and removal of inhaled particles and pathogens. Alveolar macrophages (AMs) and myeloid DCs (mDCs) patrol the airway to phagocytose inhaled particles and pathogens, and prevent unnecessary inflammatory responses to innocuous antigens.[33] The various types of alveolar and bronchial epithelial cells mediate gas exchange of O_2 and CO_2, as well as surfactant and/or mucus production on their apical surface.[34-36] Airway epithelial cells (AECs) express Toll-like receptors (TLRs) on their apical surface and stimulation of these or other pattern recognition receptors (PRRs) by exposure to inhaled pathogens or other insults induces airway localized production of inflammatory cytokines and chemokines.[34-36] These inflammatory signals, as well as mucus, surfactants, and motile, non-stromal immune cells present in the airway can be directly collected and examined *ex vivo* by bronchoalveolar lavage (BAL).[37] At steady state in most mammals, the majority of immune cells captured by BAL will be AMs and mDCs, though acute inflammation drives recruitment of other cell types such as neutrophils[38-42]

and $CD4^+$ T-cells[42-45] to the airway.

The lung vasculature is the dedicated network of blood vessels mediating transport of cells, nutrients, and gases to and from the lung. Expression of integrins and other trafficking/extravasation molecules on the vasculature drives recruitment of cell types into the lung tissue from circulation.[46,47] Immune cells localized in the vasculature can easily be determined by intravascular (i.v.) injection directly prior to harvest of lung tissue.[48,49] I.v. labeling determines the relative proportion of a given immune cell type in the vasculature compared to the lung tissue, and thus can be used to examine migration of recruited myeloid and lymphoid cell types into the lung.

The interstitium of the lung is the compartment between the airway epithelium and the vasculature, broadly considered the "tissue" of the lung. The interstitial compartment is where most immune cells, including recruited neutrophils, monocytes, and lymphocytes, migrate to in response to inflammatory signals from the airway at the induction of the pulmonary immune response.[31,32] The interstitium is therefore the main site for formation of complex immune structures such as granulomas and inducible bronchus associated lymphoid tissue (iBALT).[50,51] AECs produce inflammatory signals to their basal surface in response to airway inflammation at the apical surface, thus demonstrating differential interactions with airway immune cells as compared to interstitial immune cells.[34,35,52] Localization of immune cells within the interstitium can generally be determined histologically or by stain exclusion as i.v. label negative using flow cytometry. [53,54]

The differential roles of the various compartments of the lung become even more pronounced during inflammatory response or infection. Throughout this body of work, my studies examine how the various functions of immune cells are altered based on their locations

and the implications of cellular location on pulmonary immunity during *Mtb* infection.

1.3 *Mtb* pathogenesis and early pulmonary immune responses

1.3.1 *Initial exposure, Mtb sensing and phagocytic uptake*

Mtb pathogenesis begins in the airway of the host with the inhalation of aerosolized water droplets containing *Mtb* bacilli. These aerosolized *Mtb* are expelled from another infected host, usually by coughing or sneezing.[55-59] *Mtb* sensing in the airway relies on the expression of PRRs by AMs and AECs, which drive several key processes that induce early inflammation and initiate the immune response.

Recognition of inhaled pathogens and associated factors by epithelial cells leads to the production of mucus, antimicrobial peptides, and surfactants that aid in neutralizing and sequestering *Mtb*.[35,36,52,60] Furthermore, this sensing and stimulation driven by *Mtb* lipids induces local production of prostaglandins, bradykinins, and other inflammatory molecules that activate afferent neuronal C-fibers in the lung mucosa to induce the aforementioned cough reflex[58,61] in most larger mammals. Interestingly, the cough reflex, which is a host attempt to dislodge and expel the pathogen from the lung to prevent disease, actually helps drive aerosolization and dissemination of the bacteria to other potential hosts.[56,57,59] Considering that *Mtb* has specialized its early pathogenesis and replication to take advantage of pro-inflammatory interactions between airway AMs and AECs, the induction of cough can be viewed as an extremely effective strategy to drive population persistence and spread of *Mtb* after establishment of disease.

Upon inhalation by the host, *Mtb* bacilli deposited in the lower airway are recognized and phagocytosed by pulmonary AMs, which are tissue resident, fetal yolk sac derived, self-replicating innate immune cells present in the airway of the mammalian lung.[37,62,63] These

macrophages patrol the airway[64-67] and are believed to be the initial contact and primary reservoir of *Mtb* replication and persistence in the host.[34,68-70]

Phagocytic processes are induced by stimulation and binding of PRRs such as Mannose receptor (MR),[71,72] Dectin-1,[73] or Complement Receptors (CRs)[73-75] that are expressed on AMs.[76-78] Stimulation of these PRRs initiates a cascade of signaling events that drive actin cytoskeletal rearrangement to surround and uptake the bacteria, thus driving the formation of an early phagosome.[77,79] This phagosome then "matures" via fusion events with several endosomes that contain a variety of complexes designed to acidify the phagosome.

Effective "late" phagosome maturation includes addition of several components; the vacuolar ATPase that pumps protons to acidify the compartment,[79] the NADPH Oxidase and inducible Nitric Oxide Synthase (iNOS)[80-83] that produce reactive oxygen and nitrogen species (ROS & RNS), and various other lipases, DNAses, and proteases. These components and their products optimally function at low pH and make the acidic late phagosome a more hostile environment for destruction of the pathogen.[79,84-86] This late phagosome eventually fuses with a lysosome to become the phagolysosome, which is the ultimate step of this microbicidal process. The phagolysosome also interacts with other cellular organelles such as the Golgi apparatus, endoplasmic reticulum (ER), and mitochondria,[87,88] which all contribute to further activation of the phagocyte. This phagocytic activation induces metabolic reprogramming,[89-91] inflammatory signaling,[92] and antigen presentation.[79,86,93] Interestingly, *Mtb* has developed a sophisticated array of strategies for evading, impeding, or exploiting almost all of the aforementioned processes, which I will outline in greater detail in a background section 1.4.

1.3.2 Early AM effector functions dictate the overall pulmonary immune response

Despite being the primary reservoir for *Mtb* pathogenesis and persistence and the critical initiator of the pulmonary immune response, characterizing the role of innate phagocytes like AMs during infection has proven difficult. Historically, depletion of AMs in the context of lung infection and inflammation models have yielded mixed results (**Table 1**).[94-99] In some of these studies, airway localized AMs and DCs were transiently depleted using intratracheal (i.t.) or intranasal (i.n.) delivery of clodronate liposomes. In the context of pulmonary *Mtb* infection, this depletion yielded improved disease outcomes as marked by improved T-cell priming,[100] decreased pulmonary inflammation, gross lung damage, and total pathogen burden.[96] It is postulated that these improved outcomes may be due to AMs being an early replicative niche for *Mtb*, and therefore removal of that reservoir impedes pathogenesis. Furthermore, improved outcomes in this model can also be partially attributed to induction of macrophage apoptosis instead of necrosis,[101] thus yielding a more "beneficial" and less damaging form of cell death. This clodronate depletion model likewise yielded improved outcomes during pulmonary Pneumovirus (PMV) infection.[102]

In other studies, transient depletion was achieved with transgenic diphtheria toxin receptor (DTR) models to target AMs and/or DCs (CD11c, CD169, etc.).[98,99,103,104] In these studies, AM/DC depletion yielded similarly mixed outcomes in a similar panel of lung infections and inflammation models, where transient depletion of AMs/DCs was found to exacerbate inflammation and pulmonary infection with *Mtb*, *Francisella tularensis,* Influenza and Respiratory Syncytial Virus (RSV), [98,103-105] but yielded improved outcomes in the context of allergic inflammation.[99]

These findings are in contrast to the previous studies and suggest that AMs may be

beneficial during pulmonary infection by helping control inflammation. These outcomes could be attributed to the general anti-inflammatory functions of AMs, whereby production of IL-10 and "M2" effector functions aim to maintain homeostasis and decrease/resolve inflammation.[76,106-108] In this scenario, a lack of these anti-inflammatory signals would indeed drive exacerbated and uncontrolled damaging inflammation.

The caveats for interpretation of these conflicting findings across models should be mentioned. The models and techniques used involved differences in the timing, duration, and mechanism of cellular depletion which yield distinct physiological consequences. Similarly, the type of cell death achieved by the different methods influenced the type and severity of overall inflammation induced, thus affecting "unintentional" tissue damage and pathology. All of these factors together contribute to these mixed findings across models, making the positive or negative contribution of airway AMs and their overall role in lung defense context dependent and difficult to concisely ascertain. It is interesting to note that *no studies to date have found AMs/mDC depletion to have no consequential role in pulmonary defense against infection*, thus demonstrating how critical these cells are for the benefit of either the pathogen or the host.

Table 1: Alveolar macrophage/pulmonary mDC depletion models yield mixed results in various infection and inflammation contexts			
Depletion Model	Infectious or Inflammatory Agent	Result of Depletion	References
Clodronate Liposomes	• *M. tuberculosis*	• decreased bacterial burden • decreased inflammation • improved T cell priming	Huang 2018 Leemans 2001 Samstein 2013
	• PMV	• decreased viral burden	Rigaux 2012
Diphtheria Toxin/Receptor	• *M. tuberculosis* • *F. tularensis* • Influenza • RSV	• increased inflammation • Increased pathogen burden	Oh 2017 Tian 2005 Roberts 2015 Purnama 2014
	• Allergic inflammation	• decreased inflammation • decreased pathology • decreased lung damage	Van Rijt 2005

Table 1:Alveolar macrophage/pulmonary mDC depletion models yield mixed results in various infection and inflammation contexts. Depending upon method and infectious/inflammatory model used, depletion of airway macrophages drives divergent outcomes. Timing of depletion, though not mentioned here, may also be a significant factor. No studies to date have found AM/mDC depletion to have no effect. PMV=Pneumovirus; RSV=Respiratory Syncytial Virus

1.3.3 M1 vs M2 effector functions for AMs

The M1-M2 binary of macrophage activation and function is a useful convention for determining suites of genes and general functional effector responses for macrophages.[109] M1 profiles are associated with increased iNOS production, improved phagocytosis and microbicidal

function, increased inflammatory cytokine production,[110-112] and a metabolic shift towards glycolysis.[67,89,109] On the other hand, M2 activation is characterized by decreased iNOS production and inhibited microbicidal function, improved nutrient availability for pathogens like *Mtb*, decreased production of pro-inflammatory cytokines,[110-112] and a metabolic shift to fatty acid oxidation (FAO) that actually provides a hospitable environment for *Mtb*.[67]

AMs and interstitial macrophages (IMs) can be distinguished not only by their compartmental locations within the lung, but also by their differential expression of lineage, macrophage, and monocyte markers, such as CD11b, CD11c, Siglec-F, CD64 (FcγRI), MerTK, CX3CR1, CCR2, CD115 (CSF1R, M-CSFR), CD116 (CSF2R, GM-CSFR), and MHC-II.[113-120] Generally, monocyte-derived[67,120] IMs are recruited from the bone marrow to the lung and are considered M1-like. Accumulation of monocytic precursors and IMs correlates with pulmonary protection and IMs yield improved *Mtb* clearance *in vitro*.[67,109]

On the other hand, AMs are associated with M2 anti-inflammatory activation, and are historically regarded as being permissive to *Mtb* replication and persistence.[67,109,121,122] Contrary to this idea, *Mtb* DNA but not live bacteria has been found within AMs from histologically normal lung samples.[26] This finding suggests that AMs may have the ability to directly or indirectly clear infection,[25,26] thus supporting a microbicidal M1 phenotype and the idea that AMs may not always be permissive as previously thought.

Recent work has demonstrated that many factors can alter macrophage phenotype and effector function, thus suggesting that the M1-M2 binary dogma should be redefined as more of a spectrum of responses across various contexts.[123,124] *Mtb* factors have the ability to alter the metabolic profile of macrophages, thus shifting "energy states", favored carbon sources, effector functions, and cytokine production.[89,125] M1 activation is generally viewed as "inflammatory and

protective" and M2 activation is regarded as "anti-inflammatory and permissive" with regard to pulmonary infection. However, the timing, context, location, and magnitude of these responses determines the helpful or detrimental nature of the overall outcomes.[20,51] My work and others have also demonstrated that M1 vs M2 polarization can be affected by localization within the lung,[109,110,113,126] suggesting that cellular microenvironment also plays a key role in determining effector functions.

M1 activation and the IL-1β-inflammasome pathway are critical for macrophage mediated *Mtb* responses and induction of early inflammation,[127] though this interaction has also been shown to contribute to detrimental and damaging responses for the host. *Mtb* targets the activation of the inflammasome via ESAT-6 to induce IL-1β and pyroptotic or necrotic cell death.[128-131] Mice genetically deficient in IL-1β production or responses are much more susceptible to acute *Mtb* infection.[132] Pharmacological or genetic inhibition of the inflammasome during infection with either *Mtb* or Influenza induced decreased inflammatory responses as expected,[133,134] but also surprisingly drove protective immunity by decreasing pathogen replication/persistence.[83,135] Thus, it is hypothesized that macrophage inflammasome activation may be used by *Mtb* to induce and exacerbate persistent inflammation and necrotic or pyroptotic cell death,[130,131,136] though it is not likely used as a mechanism of improved virulence.[128,136,137]

Interestingly, both M1 activation and the IL-1β-inflammasome pathway are negatively regulated by the IκB kinase complex subunit 2 (Iκκ2, Iκκβ) of the NF-κB complex, which is a major node for inflammatory signaling in most cell types. Using pharmacological inhibition[138] and/or genetic models[139,140] to decrease Iκκ2 functionality, it was demonstrated that Iκκ2 negatively regulates inflammatory responses by specifically antagonizing M1 activation, MHC-II expression, and inflammatory Type 1 cytokine production. Furthermore, Iκκ2 inhibition

surprisingly drove increased *Mtb* control *in vitro*, due to heightened apoptosis driven by increased IL-1β and inflammasome activity, thus also leading to increased local cytokine production, tissue damage, and inflammation.[138] We have observed similar phenotypes involving NF-κB associated genes and M1 functional responses in my work, which I will discuss in detail in **Aims 1 & 2**.

Taken together, these prior findings suggest that AMs have an important yet controversial role, whether positive or negative, in pulmonary innate immune responses to infection, including TB. Our knowledge of these cell types and targeting techniques generally focus on their role specifically in the airway, although both mDCs and AMs are known to migrate to the lung draining lymph nodes to present antigen.[22,141,142] However, migration of these cell types *within* the lung tissue, including migration to the interstitium[109,126] and homing to granulomas, was previously unknown prior to my first published manuscript, and was the focus of **Aim 1** of my dissertation.[113] **Aim 2** of my thesis work expanded upon the known effector functions of AMs during *Mtb* infection, and elucidated further NF-κB-mediated M1 functions and interactions that drive the previously observed differences in the immune role of airway and non-airway AMs.

1.3.4 Early coordinated inflammatory signals

AMs are the first contact interaction between inhaled pathogens and the host, and as such are poised to initiate and control most inflammatory responses to inhaled potential insults. In the context of *Mtb* pathogenesis, this process begins when *Mtb* specific cell wall lipid factors are recognized by surface expressed PRRs on macrophages and AECs. Macrophages independently and by coordinated interactions with AECs[34-36,60] induce and amplify the local production of inflammatory cytokines and chemokines via aforementioned NF-κB and/or inflammasome

activation.[64,125,143] This inflammatory signaling cascade drives the initial "first wave" recruitment of myeloid cells from the bone marrow to the site of infection.[51,52,144,145] Coordinated and amplified production of cytokines and chemokines is the key to the initial "tailoring" of the inflammatory response, which dictates the primary innate immune cells recruited to the site of infection, and then later, the type of helper T-cell response that is generated.[146] The interactions between *Mtb*, AMs, and AECs that recruit this primary wave of inflammatory myeloid immune cells are the first and most consequential steps in modulating both short and long term immunity. Furthermore, the magnitude and type of inflammatory response generated by these interactions can determine disease severity and outcome.[51,64] These central themes can be seen throughout **Aims 1-3**, and for these reasons I have chosen to focus my thesis work on early immunity, specifically AMs and their interactions with *Mtb* and AECs.

The early drivers and controllers of inflammation include cytokines such as granulocyte colony stimulating factor (G-CSF) and IL-17, which coordinate neutrophil dominated Th17 responses,[147-152] Type 1 interferons (T1-IFNs) that regulate macrophage antimicrobial responses,[153] as well as IL-6, TNF-α, and IL-1β, which are general inflammatory mediators that also drive M1-macrophage activation and Th1 responses (**Table 2)**.[91,148,154-158] Both of these types of responses have been demonstrated to be crucial for *Mtb* control, both separately and coordinated.[159,160] To balance these inflammatory signals, the anti-inflammatory mediator IL-10 is also crucial for preventing overt tissue damage induced by an overactive immune response.[161,162] Together, these soluble signals initially produced by AMs and AECs play distinct and balancing roles in activating, recruiting, and controlling the short and long term immune responses to *Mtb*.

Table 2: Early cytokine drivers and controllers of *Mtb* infection associated inflammation		
Cytokines	Type of Responses	References
G-CSF & IL-17	• earliest responses • neutrophils • Th17	Torrado and Cooper 2010 Monin 2015 Khader and Cooper 2008 Kolls and Khader 2011 Lin 2010 Khader 2009
Type 1 Interferons	• macrophage activation • phagocytosis • anti-microbial responses	Divangahi 2015
IL-6, TNF-α, IL-1β	• general inflammation • M1 macrophage activation • Th1	Salgame 2005 Bai 2004 Abebe 2019 Vesosky 2006
IL-10	• anti-inflammatory • prevention of overt tissue damage • induction of Tregs	Fillatreau and O'Garra 2014 Ouyang and O'Garra 2019

Table 2: Early cytokine drivers and controllers of inflammation. The types of early pro-inflammatory cytokines induced during infection depend on a variety of factors, including the host cell of origin, the type of pathogen associated molecular pattern (PAMP) recognized, and the type of PRR stimulated. The various combinations of cytokines produced drive different suites of host responses tailored to specific classes of pathogens.

1.3.5 *Chemokine signals mediate homing to the lung and compartmental migration*

Organization of immune cells within the various lung compartments is driven by multiple chemokine: receptor axes produced by AMs, AECs, and other inflammatory immune cells, which have been exhaustively discussed in previous reviews on the subject.[23,64,143] These axes are evolutionarily conserved across species, and often have either competing or redundant roles for guiding migration/organization within the various compartments of the lung, though most are involved in general recruitment to the lung from the periphery or specific homing within granulomas.

While the focus of my dissertation work is on innate immunity, compartmental migration has been observed and explored much more thoroughly in adaptive responses of $CD4^+$ T-cells. Sharp differences in effector functions are observed with differential lung localization in the airway, parenchyma, or vasculature, suggesting cellular microenvironment plays a significant role in determining effector function. It has been previously demonstrated that for helper $CD4^+$ T-cells to exert protective effects during TB, they must have direct MHC-II-dependent contact with *Mtb* infected macrophages in the lung. Thus $CD4^+$ T-cell migration into the parenchyma is required for protection.[163] Furthermore, this migration phenotype correlates with differentiation status, where less differentiated $CD4^+$ T-cells express C-X-C Motif Chemokine Receptor 3 (CXCR3) and migrate from the vasculature into the lung parenchyma and control *Mtb* growth, whereas terminally differentiated, $CX3CR1^+$ $CD4^+$ T-cells remain in the vasculature and fail to exert a protective role.[164-166] However, differentiation status may not be the most defining feature that limits T-cell migration,[167] suggesting other factors likely contribute to this phenotype. Interestingly, CX3CR1 deficiency improved $CD4^+$ T-cell migration into the lung, suggesting that these chemokine signals are in competition and potentially antagonistic.[168] Beyond T-cells, CX3CR1 is also associated with pulmonary homing of innate immune cells,[166,169] and mediates airway migration of DCs, macrophages, and neutrophils in response to intratracheal infection or intravenous vaccination with BCG.[169]

Interestingly, despite the strong phenotypes associated with this differential chemokine receptor expression and localization, no single chemokine receptor or ligand knockout fully abrogated pulmonary $CD4^+$ T-cell responses to pulmonary infection.[168] While CXCR3 deficiency did indeed significantly decrease T-cell homing to the lung, other chemokine receptors such as C-C Chemokine Receptor Type 2 (CCR2, discussed below), CXCR5, and

others also contribute to pulmonary migration. Consistently, knockouts of these other receptors also yielded minor defects in pulmonary migration.

CXCR5 expression on lymphocytes and innate lymphoid cells (ILCs) mediates migration/homing from uninvolved lung interstitium tissue into iBALT-containing granulomas via CXCL13, and this B and T cell homing correlates with protection in pulmonary TB models across species.[170-173] iBALT containing granulomas are a distinct functional microenvironment specific to the inflamed/infected lung, and these immune structures facilitate antigen presentation, affinity maturation and clonal expansion of antigen specific lymphocytes.[51]

Another key driver of pulmonary interstitial migration and granuloma organization is CCR2. CCR2 is a major contributing axis for the recruitment of myeloid and lymphoid cells from the bone marrow to the inflamed lung for both Th1 and Th17 responses.[174] Inflammatory cytokines and chemokines, especially monocyte chemoattractant protein 1 (MCP-1, CCL2), the main ligand for CCR2, are produced from early onset of infection to promote recruitment of innate immune cells, contributing to the massive first wave of the TB immune response.[64,143] Many key cell types in the lung express CCR2, with monocytes and neutrophils being the most well-characterized.[100,144,145] Immature $CD4^+$ T-cells, as well as airway resident mDCs and AMs, also express CCR2.[113,174,175] Interestingly, despite the expression of CCR2 on many key cell types, previous studies have found a limited role for CCR2 during pulmonary TB,[100,174,176] suggesting this axis may be dispensable.[143] **Aim 1** of my dissertation research focused on re-examining the CCR2 axis in the context of *Mtb* strain specific immune responses. In the process, we observed a previously unknown migratory function of AMs into granulomas and described a novel technique for examining compartmental localization of immune cells.[113,126] These studies further observed that AM effector functions can be location/compartment specific,[109,113,126] and

will be further discussed in **Aims 1 & 2**.

Taken together, these findings demonstrate the presence of distinct compartmental microenvironments in the lung both at steady state and during infection. These compartments induce specific homing/migratory signals and effector functions for a variety of immune cells. Furthermore, these studies observe significant, overlapping contributions and redundant function for multiple chemokine receptors, which is likely a fail-safe mechanism employed by the host to ensure this functionality. Contribution of multiple chemokine receptors to this critical compartmental localization phenotype is likely not exclusive to $CD4^+$ T-cells, and a similar phenotype may be present in AMs and/or other innate immune cells, though my studies have not yet covered that possibility.

1.3.6 Early adaptive immunity and the formation of granulomas

The initial influx of bone marrow derived myeloid cells, guided by the aforementioned inflammatory cytokines and chemokines, marks the first major wave of the pulmonary immune response to *Mtb*. As *Mtb* continues to replicate and persist in permissive phagocytes, DCs migrate to the dLNs and present *Mtb* antigen to naive $CD4^+$ helper T-cells.[20-22,177,178] It was previously demonstrated that the characteristic "delay" in the adaptive immune response to *Mtb* involves these processes, and priming/activation of $CD4^+$ T-cells in the mediastinal lymph node is the limiting step. This "bottleneck" is at least partially dependent on type of antigen, antigen availability, and the number of viable bacilli present in the lymph node.[22,142] Furthermore, it was shown that intratracheal (i.t.) administration of activated DCs can resolve this "bottleneck" delay.[21] This therapy drove a much quicker and larger *Mtb* specific adaptive immune response, resulting in near sterilizing immunity at early time points post-infection. After DCs activate *Mtb*

antigen specific $CD4^+$ T-cells, these T-cells clonally expand and migrate back to the lung as the second major wave of the pulmonary immune response, which leads to the formation of granulomas and iBALT.[179-181]

While difficult to test experimentally, it is widely accepted that infected phagocytes, likely AMs and DCs, are the "seeds" of new granulomas.[179,182] It has been demonstrated that heavily *Mtb*-infected phagocytes cannot control *Mtb* growth but continue to produce inflammatory cytokines and chemokines, thus attracting more phagocytes to serve as permissive reservoirs.[183-185] Heavily *Mtb*-infected cells are less bioenergetically active,[90,186] likely less motile, and also induce caspase dependent necrosis.[131] Taken together, these functions likely drive a localized inflammatory focus and induce homing of immune cells to the area. This nascent granuloma is at first composed mainly of monocytes, macrophages, and neutrophils, and then later by the aforementioned secondary wave of T-cells. These granulomatous foci drive further tissue remodeling and localized inflammatory responses that lead to even more drastic changes over time.[179]

Granulomas are the hallmark immune structures associated with TB disease, and depending on a variety of factors, can be either protective or non-protective.[51,64] Protective granulomas serve to contain *Mtb* for sequestration and killing and are generally dominated by Th1 responses and M1 macrophages.[113] These macrophages perform several roles in order to effectively contain and sequester free bacilli and *Mtb* infected cells to prevent spread outside of the area. Furthermore, protective granulomas are also demarcated by the presence of ectopic tertiary lymphoid follicles called iBALT,[23,50,173,187] which contain a local pool of antigen specific lymphocytes that aid in pulmonary defense and secondary responses to later infection.

On the other hand, non-protective granulomas are generally dominated by a hypoxic core

of neutrophils and M2 macrophages[89] and a concentric ring or "cuff" of T-cells around the outside which are unable to penetrate into the granuloma.[172] Th17 responses, which are coordinated by early epithelial cell signals that drive neutrophil recruitment, have been demonstrated to be protective against *Mtb* infection.[148,149,151,152,188] However, as discussed previously, it is likely that an *overabundance* of neutrophils is what drives uncontrolled inflammation and tissue damage, as the extrema of inflammatory responses are considered pathological. This neutrophil-dominated core allows for *Mtb* replication, large scale cell death and overt tissue damage.[189,190] These processes drive lung-damaging hypoxia and eventual necrotic decomposition of the core,[189,191] which leads to structural breakdown of the entire granuloma. This breakdown prevents protective cellular interactions and proper containment, thus driving *Mtb* persistence, replication, and dissemination to other areas of the lung and spread to other tissues.[51,64] The persistence of long term infection, the establishment of latent infection, and dissemination to other tissues are beyond the scope of this dissertation and will not be discussed in this body of work.

Aims 2 & 3 of my dissertation research draw connections between the early innate immune response and the development of aforementioned adaptive immune structures. The critical yet largely overlooked role of early innate immune responses, specifically focusing on interactions between macrophages, pulmonary epithelial cells, and *Mtb* cell wall virulence factors, was the focus of my second published manuscript presented as **Aim 3**.[192] My work demonstrates that macrophage effector functions such as cell migration, cytokine production, apoptosis, and *Mtb* killing indeed broadly affect later adaptive immune responses, namely formation of protective granulomas and iBALT. These immune structures ultimately determine the individual's sustained systemic response to *Mtb* infection and influence overall disease

severity and outcome, highlighting the importance of examining and targeting these early interactions in my work.

1.4 *Mtb* specific factors that influence immune responses

1.4.1 *Mtb cell wall/capsule structure and composition*

Mycobacteriaceae family species are a subgroup of *Corynebacterineae* and classified as Gram positive bacteria.[193,194] Interestingly, the slow-growing pathogenic *Mycobacteriaceae* family species such as *tuberculosis, ulcerans,* and *leprae* display characteristics of both Gram positive and Gram negative bacteria,[193,195-197] which is indicative of the relative complexity of these species' cell walls. Furthermore, these pathogenic species share ~60-80% genome sequence homology,[198,199] suggesting that the relative complexity of the cell wall is a conserved pathogenic strategy across species. This cell wall complexity is a key driver of the various host evasion and exploitation strategies available to *Mtb* that drive overall pathogenicity. Several excellent reviews focusing on the structure and biochemistry of the *Mtb* cell wall and capsule have been published, which I will briefly summarize. Please see Figure 1 of Guenin-Mace et al 2009, Figure 2 of Kalscheuer et al 2019, or Figure 5 of Bansal-Mutalik et al 2014 for schematic images of the *Mtb* cell wall/capsule as discussed below.[193,194,200]

The cell wall of *Mtb* is mainly composed of lipids and polysaccharides[195,196,200,201] (~30-60% dry weight) and is organized into four layers:[193,194,200,202] (1) the plasma membrane or inner membrane, (2) the arabinogalactan-peptidoglycan complex (AGP), (3) the mycobacterial outer membrane (MOM) which is linked covalently to the AGP via mycolic acids, and (4) the outer capsule.

The inner membrane (layer #1) is an asymmetric bilayer mainly composed of

phospholipids and membrane proteins, similar to other bacteria. The AGP (layer #2) is, as the name suggests, mainly composed of arabinogalactan and peptidoglycan.[203] The AGP anchors the MOM (layer #3) through covalent bonds with mycolic acids.[200] Mycolic acids are essential for *Mtb* survival,[204] and are critical for the structure and organization of the MOM that drives the characteristic low permeability of the *Mtb* cell envelope. These properties make *Mtb* resistant to many mechanisms of destruction or perturbation by a variety of host strategies,[204,205] such as defensins[206] and complement,[207,208] and also contribute to the difficulty in classifying *Mtb* as Gram positive or Gram negative.[196,209,210]

The MOM (layer #3) is an asymmetric bilayer mainly composed of long chain fatty acids on the inner leaflet, and a complex outer leaflet composed of glycolipids and lipoglycans, including: trehalose mono- (TMM) and dimycolates (TDM), sulfoglycolipids (SGL), phosphatidylinositol mannosides (PIMs), lipomannan (LM), and lipoarabinomannan (LAM).

The outer capsule (layer #4) is composed of loosely packed polysaccharides such as α-glucan and small amounts of mannan and arabinomannan. There are also abundant lipid species such as trehaloses (including diacyl (DATs) and sulpholipids (SLs)), phthiocerol dimycocerosates (PDIMs), including phenolic glycolipids (PGLs), and also PIMs.[193,200]

Many of these lipid virulence factors, especially those of the MOM and outer capsule layers, directly interact with the host and are critically involved in modulating the host cellular immune response during *Mtb* infection. These factors target specific PRRs to drive or modulate cellular entry into specific compartments, induce or abrogate cytokine/chemokine production, or evade host intracellular mechanisms of phagocytosis, degradation, and/or antigen presentation.

Interestingly, most of these factors are biosynthesized by enzymes from a relatively small suite of genes, suggesting convergence of many important biosynthetic pathways into a limited

set of critical backbone processes needed for virulence and pathogenesis. A key biosynthetic nexus that *Mtb* cell envelope lipid factors critically utilize for virulence is the polyketide synthase (PKS, *pks1-15* genes) family of enzymes, which are multifunctional enzymes present in many bacterial families that are involved in the production of secondary metabolites called polyketides.[193,211] The slow growing pathogenic *Mycobacteria* such as *tuberculosis, ulcerans,* and *leprae* all express PKS, suggesting that these pathogenic species have evolved to utilize these enzymes and their lipid products for pathogenesis. The aforementioned lipid virulence factors such as mycolic acids,[212,213] DAT and PAT,[214] DIM and PGL,[144,145,214,215] and sulfolipid[216] are all products of PKS family enzymes, and will be discussed below. Importantly, disrupting either *pks* genes themselves,[144,145,217] or some of their specific lipid products,[217-219] leads to abrogated virulence *in vivo*. However, it should be noted that diverse *Mtb* strains express differing ratios of PKS-associated virulence lipids,[74,220-222] and depending on background strain, modulation of these genes or individual lipid factors yields divergent immune responses.[113,125,223-225]

The mycobacterial membrane protein large (*Mmpl*) family is a group of genes that encode inner membrane transporters for *Mtb* cell wall lipid factors. Some of these transporters, such as *Mmpl7*, are well characterized with regards to function, target substrate, etc, while others, such as *Mmpl2*, remain relatively unidentified. *Mmpl7* is an inner membrane protein responsible for transport of PDIM to the MOM.[226-228] These proteins are critical for maintenance of the *Mtb* cell wall via the transport of lipids between the inner and outer membranes. Indeed, mutants of *Mmpl* genes yield virulence and growth defects *in vivo*.[226,227]

Of the *Mtb* lipid factors mentioned above, the contributions of the aforementioned DATs, PDIMs, and PGLs in modulating host immune responses, phagocyte interactions, and

macrophage effector functions will be discussed throughout all three aims of my work.

1.4.2 Interactions between Mtb Capsular/Outer Membrane lipids and Host Surface PRRs

As discussed previously, the main host cells targeted in early *Mtb* pathogenesis are professional airway phagocytes such as AMs and DCs, but lung epithelial cells throughout the airway tract are also heavily involved. These host cells express a variety of PRRs that recognize pathogen associated molecular patterns (PAMPs) in order to properly respond to foreign substances, allergens, viruses, and bacteria. PRRs on innate phagocytes are utilized by *Mtb* lipid factors to mediate cell entry by phagocytosis, including several complement receptors, DC-SIGN, mannose receptor (MR), and Fc receptors.[200,229,230]

Complement Receptor 3 (CR3) is a heterodimeric complex of integrins CD11b and CD18 and is expressed on innate phagocytes at varying levels. Capsular α-glucan and PGL lipid factors of *Mtb* are recognized by CR3 to enhance uptake and mediate cellular entry,[74,231-234] thus contributing to the initial steps of *Mtb* pathogenesis. Depending on the cell type involved in uptake by phagocytosis, the other CRs can also play a major role in phagocytosis.[75,233,235] However, to date none of the CRs have been shown to directly contribute to the phagosomal sorting and eventual intracellular fate of the ingested bacterium.

DC-SIGN (CD209) is a C-type lectin that is constitutively expressed on DCs and can be induced on AMs.[236,237] DC-SIGN recognizes both capsular α-glucan and LAM from the MOM to also mediate phagocytosis,[236-239] and has been implicated in dampening immune responses.[240,241] LAM from the MOM, as well as arabinomannan and mannan from the capsule, are also recognized by MR. This binding interaction is critically involved in cellular entry and several other immune mechanisms to be discussed below.[71,242]

Arabinomannan specific antibodies on opsonized *Mtb* can be bound by Fc receptors,[243,244] thus demonstrating another mode of cellular entry if vaccination or previous exposure have induced a previous adaptive immune response. Taken together, these studies have demonstrated that *Mtb* utilizes a variety of capsular and MOM associated factors to target several phagocytic PRRs for enhanced uptake that drives cellular entry into specific, beneficial compartments for *Mtb* growth and persistence.

Mtb lipid virulence factors have also been shown to target other PRR receptors, such as TLRs, NLRs, and lectin receptors, are involved in modulating host pro-inflammatory responses and cytokine production. As with the aforementioned phagocytic receptors, the expression of these PRRs is known to vary between different cell types,[245] so *Mtb* virulence factors that target specific TLRs often drive divergent responses across models. Many *Mtb* lipid factors have varied and often competing roles in the induction or abrogation of inflammatory cytokine responses, depending on factors such as targeted cell type, specific receptor binding and interactions, intracellular compartment location, and *Mtb* background strain. Pro-inflammatory cytokine production initiated by TLR-*Mtb* lipid interactions is generally driven by the key inflammatory signaling pathways mentioned previously, namely the inflammasome and/or the NF-κB pathway. Anti-inflammatory responses that dampen cytokine production are generally driven by increased production of IL-10 or modulation of host cell metabolism. Below I will summarize the complex cytokine responses to several of the key *Mtb* lipid factors I discuss throughout this document (**Table 3**).

Table 3: *Mtb* lipid factors modulate early immunity by manipulating PRR responses			
Mtb determinant	Interacting host factor/PRR	Overall response	References
Pro-inflammatory			
α-glucan	CR3 (CD11b and CD18)	• enhanced uptake • enhanced cellular entry	Cywes 1996,1997 Oldenburg and Demangel 2017
α-glucan	DC-SIGN (CD209)	• enhanced uptake	Tailleux 2003 Geurtsen 2009 Ehlers 2010
Mannan species (LAM, LM, PIM Arabinomannan)	TLR2 +/- Dectin1 (β–glucan receptor)	increased production • TNF-α • IL-6 • RANTES	Yadav and Schorey 2006 Quesniaux 2004 Gilleron 2006
PGL	TLR2/4 CR3	increased production • CCL2 • pro-inflammatory cytokines • neutrophil activation	Cambier 2014,2017 Faldt 1999 Gopal 2013 Dunlap 2018 Howard 2018 Scott 2020 Sinsimer 2008 Manca 2005
SL-1	NOD2	increased production • pro-inflammatory cytokines • ROS	Pabst 1988 Zhang 1988 Brozna 1991 Zhang 1991 Nabatov 2013
Anti-inflammatory			
ManLAM	MR DC-SIGN	decreased production • IL-12 • TNF-α	Nigou 2001,2002 Johansson 2001
LM	MR DC-SIGN	decreased production • IL-12 • TNF-α • NO	Quesniaux 2004 Astarie-Dequeker 1999
Mannan species (LAM, LM, PIM Arabinomannan)	DC-SIGN	increased production • IL-10	Geijtenbeek 2003 Van Kooyk and Geijtenbeek 2003
PGL	TLR2/4 CR3	decreased production • IL-12 • TNF-α • IL-6	Arbues 2016 Reed 2004
PDIM	prevents TLR recognition	decreased production • IL-6 • TNF-α	Rousseau 2004 Cambier 2014 Arbues 2014
DAT	Mincle independent	decreased production • IL-12 • TNF-α • IL-6	Lee 2007
SL-1	NOD2	decreased production • pro-inflammatory cytokines • ROS	Pabst 1988 Zhang 1988 Brozna 1991 Zhang 1991 Nabatov 2013

Table 3: *Mtb* lipid factors modulate early immunity by manipulating PRR responses. Different immune cell types in the lung display varying distributions of PRRs. Distinct *Mtb* lipid virulence factors are recognized by specific PRRs individually or in combination. In turn, these PRRs drive specific pro- or anti-inflammatory responses of secreted cytokines or intracellular molecules.

Beyond their previously mentioned roles in modulating phagocytosis, MOM and capsular mannan species such as LAM, LM, and PIM are recognized by surface TLR2[246,247] either in isolation or in cooperation with β-glucan receptor Dectin-1.[73] These interactions have been shown to drive NF-κB mediated production of TNF-α, IL-6, and RANTES by macrophages in a TLR2 and Dectin-1-dependent manner.[73] Interestingly, it has been documented that these mannan lipid species can also mediate inhibition of inflammatory responses by utilizing interactions with other PRRs. ManLAM, through aforementioned interactions with MR and DC-SIGN, directly inhibits production of Th1 cytokine IL-12 and TNF-α[248-250] while LM inhibits production of TNF-α, IL-12, and NO in a TLR2-independent manner.[72,247] These inhibitory effects are likely due to the competing contributions of multiple receptors and their associated signaling. Additionally, the differential expression of these receptors on distinct cell types likely contributes to these divergent responses. Furthermore, the decreased production of pro-inflammatory cytokines may also be due to the interactions of mannan species with DC-SIGN on activated phagocytes, which can drive increased production of anti-inflammatory IL-10.[240,241]

Similar to mannans, *Mtb* outer capsule PGLs are recognized by TLR2/4[231] and also CR3,[234] and have been demonstrated to either induce or inhibit NF-κB mediated pro-inflammatory cytokine responses, depending on context.[113,223,225] In a zebrafish model using a model of *M. marinum,* PGLs were shown to augment inflammatory cytokine and chemokine production, namely CCL2, leading to recruitment of permissive CCR2+ monocytes that enhanced *Mtb* persistence and growth.[144,145]

PGLs are highly expressed by lineage 2 W-Beijing family strains of *Mtb*,[225,251,252] which are specifically associated with hypervirulence in humans and mammalian models.[218,223,253] PGLs can directly activate human neutrophils *in vitro*,[254] and infection with PGL-expressing W-Beijing family member *Mtb* HN878 correlates with accumulation of hyper-inflammatory monocytes and neutrophils in the mouse model.[14,113,125,224] These findings suggest that PGL utilization in virulence may be an important and conserved strategy across host species.

Mouse studies demonstrate that *Mtb* strain HN878 also drives heightened pro-inflammatory cytokine responses and sustained increased disease severity,[113,125,223,253] marked by specific upregulation of the CCR2-CCL2 axis in the lung. This heightened inflammatory response was not observed in the commonly used *Mtb* strain H37Rv, as this strain lacks PGLs due to a frame-shift mutation in the *Mtb pks15-1* gene.[210] This suggests that PGLs play an important role in this hyperinflammatory phenotype. Interestingly, when using a similar *pks15-1* mutant on the HN878 strain background, our lab and others have surprisingly observed heightened virulence and pro-inflammatory responses when compared to wildtype HN878.[113,225] Taken together, these findings suggest that the specific contribution of PGLs and/or the PKS enzymes may be more complex than previously thought, and other lipid virulence factors are likely involved and counter-regulated in this model.

In contrast to this aforementioned pro-inflammatory role, purified PGLs derived from *Mtb* directly bind to and inhibit TLR2, thus abrogating NF-κB activation.[231] Indeed, *Mtb* that overexpressed PGLs inhibited production of TNF-α IL-6, and IL-12 *in vitro* in macrophages.[225,231] This divergent role compared to *in vivo* studies is likely due to as yet unknown interactions between *Mtb* and multiple other cell types, such as epithelial cells and DCs, suggesting that *Mtb*-macrophage interactions in isolation may not be representative of the

overall immune response. Taken together from studies of mannans and PGLs, it has been demonstrated that these *Mtb* lipids have differing effects across both *Mtb* and host backgrounds, and have contrasting roles in modulating immunity, thus making their isolated definitive contributions difficult to surmise.

Another *Mtb* outer capsule glycolipid involved in modulating host pro-inflammatory responses is SL-1. Sulfolipids like SL-1 are recognized by the intracellular PRR Nuclear Oligomerization Domain 2 (NOD2),[255] which in activated phagocytes triggers *Mtb* neutralizing autophagy processes and pro-inflammatory cytokine production mediated by NF-κB and the inflammasome. Similar to the other lipids discussed, SL-1 both stimulates and suppresses the production of cytokines and ROS in activated phagocytes *in vitro*,[256-259] thus demonstrating the context dependent variety of responses elicited by the same molecule as a theme.

On the organismal level, SL-1 has recently been shown to drive the cough reflex in guinea pigs and humans, thus augmenting transmission events as a pathogenic strategy.[56-58] The cough reflex is caused by activation of nociceptive C-afferent neurons, which are stimulated by the local production of prostaglandins, bradykinins, and other inflammatory molecules by epithelial cells. These studies demonstrate that neurons and epithelial cells are both directly targeted by SL-1.[61] Interestingly, despite its involvement in a variety of pathogenic strategies, SL-1 is not required for virulence of *Mtb* H37Rv in the murine model,[260] though its contribution to virulence functions in other background strains has not yet been assessed. These studies further highlight that isolated interactions between *Mtb* lipid factors and individual cell types must be taken in context of the gestalt of interactions, where *in vivo* lung responses may be quite different than isolated cellular responses *in vitro*.

PDIMs and DATs, which are structurally similar to the aforementioned PGLs and SL-1,

respectively, are another topic of focus in my work. These lipids, like PGLs and SL-1, have also been shown to directly inhibit pro-inflammatory cytokine production through several direct and indirect mechanisms. PDIMs are a non-glycosylated structural precursor of PGLs,[261] and are known to mask *Mtb* PAMPs,[145] thus inhibiting PRR recognition and downstream cytokine signaling. Furthermore, PDIM also directly inhibits production of TNF-α and IL-6, as a PDIM deficient mutant *Mtb* strain was observed to drive increased production of these cytokines in macrophages and DCs.[260] DATs are non-sulfated trehalose species which are recognized by Macrophage inducible C-type lectin (Mincle).[262-264] DATs have been shown to inhibit production of TNF-α, IL-12, and IL-6 production in stimulated or infected THP-1 cells,[265] though Mincle is likely not required for this function. Similarly, DATs have also been shown to inhibit T-cell proliferation, thus leading to an overall decreased inflammatory response.[266]

These findings demonstrate the complexity of *Mtb* lipid interactions with the host and suggest that the individual contributions to inflammation are often interconnected amongst multiple lipid factors and host cell receptors in concert.

1.4.3 *Mtb lipid factors and intracellular immune evasion strategies*

Beyond stimulating and modulating inflammatory responses, *Mtb* has evolved a robust tool set of strategies for evading host defense mechanisms after cellular entry, targeted at persisting within professional phagocytes like AMs and DCs. As mentioned above, *Mtb* utilizes OM associated lipid factors in conjunction with host PRRs to skew cellular entry away from bactericidal phagosomes. Even after cellular entry, a host of the aforementioned lipid factors are involved in impeding *Mtb* killing within phagosomes and establishing a permissive environment within the host cell for *Mtb* growth. For example, PDIM, in cooperation with ESX-1,[267]

contributes to phagosomal damage which leads to *Mtb* escape into the cytosol and eventual host cell necrosis.[268]

Even if the bacterium is phagocytosed, *Mtb* factors such as manLAM[269,270] and TDM[72,271] prevent phagosome-lysosome fusion, thus bypassing mycobactericidal functions in macrophages.[71,242] Within the phagosome, PDIM is also required for early *Mtb* defense[272] by resisting the microbicidal action of NO.[260] Along with this, PIMs establish a permissive niche for growth of *Mtb* within phagocytes by driving phagosome fusion with early endosomes, thus delivering essential nutrients for *Mtb* survival.[273] SL-1 is also implicated in several of these evasion strategies. SL-1 contributes to the alteration of phagosome-lysosome fusion[274-276] and also functions to shut down the respiratory burst of infected phagocytes via inhibition of mitochondrial oxidative phosphorylation[277] and suppression of ROS.[256-259]

These early subversion mechanisms are critical to pathogenesis and serve to delay the generation of *Mtb* specific helper $CD4^+$ and killer $CD8^+$ T-cells and the onset of adaptive immunity. Beyond targeting short term persistence of phagocytes, *Mtb* also has a variety of strategies for driving sustained responses and evading adaptive immunity. *Mtb* induces downregulation of MHC-II molecules on phagocytes,[278-282] and utilizes mycobacterial lipoprotein to specifically inhibit AM expression of MHC-II and CD80,[283] thus impairing antigen presentation and associated T-cell priming.[121,284] Many of these *Mtb* lipid factors are also involved in the broader long-term host immune response, and have been demonstrated to skew formation of immune structures such as granulomas and iBALT. [192,285,286]

Despite these sophisticated mechanisms *Mtb* has to thwart, evade, and delay the host immune response, approximately 50% of exposed individuals remain uninfected, and in most of these there is no evidence of an adaptive response at all, suggesting a critical role for early innate

immunity and mucosal responses in early defense and rapid pathogen clearance.[24,25] This would be the ideal goal for a host directed therapeutic or vaccine; to elicit a primed innate response that clears the pathogen quickly without the need to wait for adaptive immunity.[287] Along these lines, my research efforts have focused on understanding early innate immunity, specifically how *Mtb* modulates inflammatory responses in airway phagocytes and epithelial cells to induce stark long lasting effects that skew granuloma and iBALT formation, and overall disease outcome.

Chapter 2: Identifying the critical role of CCR2^{+} Alveolar Macrophages in protective immunity during pulmonary *Mtb* infection

This chapter is excerpted from the following manuscript:

Dunlap et al. A novel role for CCR2 during infection with hypervirulent Mycobacterium tuberculosis. *Nature Muc Immunol*. (2018) PMID: 30115997

Please refer to the above publication and/or attached appendix for supplemental data referenced in this chapter

2.1 Introduction

A major chemokine axis that recruits innate immune cells to the lungs is CCR2. $CCR2^{-/-}$ mice aerosol-infected with Euro-American lineage 4 *Mtb* strains showed defective accumulation of mDCs and macrophage/monocyte populations in the *Mtb*-infected lung, with coincident delayed T cell responses.[100,176] Despite decreased innate cellular recruitment, $CCR2^{-/-}$ mice were surprisingly not more susceptible to *Mtb* infection,[174,176] propagating the idea that the CCR2 axis is dispensable for protective immunity to infection with *Mtb*.[143]

A major ligand for CCR2 is MCP-1 (CCL2), along with the ligands CCL7 and CCL12. In human populations, meta-analysis of the identified −2518 A/G single nucleotide polymorphism (SNP) in the promoter region of the CCL2 gene show significantly elevated risk for pulmonary TB.[288] Recent studies have highlighted differences in cytokine induction and immune requirements for *Mtb* control to be dependent on the infecting *Mtb* strain.[224,225,253,289] Studies using the zebrafish granuloma model have described that *M. marinum* expressing virulence factors such as PGLs drive increased expression of CCL2, and mediate recruitment of $CCR2^{+}$ permissive monocytes to promote pathogenesis.[144,145] Thus, murine studies suggest a dispensable role for CCR2, zebrafish and *M. marinum* infection models suggest a pathological role for CCR2, while human studies propose a critical but as yet undefined role for the ligand, CCL2.

AMs are tissue-resident phagocytes localized to the airway and are believed to be the first contact and primary reservoir for replication of *Mtb* following inhalation of the bacteria.[65,66] During acute *Mtb* infection, AMs can exacerbate spreading of bacteria and formation of necrotic granulomas.[65] However, despite the consensus that AMs are the first innate cells that interact with *Mtb*, not much is known about how AMs participate to mediate control of *Mtb* infection.

In the current work, we show that AMs are amongst the earliest infected cells upon

exposure to W-Beijing family *Mtb* strain HN878, they accumulate in the airways and express CCR2. During disease progression, we demonstrate that AMs exit the airways and localize within the TB granulomas. Importantly, following *Mtb* HN878 infection, sorted non-airway AMs highly express genes belonging to classical macrophage activation, when compared to airway AMs that express a unique transcriptional signature. Depletion of CCR2-expressing cells, specifically at the timing of CCL2 induction and AM egress from the airways, resulted in increased susceptibility to *Mtb* infection, with the accumulation of neutrophils and loss of *Mtb* control. Additionally, we provide new evidence that mutant HN878 lacking PGL expression surprisingly resulted in increased susceptibility, even in $CCR2^{-/-}$ mice.

In this study and another contemporary work, our lab and others developed a technique for examining airway localization of immune cells.[113,126] I.t. instillation[49] of fluorophore conjugated antibody to live mice prior to lung harvest allows for "airway labeling" of immune cells by flow cytometry, giving us the ability to validate BAL techniques and importantly determine the relative proportion of a given immune cell type present in the airway vs the lung tissue (see supplementary data from **Aim 1** manuscript[113] for robust validation of this technique). We determined that both populations of airway and non-airway cells were indeed bonafide, tissue resident AMs, not replenishing monocyte-derived cells adopting an "AM-like" niche in the airway.[117,118,290] This novel technique is a critical component of the findings presented in **Aim 1** and **Aim 2** of my work, and helped determine a previously unknown migratory function of AMs out of the airway and into granulomas. Localization of immune cells within the interstitium can now be determined by exclusion of the i.t. and i.v. techniques mentioned, where airway and/or vascular label "double negative" cells can be quantified as interstitial.

We show that migration out of the airway is guided by *Mtb*-strain specific upregulation of

CCR2 on AMs and CCL2 expressed within and around *Mtb* granulomas at early time points.[113] While we found the utility of the CCR2 axis to be *Mtb* strain dependent, specifically driven by hypervirulent *Mtb* HN878 infection. The overall migration phenotype out of the airway was also independently confirmed by another group using a different strain of *Mtb,* and involved IL-1β and the inflammasome.[126] In other separate studies, infected macrophages localized in the interstitium or granulomas were observed to be more M1-like and infected airway macrophages were observed to be more M2-like,[109,110] thus validating our findings and demonstrating that compartmental location can dictate differential macrophage responses in the context of the same pathogen.

Together, our data provide novel evidence for a protective role for CCR2 in mediating AM localization and immunity against emerging *Mtb* infections. Furthermore, this work demonstrates an effective and novel protocol for examining airway and non-airway cells, and defines a novel function for AMs in pulmonary defense.

2.2 Results

2.2.1 *CCR2 is required for AM accumulation and protective granuloma formation following infection with emerging W-Beijing Mtb*

Published studies thus far have shown a redundant role for CCR2 in *Mtb* infection, specifically using Euro-American lineage 4 strains such as H37Rv and Erdman.[100,176] These studies have documented either negligible[100] or small[291] increases in *Mtb* burden in CCR2$^{-/-}$ mice, unless CCR2$^{-/-}$ mice were infected with high doses of *Mtb* administered intravenously.[174,291] Our data confirms these findings as CCR2$^{-/-}$ mice showed similar lung *Mtb* burden when compared with C57BL/6J (B6) mice following infection with *Mtb* H37Rv (H37Rv) (**Figure 1A**). Additionally, CCR2$^{-/-}$ mice only showed a small increase in lung burden when infected with another Euro-American lineage 4 clinical *Mtb* strain, CDC1551 (**Figure 1B**). Infection with neither H37Rv nor CDC1551 resulted in increased dissemination to the spleen in CCR2$^{-/-}$ infected mice (**Figure 1A,B**). In addition, infection with an Indo-Oceanic lineage1 clinical *Mtb* strain, T17x,[292] also resulted in a small increase in lung and spleen *Mtb* burden in CCR2$^{-/-}$ mice, when compared to B6 infected mice (**Figure 1C**). In sharp contrast, when infected with lineage 2 *Mtb* HN878 (HN878), CCR2$^{-/-}$ mice showed significantly increased *Mtb* burden at early days post infection (d.p.i.) which was also maintained during chronic infection (**Figure 1D**). Indeed, CCR2$^{-/-}$ HN878-infected mice also exhibited increased dissemination to the spleen, when compared to HN878-infected B6 mice (**Figure 1D**). Severe susceptibility with increased lung and spleen *Mtb* burden was also observed when CCR2$^{-/-}$ mice were infected with a pyrazinamide-resistant lineage 2 *Mtb* clinical strain, HN563 (**Figure 1E**). These results together show a previously undocumented susceptibility of CCR2$^{-/-}$ mice to *Mtb* infection, projecting a protective role for CCR2 in virulent, emerging W-Beijing *Mtb* infections.

To delineate the cellular mechanisms by which CCR2 mediates protective immunity

against HN878 infection, we determined myeloid cell recruitment to the lungs of infected B6 and CCR2$^{-/-}$ *Mtb*-infected mice (**Supplementary Figure 1** - gating strategy by flow cytometry, **Appendix**). Following H37Rv infection, we observed a trend towards decreased accumulation of monocytes, AMs, recruited macrophages (RMs), mDCs, and neutrophils in the lungs of CCR2$^{-/-}$ H37Rv-infected mice when compared to B6 H37Rv-infected mice (**Supplementary Figure 2A-E, Appendix**) confirming previous findings.[100,174,293] CCR2$^{-/-}$ mice also exhibited lower numbers of RMs, mDCs, and monocytes in the uninfected lungs (**Figure 1F**, day 0). Upon infection with HN878, CCR2$^{-/-}$ mice showed significantly decreased early AM and RM accumulation and maintained a small reduction in monocyte accumulation, when compared with B6 HN878-infected lungs (**Figure 1F**). Although mDC numbers were lower in uninfected lungs of CCR2$^{-/-}$ mice, there were no significant changes in mDC numbers in CCR2$^{-/-}$ HN878-infected mice when compared to B6 HN878-infected mice (**Figure 1F**). Also, the accumulation of activated lung IFN-γ-producing CD4^{+} T-cells was comparable between B6 and CCR2$^{-/-}$ mice infected with either H37Rv or HN878 (**Supplementary Figure 1F-H, Appendix**). These results demonstrate that early macrophage accumulation and protective immunity are dependent on CCR2 expression during HN878 infection, but that this requirement is dispensable for H37Rv infection.

The decreased early accumulation of macrophage populations in CCR2$^{-/-}$ HN878-infected mice coincided with significantly increased early accumulation of neutrophils, which was maintained during chronic infection (**Figure 1F**). Incidentally, neutrophil accumulation is associated with failed immunity to *Mtb* infection and neutrophils are the predominant infected myeloid cell type.[189,294-296] In support of this, we observed increased fibrosis and formation of necrotic granulomas in lungs of HN878-infected CCR2$^{-/-}$ mice, when compared with lungs of

B6 HN878-infected mice (**Figure 1G,H**). Expression of mRNA for tissue remodeling markers such as Arginase-1 (*Arg1)*, transforming growth factor (*Tgfb1)* and tumor necrosis factor alpha *(Tnf*α) were also increased in CCR2$^{-/-}$ HN878-infected lungs (**Figure 1I**). Additionally, fewer granulomas were found in CCR2$^{-/-}$ HN878-infected lungs, when compared with well-formed granulomas present in B6 HN878-infected lungs (**Figure 1J,K**). Finally, although there was decreased accumulation of AMs in CCR2$^{-/-}$ HN878-infected lungs (**Figure 1F**), more CD11c^{+} macrophages were infected with *Mtb* within granulomas of CCR2$^{-/-}$ mice, when compared to the AMs in granulomas from B6 mice (**Figure 1L**). Together, these data imply that the CCR2 axis is required for formation of protective granulomas during TB. In the absence of CCR2, there are fewer macrophages and fewer protective granulomas formed, instead resulting in an influx of neutrophils and development of necrotic granulomas that do not effectively control *Mtb* thus leading to increased susceptibility.

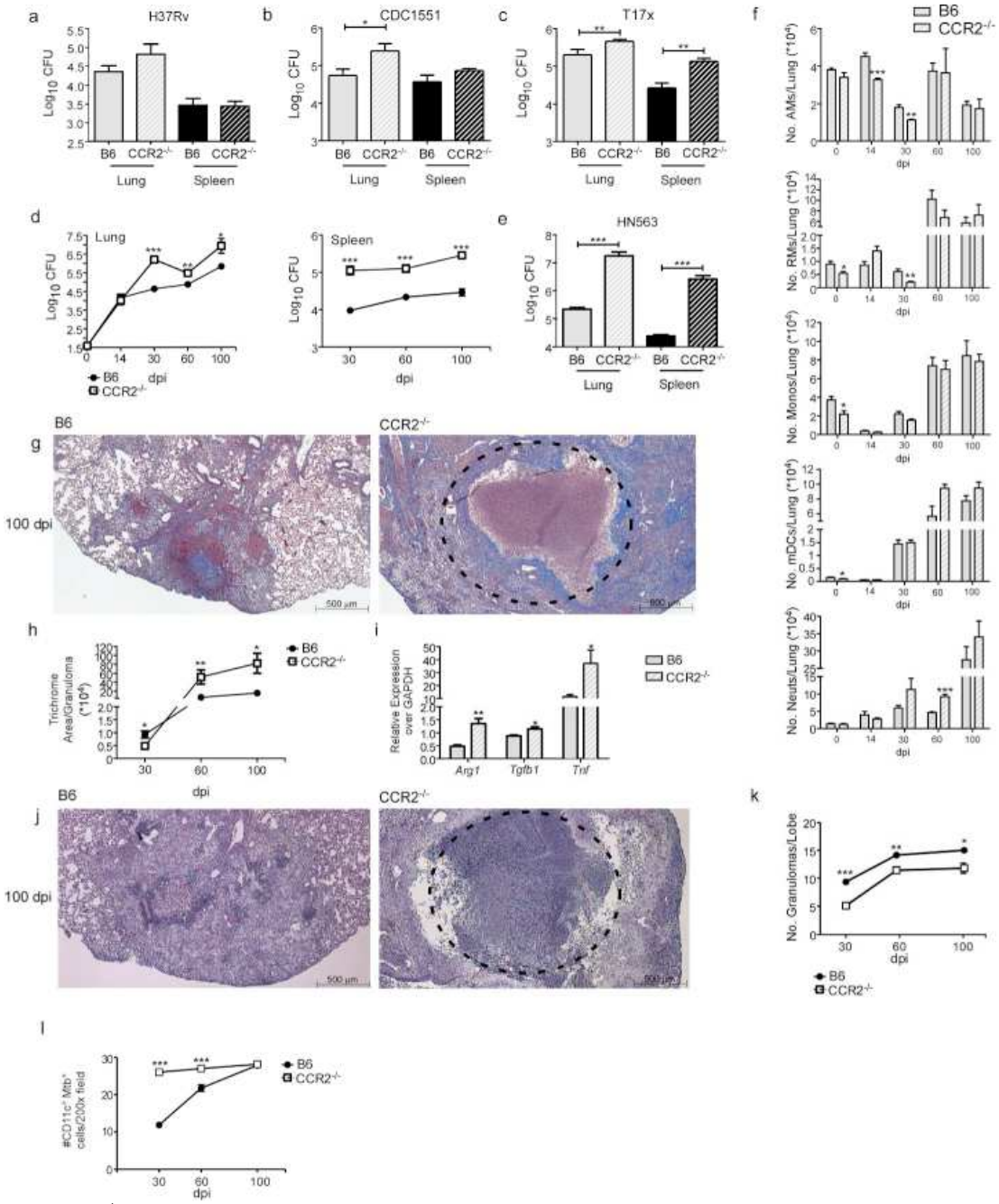

Figure 1: CCR2$^{-/-}$ mice show increased susceptibility to low dose aerosol HN878 infection. B6 and CCR2$^{-/-}$ mice were aerosol-infected with ~100 CFU of (A) H37Rv, (B) CDC1551, (C) T17x, (D) HN878, or (E) HN563. Bacterial burden in the lung and spleen was determined by plating (A-C and E) at 30 d.p.i. or (D) at different d.p.i. (F) Lung myeloid cell populations were enumerated in B6 and CCR2 $^{-/-}$ HN878-infected mice using flow cytometry at indicated d.p.i. (G-K) Pulmonary histology was assessed on FFPE lung sections from 30, 60 and 100 d.p.i samples stained with (G) Trichrome staining or (J) H&E staining. (H) Inflammatory area expressing collagen was quantified using Visiomorph image processing software to determine lung fibrosis (I) RNA was extracted from B6 and CCR2$^{-/-}$ HN878-infected lungs and relative mRNA expression of specific genes was determined by qRT-PCR. *Gapdh* was used as internal control. (K) Inflammation was quantified using the morphometric tool of the Zeiss Axioplan microscope to determine the total number of granulomas per lobe. (L) The total number of CD11c^{+} *Mtb* containing cells per 200X was determined by counting in FFPE lung sections of B6 and CCR2$^{-/-}$ mice. AMs=Alveolar Macrophages, RMs=Recruited Macrophages, Monos=Monocytes, mDCs=Myeloid Dendritic Cells,

Neuts=Neutrophils. n=5, (A-E) Student's t-test between B6 and CCR2$^{-/-}$, (F) 2-way ANOVA with Bonferroni's post-test. (H-L) Student's t-test was used to determine differences per time point.

2.2.2 AMs are preferentially infected with Mtb HN878 and require lung epithelial signaling for accumulation upon infection

To delineate the unique requirement for CCR2 expression during HN878 infection, we used H37Rv-GFP and HN878–GFP *Mtb* reporter strains and addressed if they similarly infect myeloid cell populations, and if *Mtb* infection modulated CCR2 expression on myeloid cells. Following *in vivo* infection with *Mtb*-GFP reporter strains, AMs more significantly uptake HN878 than H37Rv, suggesting a preferential localization of *Mtb* HN878 within AMs (**Figure 2A,B**). Several lung myeloid subsets expressed CCR2 in H37Rv- and HN878-infected mice, including AMs and RMs, monocytes, neutrophils, and mDCs (**Figure 2C-E**). Overall, significantly higher numbers of AMs, monocytes, and neutrophils expressing CCR2 were found in the lungs of HN878-infected mice, when compared to H37Rv-infected mice and uninfected mice (**Figure 2C-E**). Following H37Rv infection, the RM population predominantly expressed CCR2 when compared to expression levels in uninfected mice (**Figure 2D**). In contrast, during HN878 infection, the predominant myeloid cell type expressing CCR2 was the AM population (**Figure 2D**). Furthermore, we observed significantly increased CCR2 expression on AMs on a per cell basis during HN878 infection, when compared with AMs during H37Rv infection (**Figure 2F**). Thus, our data suggest that AMs preferentially uptake HN878 and specifically upregulate the expression of CCR2.

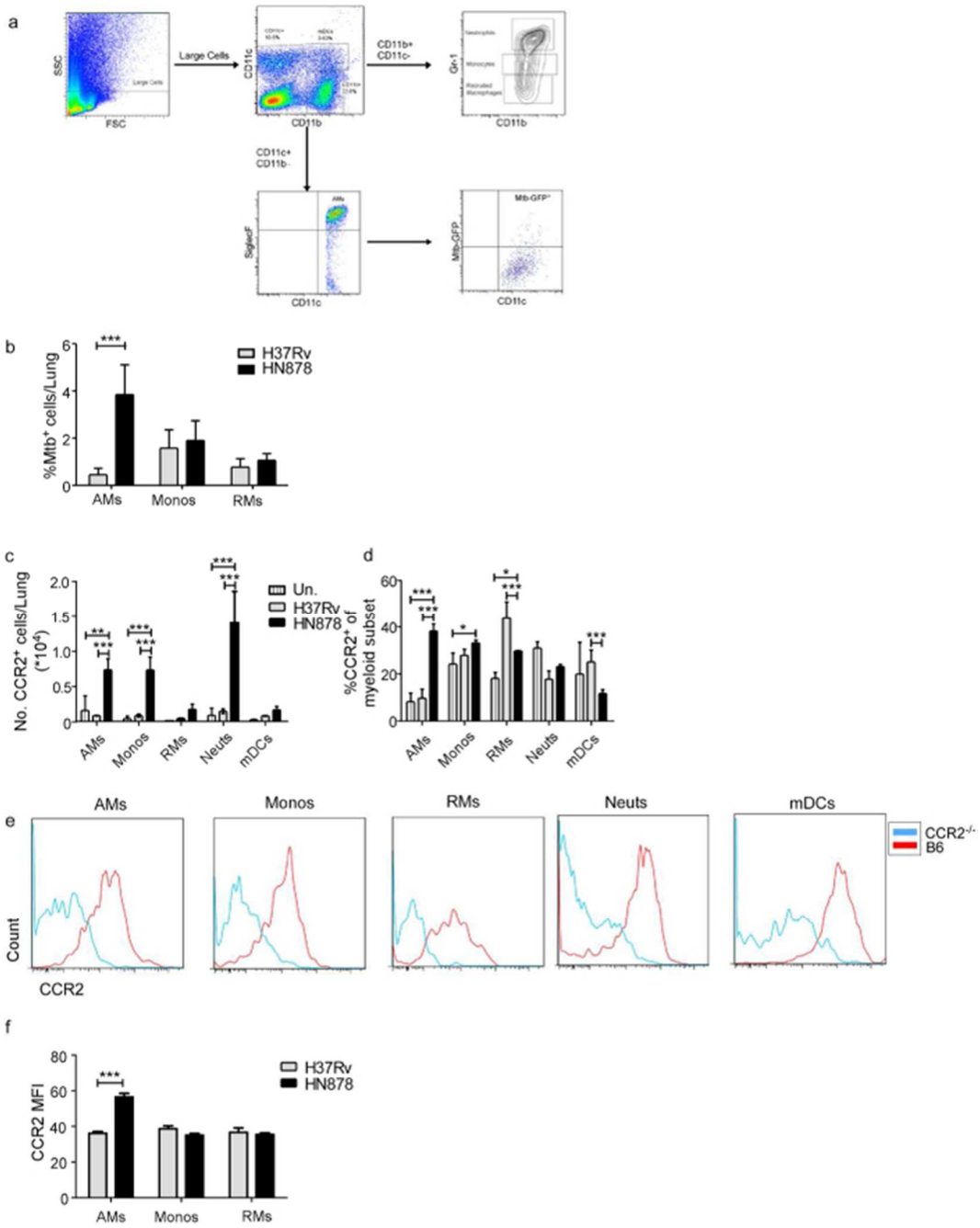

Figure 2: AMs are preferentially infected with HN878 and CCR2 expression on AMs is *Mtb* strain dependent. (A) The flow cytometry gating strategy for myeloid populations. Briefly, AMs were defined as $CD11b^{-}CD11c^{+}$Siglec F^{+} cells. mDCs were defined as $CD11b^{+}CD11c^{+}$ cells. Neutrophils were defined as $CD11b^{+}CD11c^{-}Gr\text{-}1^{hi}$ cells, monocytes were defined as $CD11b^{+}CD11c^{-}Gr\text{-}1^{lo}$ cells, and recruited macrophages were defined as $CD11b^{+}CD11c^{-}Gr\text{-}1^{-}$ cells. *Mtb*-GFP^{+} cells were gated from individual subsets. (B) B6 mice were aerosol-infected with ~100 CFU of H37Rv-GFP or HN878-GFP and myeloid cell subsets infected with *Mtb*-GFP were determined by flow cytometry on 30 d.p.i (n=5). (C,D) B6 mice (n=5) were infected with aerosolized H37Rv or HN878 and the total number (C) and percentage (D) of $CCR2^{+}$ myeloid lung cell populations were determined by flow cytometry and compared to uninfected controls. (E) Representative histograms of each subset displaying CCR2 expression by antibody staining compared to $CCR2^{-/-}$. (F) Mean fluorescence intensity (MFI) of CCR2 expression on myeloid populations was normalized relative to MFI of unstained, uninfected controls. Un.=uninfected, AMs=Alveolar

Macrophages, Monos=Monocytes, RMs=Recruited Macrophages, Neuts=Neutrophils, mDCs=Myeloid Dendritic Cells. (A-D) 2-Way ANOVA with Bonferroni post-test was used. (F) Student's t-test.

To further elucidate the *Mtb* strain specific requirement for the CCR2 axis, we next determined the expression of CCR2 ligands in H37Rv- and HN878-infected lungs. Early expression of mRNA for *Ccl2*, *Ccl7* and *Ccl12* was significantly higher in HN878-infected lungs, when compared to levels in H37Rv-infected lungs (**Figure 3A**). Additionally, $CCL2^{-/-}$ mice infected with *Mtb* HN878 exhibited increased *Mtb* bacterial burden (**Supplementary Figure 3a, Appendix**). However, since $CCL2^{-/-}$ mice did not fully reflect the heightened susceptibility of the $CCR2^{-/-}$ mice to HN878 infection, other ligands such as CCL7 and CCL12 may mediate CCR2 driven protection during *Mtb* HN878 infection. Given the relevance of CCL2 in human disease,[288,297] we chose to focus on CCL2 production in subsequent experiments. To determine the main cellular sources of CCL2 upon infection, we assessed CCL2 levels in supernatants of lung epithelial cells, DCs, and macrophages after *in vitro* infection with either H37Rv or HN878. We observed that CCL2 production was significantly higher upon infection with HN878 in epithelial cells and DCs (**Figure 3B**). In contrast, in macrophages as previously shown,[225] HN878 infection resulted in decreased CCL2 production when compared to H37Rv infection (**Figure 3B**).

Epithelial cells induced CCL2 in response to infection with HN878, thus we hypothesized that epithelial cell signaling may be involved in chemokine induction and coordinate the localization or myeloid cells, including AMs to form granulomas. Thus, we utilized the $I\kappa\kappa2^{fl/fl}$ Sftpc-cre mice,[298] which lack canonical Iκκ2 and NF-κB signaling in Sftpc-expressing cells, mainly lung epithelial cells.[299] Upon infection of $I\kappa\kappa2^{fl/fl}$ Sftpc-cre mice with *Mtb* HN878, we observed decreased AM (**Figure 3C**) and neutrophil (**Figure 3D**) accumulation

in HN878-infected lungs, without any changes in RM accumulation (**Figure 3E**) when compared to myeloid cell accumulation in infected littermate controls. Associated with decreased AM accumulation, Iκκ2$^{fl/fl}$ Sftpc-cre HN878-infected mice were more susceptible and exhibited increased lung *Mtb* CFU at 30 d.p.i. (**Figure 3F**). We found that total protein levels of C-C-chemokines such as CCL2 and CCL3, and CXC-chemokines such as CXCL2 were not different in lung homogenates of Iκκ2$^{fl/fl}$ Sftpc-cre mice, compared to littermate controls (**Supplementary Figure 3b, Appendix**). However, we specifically found that lungs of Iκκ2$^{fl/fl}$ Sftpc-cre mice exhibited fewer E-cadherin expressing epithelial cells producing CCL2 protein, when compared to littermate controls (**Figure 3G**). The protein levels of CXCL1, a neutrophil attracting chemokine, were reduced in total lung homogenates of Iκκ2$^{fl/fl}$ Sftpc-cre mice (**Supplementary Figure 3b, Appendix**), likely resulting in the decreased neutrophil recruitment observed in infected mice (**Figure 3D**). These findings suggest that early epithelial signaling has a role in coordinating the accumulation of myeloid cells, specifically AMs and neutrophils, to the lungs during infection.

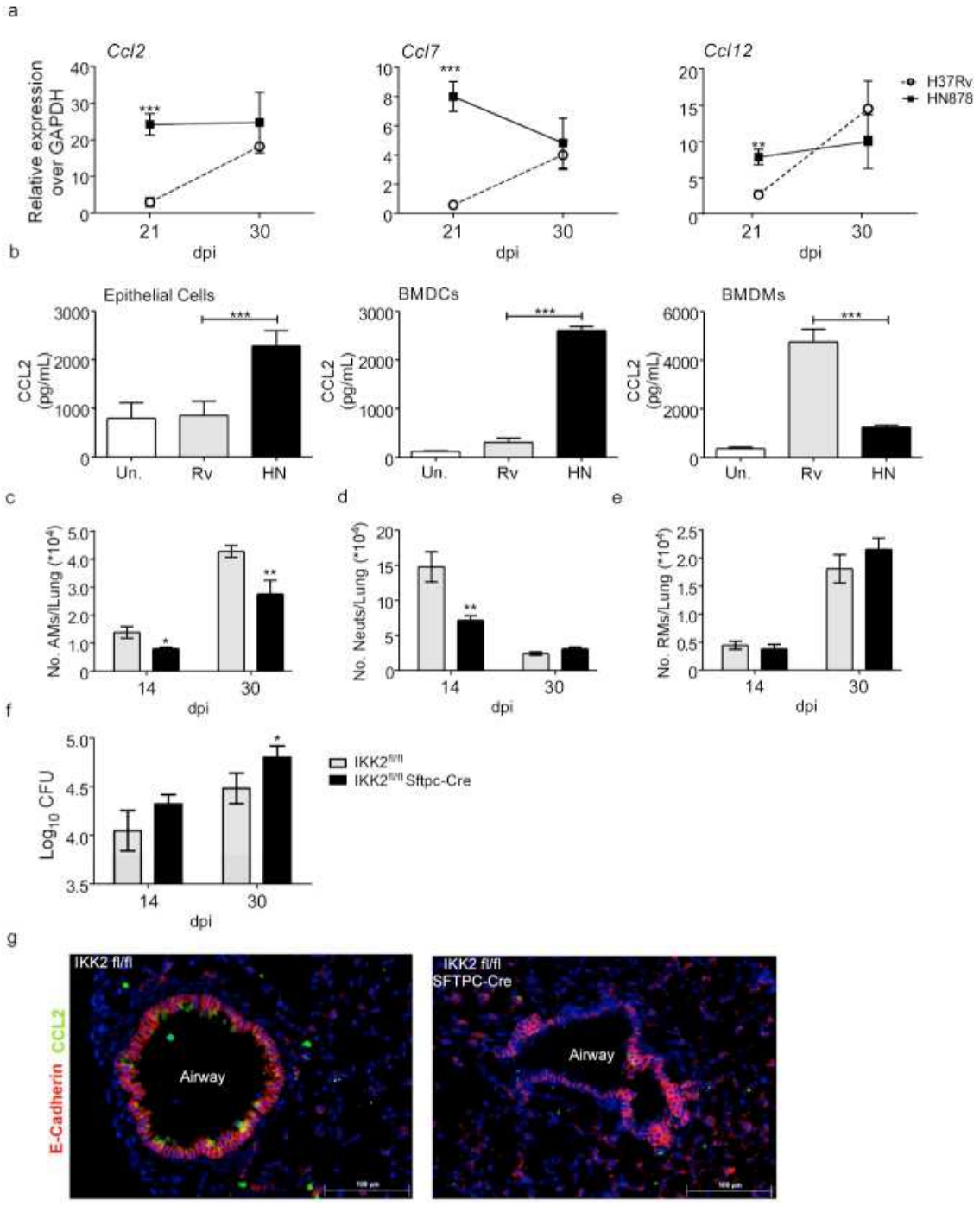

Figure 3: Increased early CCR2 ligand expression is induced in the lung following HN878 infection. (A) RT-PCR analysis was performed at 21 and 30 d.p.i. to determine mRNA expression for *Ccl2*,*Ccl7*, and *Ccl12* in lungs of H37Rv- or HN878-infected mice (n=5 per group, per time point). (B) C10 epithelia, BMDCs, and BMDMs were cultured and infected with indicated *Mtb* strains at an MOI of 1 for 48 hours (n=6). Supernatants were analyzed by multiplex or ELISA assay for CCL2. (C-E) Iκκ2$^{fl/fl}$ Sftpc-cre mice and littermate controls were infected with HN878 for 14 (n=7) and 30 (n=5) d.p.i. and the accumulation of (C) AMs, (D) neutrophils, and (E) RMs were calculated by flow cytometry. (F) Bacterial burden in the lung was determined by plating at 14 (n=7 per group) and 30 d.p.i. (n=5 per group) in Iκκ2$^{fl/fl}$ Sftpc-cre mice and littermate controls. (G) Confocal microscopy of lung sections stained for E-cadherin (red) and CCL2 (green) in Iκκ2$^{fl/fl}$ Sftpc-cre mice and littermate controls. AMs=Alveolar Macrophages,

Neuts=Neutrophils, RMs=Recruited Macrophages. (A) 2-way ANOVA with Bonferroni post-test (B) 1-way ANOVA with Tukey's post-test. (C-F) Student's t-test was used to compare between groups per time point.

2.2.3 CCR2 expression mediates AMs to egress from airways and localize within TB granulomas

CCL2 is produced by HN878-infected epithelial cells and DCs, and thus we next examined if the CCR2 axis was involved in AM movement out of the airways. To address this, we specifically labeled myeloid cells within the airways by delivering fluorophore-conjugated CD45.2 antibody i.t. to *Mtb* HN878-infected mice prior to harvest (**Supplementary Figure 4a-d, Appendix**). This technique allowed us to distinguish between BAL stain positive airway $CCR2^+$ AMs ($CD45.2^+$ $CCR2^+$ $CD11c^+$ $SiglecF^+$) and BAL stain negative non-airway $CCR2^+$ AMs that are not exposed to the CD45.2 antibody ($CD45.2^-$ $CCR2^+$ $CD11c^+$ $SiglecF^+$) (**Figure 4A**). To validate the technique, we demonstrated that delivery of CD45.2 antibody into the airways does not leak into the interstitium in naïve mice (**Supplementary Figure 4d, Appendix**). However, when lung injury is induced in mice by i.t. instillation of hydrochloric acid (HCl), we observed increased dispersion of CD45 antibody into the interstitium (**Supplementary Figure 4d, Appendix**). Additionally, mice undergoing lung injury due to treatment with HCl showed increased frequency of total lung cells and myeloid cells stained with CD45.2 antibody when compared with $CD45.2^+$ lung cells in naïve PBS-treated mice (**Supplementary Figure 4a, Appendix**) Furthermore, when BAL was collected immediately after delivery of CD45.2 antibody i.t., we found that the airway localized AMs were ~99% $CD45.2^+$ in both uninfected and *Mtb*-infected mice (**Supplementary Figure 4e**, left panel**, Appendix**), though AMs were a smaller proportion of the total airway cells during infection (**Supplementary Figure 4e**, right panel**, Appendix**).

During *Mtb* infection, we observed an overall increase in AM accumulation in the lung

(**Figure 4B**). In addition, we found that early during infection, of the airway labeled myeloid cells, AMs were the most represented cell type, followed by DCs (**Figure 4C**). However, as infection progressed, neutrophils along with monocytes were increasingly represented in the airway, while AMs were less represented (**Figure 4C**). We observed increased $CCR2^+$ AM accumulation early following infection, especially within the airways (**Figure 4D**). As infection progressed, we observed decreased $CD45.2^+$ $CCR2^+$ AMs localizing within the airways and increased non-airway $CD45.2^-$ $CCR2^+$ AMs, suggesting either an egress of bonafide AMs from the airway, or the presence of recruited, monocyte-derived, AM-like cells within the tissue (**Figure 4D**). The timing of these changes in localization coincided with the timing of increased CCR2 ligand expression in the lung at 21 d.p.i. (**Figure 3A**).

To determine the identity and functional relevance of the AM populations, we sorted for highly purified airway AMs (~99% purity, **Supplementary Figure 5a, Appendix**) ($CD45.2^+$ $CD11c^+$ $SiglecF^+$) from uninfected and infected mice, and non-airway AMs from infected mice (~95% purity, **Supplementary Figure 5a, Appendix**) ($CD45.2^-$ $CD11c^+$ $SiglecF^+$) and carried out RNA sequencing. We confirmed that both populations were in fact bonafide AMs by examining the common AM gene signature[115,300] between groups (i.e. *Siglecf*, *Pparg*, *Tgfbr2*, *Csf2r, Mertk, Itgax, Lyz2*, and *Fcgr1*). We also confirmed that the AM populations did not highly express genes associated with monocyte-derived interstitial or recruited macrophages[67] (*Ly6c1, Itgam*, and *CD163*)(**Supplementary Table 1, 2a-b, Appendix**). These data support our hypothesis that the both airway and non-airway AMs are not interstitial monocyte-derived macrophages[67] but in fact bonafide AM populations.

According to the RNA-Seq analysis, non-airway AMs expressed significantly higher mRNA levels (according to DESeq2[301]) for genes belonging to classical macrophage activation

including inducible nitric oxide synthase (*Nos2*), CD40 antigen (*Cd40*), S100 calcium binding protein A8 (*S100a8*), Guanylate binding protein 2 (*Gbp2*), Lysozyme 1 (*Lyz1*) and Lipocalin (*Lcn2*), when compared with sorted airway AMs (**Figure 4E** and **Supplementary Table 3, see Dunlap et al, 2018**). Additionally, non-airway AMs also expressed significantly higher mRNA for genes such as Matrix metallopeptidases (*Mmp2*, *Mmp14*) and proinflammatory chemokines such as *Cxcl9*, *Cxcl16*. In addition, mRNA belonging to classical macrophage transcriptional signatures such as Basic leucine zipper transcription factor, ATF-like 2 (*Batf2*)[302] and Interferon regulatory factor 8 (*Irf8*),[303] were significantly higher in sorted non-airway AMs than airway AMs. Transcriptional profiles of non-airway AMs when compared with airway AMs showed significantly higher expression of pathways associated with infections, complement cascade, and the phagosome activation (**Supplementary Table 4, Appendix**).

Alternatively, only 12 genes were significantly expressed at higher levels in airway AMs during infection, when compared with non-airway AMs isolated from *Mtb*-infected mice (**Figure 4E** and **Supplementary Table 5, Appendix**), including inhibitor of DNA binding 1[304] (*Id1;* expressed by tissue-resident macrophages) and growth differentiation factor-15 (*Gdf15*), which has been reported to drive expression of CCR2 in macrophages.[305] Further, significantly higher gene expression in airway AMs was observed for TLR-induced inflammatory responses such as Polo-like kinase 3 (*Plk3*)[306] and Pleckstrin homology like domain, family A, member 1 (*Phlda1*)[307] and the cholesterol–trafficking START domain containing 9 (*Stard9*) genes. Genes significantly higher in airway AMs from infected mice compared to uninfected mice demonstrated significant enrichment for pathways associated with metabolic pathways, antigen processing and phagocytosis (**Supplementary Table 6, see Dunlap et al, 2018**). In addition, genes associated with several key signaling pathways associated with cytoskeletal rearrangement

and diapedesis were downregulated during infection in airway AMs (**Supplementary Table 7, see Dunlap et al, 2018**). Together, our results indicate that airways AMs during infection upregulate a unique transcriptional signature associated with phagocytosis and antigen-presentation, when compared to non-airway AMs, who are more classically activated for intracellular killing and T cell activation.

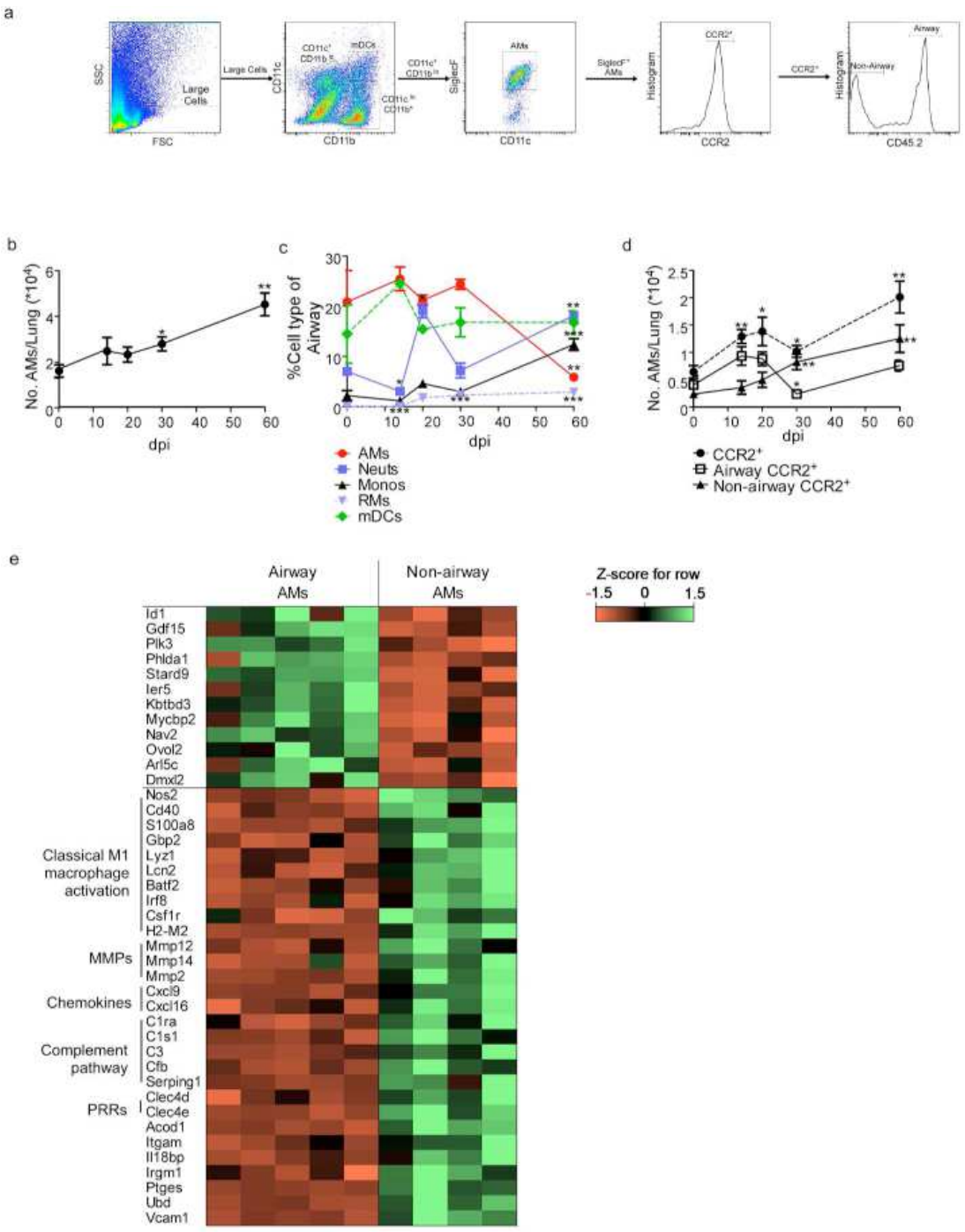

Figure 4: CCR2 expression is required for AMs to egress from airways and localize within TB granulomas. Single cell lung suspensions from uninfected and infected mice (n=5) were prepared and (A) the gating strategy for airway and non-airway AMs is shown. The percentage and number of specific cell subsets with airway label CD45.2 delivered i.t. is shown. $CD11c^{+}CD11b^{lo}SiglecF^{+}CD45.2^{+}$ cells were gated as airway AMs, while $CD11c^{+}CD11b^{lo}$ $SiglecF^{+}$ $CD45.2^{-}$ cells were gated as non-airway AMs. (B) The total number of AMs over the time course of HN878 in B6 mice was determined by flow cytometry (n=5 per time point). (C) From total airway labelled cells ($CD45.2^{+}$), the percentage of each myeloid cell type was determined in HN878-infected B6 mice by flow cytometry. (D) Total $CCR2^{+}$ AMs, $CCR2^{+}$ airway ($CD45.2^{+}$) AMs, and $CCR2^{+}$ non-airway ($CD45.2^{-}$) AMs over the course of HN878 infection in B6 mice were determined by flow cytometry. (E) Z-score Pearson correlation-based clustering of differentially expressed genes of interest (all 12 significantly differentially expressed genes in airway

AMs, and 29 genes of functional interest that were higher in non-airway AMs). AMs=Alveolar Macrophages, Neuts=Neutrophils, Monos=Monocytes, RMs=Recruited Macrophages, mDCs=Myeloid Dendritic Cells, MMPs=matrix metallopeptidases, PRRs=pattern recognition receptors. (B-D) Each time point was compared to baseline d0 counts using Student's t-test. (E) The gene expression levels of a subset of significantly differentially expressed genes between airway and non-airway AMs (according to DESeq).

To mechanistically examine the ability of $CCR2^+$ AMs to egress from the airways and localize within the TB granulomas during HN878 infection, we used an adoptive transfer model with CCR2-GFP-expressing AMs. We purified $CD11c^+$ lung cells (**Supplementary Figure 5b, Appendix**) from HN878-infected CCR2-GFP($^+$/KI) mice[308] or CCR2-GFP(KI/KI) mice. CCR2-GFP($^+$/KI) mice have one functional allele for CCR2, but also express GFP, while CCR2-GFP(KI/KI) mice have both nonfunctional, GFP^+ alleles. We adoptively transferred the $CD11c^+$ cells into the airways of HN878-infected B6 mice, and using SiglecF to further identify AMs, $CD11c^+$ $SiglecF^+$ CCR2-GFP^+ AMs were tracked within TB granulomas (**Figure 5A**). We observed that $CD11c^+$ $SiglecF^+$ CCR2-GFP($^+$/KI) AMs adoptively transferred into the airways localized within the TB granulomas (**Figure 5B**). In contrast, adoptive transfer of CCR2-GFP(KI/KI) AMs into the airways resulted in notably reduced accumulation within the TB granulomas (**Figure 5C**). Furthermore, we observed increased migration of *Mtb*-stimulated CCR2-GFP($^+$/KI) macrophages in response to HN878-infected but not H37Rv-infected epithelial cell supernatant. However, *Mtb*-stimulated CCR2-GFP(KI/KI) macrophages did not migrate in response to either *Mtb*-infected epithelial cell supernatants, suggesting that the macrophage migration in response to infection is CCR2-dependent (**Figure 5D**). Furthermore, localization of *Ccl2* mRNA is within TB granulomas in HN878-infected B6 lungs, while *Ccl2* mRNA expression was localized outside of cavitary TB granulomas in $CCR2^{-/-}$ HN878-infected lungs (**Figure 5E**). Additionally, a higher percentage of AMs were found in the airways of $CCR2^{-/-}$ HN878-infected lungs when compared to B6 HN878-infected mice (**Figure 5F**). These data

suggest that CCR2 plays a role in AM localization within the TB granuloma, and that without a functional CCR2, AMs less efficiently migrate from the airways to localize within the TB granulomas.

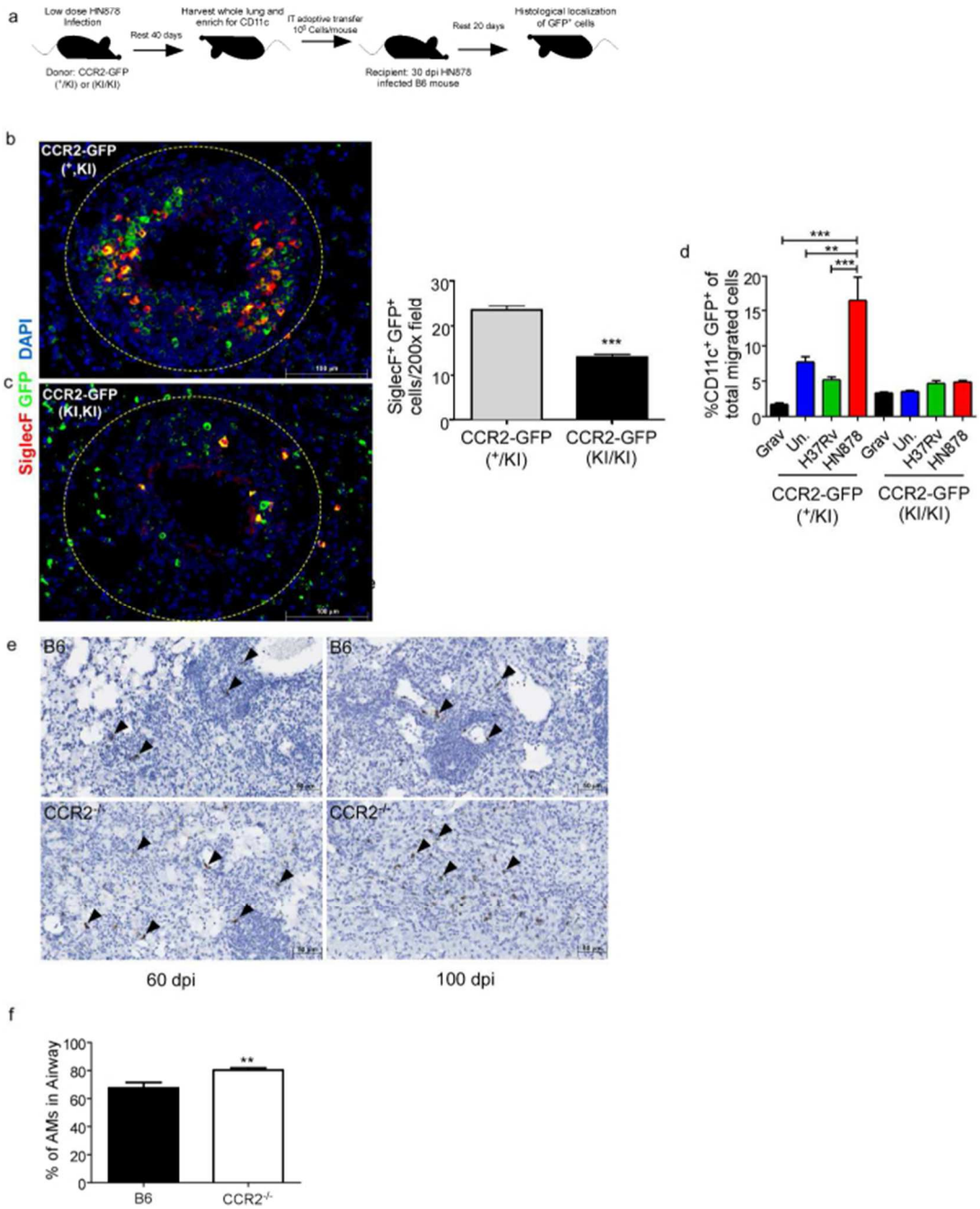

Figure 5: CCR2 is required for AM localization within TB granulomas. (A) CD11c^{+} cells were purified from lungs of 30 d.p.i. HN878-infected CCR2-GFP($^{+}$/KI) or CCR2-GFP(KI/KI) mice and 10^{6} cells were IT transferred into B6 HN878-infected mice (n=5) at 30 d.p.i.(A-C) Lungs were harvested at 50 d.p.i. and examined for localization of SiglecF^{+} GFP^{+} cells within TB granulomas using the morphometric tool of the Zeiss Axioplan microscope. (D) CCR2-GFP($^{+}$/KI) or CCR2-GFP(KI/KI) BMDMs were stimulated *in vitro* with 20 μg/mL irradiated *Mtb* HN878 for 24

hours. Migration towards uninfected, H37Rv- or HN878-infected epithelial cell supernatants was analyzed via transwell chemotaxis assays and flow cytometry (n=3). (E) *Ccl2* mRNA localization was determined within FFPE lung sections from B6 and CCR2$^{-/-}$ HN878-infected using RNAScope in situ hybridization (ISH). Arrows point to *Ccl2* mRNA localization(brown). (F) B6 and CCR2$^{-/-}$ mice (n=5) were infected with HN878 and percentage of AMs with airway label CD45.2 delivered IT was calculated on 14 d.p.i. by flow cytometry. Grav=Gravity control, Un.=uninfected, AMs=Alveolar Macrophages. n=5 (B,C) Student's t-test. n=3, (D) 2-Way ANOVA with Bonferroni post-test. (F) Student's t-test.

2.2.4 CCR2 expression at the time of airway AM egress is critical for control of Mtb HN878 infection

CCR2-DTR mice have DTR inserted between the first and second codon of CCR2,[175] and treatment of CCR2-DTR mice with diphtheria toxin (Dtx) resulted in depletion of all CCR2-expressing cells. Previously, depletion of CCR2-expressing cells following *Mtb* Erdman infection reduced monocyte and monocyte-derived populations, but did not result in increased *Mtb* susceptibility.[100] To address the timing of the CCR2 requirement for protection following HN878 infection, we similarly used CCR2-DTR mice.[100] CCR2-DTR mice were infected with HN878, and CCR2-expressing cells were depleted either early at the time of infection (−1 to 5 d.p.i.) or later at the time of AM egress from the airways (12–18 d.p.i.) (**Figure 4D**). Transient depletion of all CCR2-expressing cells around 12–18 d.p.i. but not at the time of infection resulted in a significant increase in *Mtb* burden (**Figure 6A-D**). Depletion of CCR2-expressing cells at 12–18 d.p.i. also resulted in increased accumulation of neutrophils, monocytes and RMs in the lung and sharply decreased number of AMs, when compared to PBS treated *Mtb*-infected mice (**Figure 6B**). Additionally, CCR2-DTR that received Dtx between 12–18 d.p.i. also showed increased inflammation, when compared to control CCR2-DTR mice that received PBS (**Figure 6C**). In contrast, CCR2-DTR mice that received Dtx around the time of infection did not show any differences in AM numbers, but showed decreased accumulation of neutrophils, monocytes and RMs and coincident decreased inflammation (**Figure 6E,F**). Together, these results

demonstrate that transient depletion of CCR2-expressing cells coincident with the time of AM egress from the airways resulted in decreased AM accumulation and increased susceptibility to HN878 infection. In contrast, depletion of CCR2-expressing cells around the time of infection, while dampening RM and monocyte accumulation, did not impact AM accumulation and only minimally increased *Mtb* control.

To further confirm the role of $CCR2^{+}$ AMs in protection against HN878 *Mtb* infection, we delivered B6 macrophages stimulated *in vitro* with irradiated *Mtb* into the airways of $CCR2^{-/-}$ HN878-infected mice. Adoptive transfer of B6 macrophages rescued the increased susceptibility observed in $CCR2^{-/-}$ HN878-infected mice, yielding decreased lung bacterial burden equivalent to B6 HN878-infected mice (**Figure 6G**). These data suggest that the susceptibility associated with $CCR2^{-/-}$ mice coincides with lack of macrophage accumulation in the lung, and that adoptive transfer of B6 macrophages into airways is sufficient to reverse susceptibility *Mtb* in $CCR2^{-/-}$ HN878-infected mice.

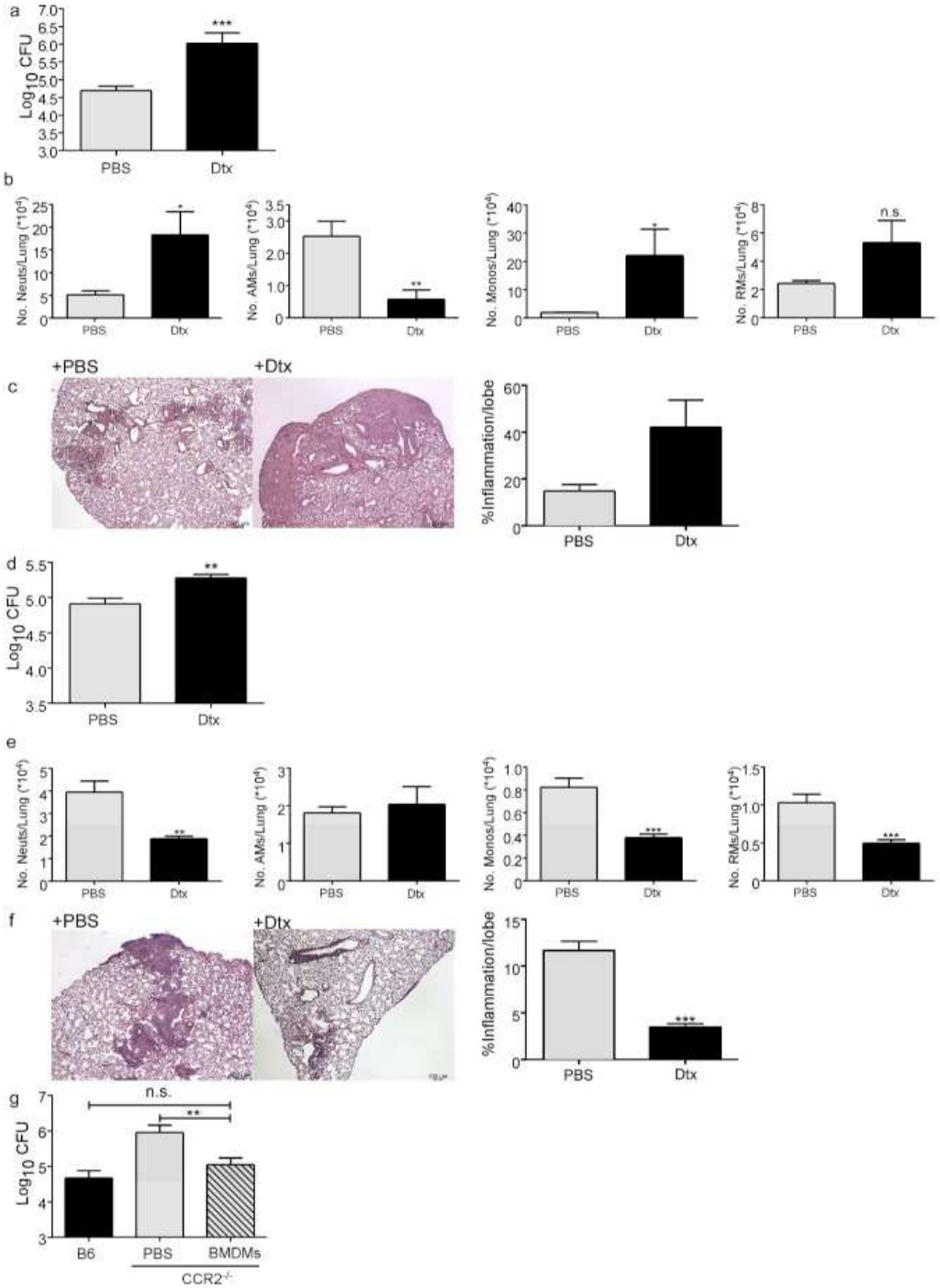

Figure 6: Depletion of CCR2^{+} cells at the time of AM egress from airways increases susceptibility to HN878 infection. CCR2-DTR mice (n=4) were infected with HN878 and administered Dtx (A-C) IP at 12, 14, and 16 d.p.i. or (D-F) at −1, 1, and 3 d.p.i. (A,D) Lung bacterial burden was determined by plating on 30 d.p.i. (B,E) Neutrophil, AM, monocyte and RM numbers were determined in PBS-treated and Dtx-treated CCR2-DTR mice at 30 d.p.i. (C,F) Pulmonary histology was assessed on FFPE lung sections stained with H&E, and inflammatory area was quantified using the morphometric tool of the Zeiss Axioplan microscope. (G) B6 (n=5) and CCR2$^{-/-}$ mice (n=8 per group) were infected with HN878, and CCR2$^{-/-}$ mice received either PBS or HN878-stimulated BMDMs delivered IT on 15 and 21 d.p.i. Lungs were harvested at 30 d.p.i. and bacterial burden was determined by plating. Neuts=Neutrophils, AMs=Alveolar Macrophages, Monos=Monocytes, RMs=Recruited Macrophages. (A-F) Student's t-test. (G) 1-way ANOVA with Tukey's post-test.

2.2.5 Dependence on CCR2 for protective immunity to Mtb HN878 is not driven solely by PGL expression

Recently, *M. marinum* expressing PGL has been shown to be involved in induction of CCL2 and recruitment of CCR2-expressing permissive macrophages in zebrafish mycobacterial infection model.[144,145] Thus, we next addressed if absence of PGL in *Mtb* HN878 would result in lack of a role for CCR2 in controlling *Mtb* HN878 infection in mice. Thus, B6 and CCR2$^{-/-}$ mice were infected with a recombinant *Mtb* HN878 mutant harboring a mutation within *pks1-15* (HN878 *pks1-15*::*hygB*) rendering *Mtb* PGL deficient.[225] Upon infection with *Mtb* HN878 *pks1–15::hygB*, CCR2$^{-/-}$ mice were still more susceptible to infection when compared with B6 infected mice (**Figure 7A**). This coincided with decreased accumulation of AMs, RMs and monocytes, increased neutrophil accumulation, (**Figure 7B**) and severe pulmonary disease (**Figure 7C**) in CCR2$^{-/-}$ infected mice when compared with B6 infected mice. Additionally, while in vitro infection of macrophages and DCs with HN878 *pks1–15::hygB* resulted in decreased CCL2 when compared to HN878 infection[225] (**Figure 7D**), comparable induction of CCL2 was observed upon infection of lung epithelial cells with HN878 and HN878 *pks1–15::hygB* (**Figure 7E**). These data are also supported by localized expression of *Ccl2* mRNA within TB granulomas in lungs of B6 and CCR2$^{-/-}$ mice infected with HN878 *pks1–15:hygB* (**Figure 7F**). These data suggest that PGL expression is not the only key determinant for a protective role for CCR2 in *Mtb* HN878 infection, as *Mtb* H37Rv and HN878 also differ in expression of several other key components in their cell walls.[222]

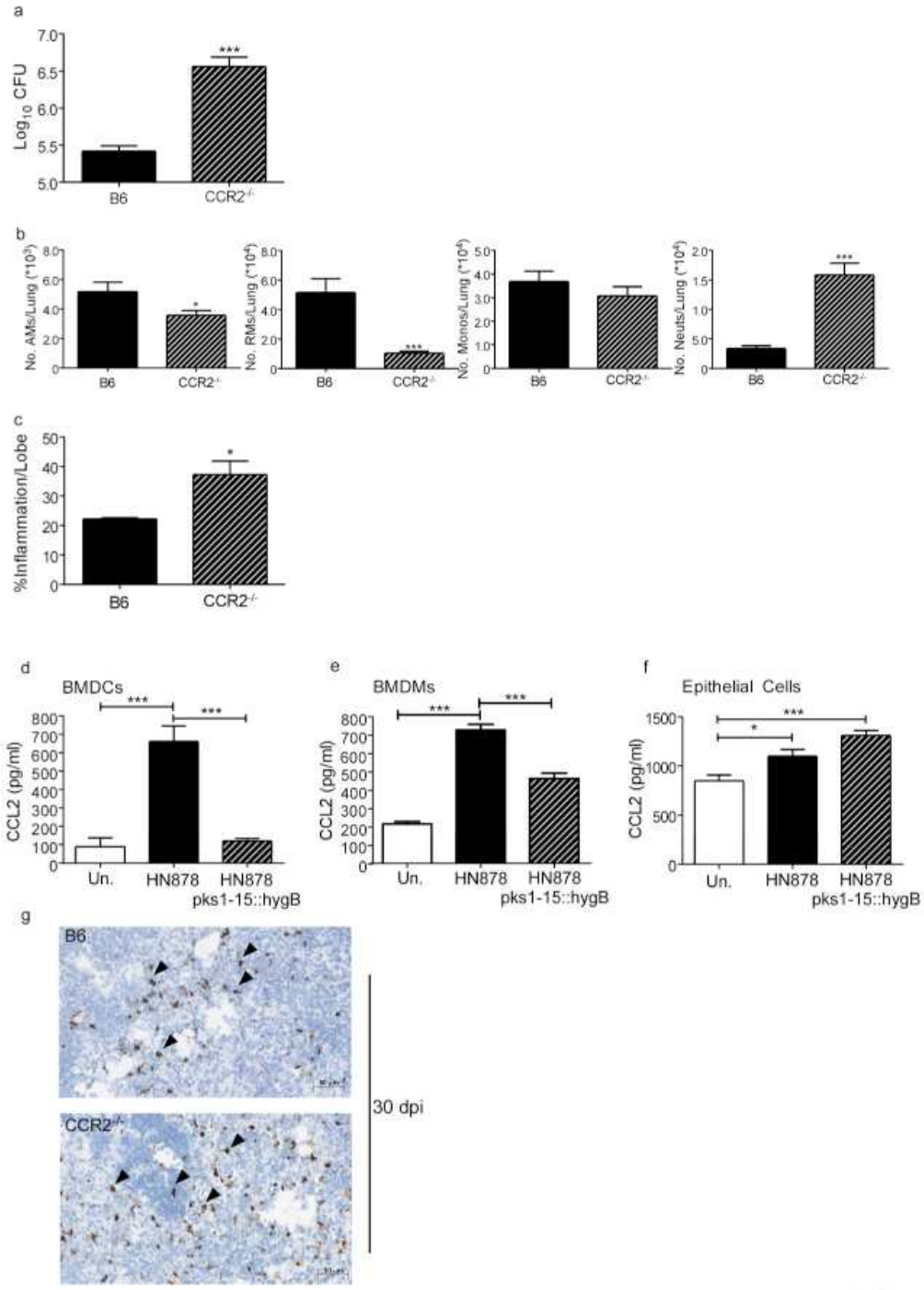

Figure 7: Dependence on CCR2 for protective immunity to Mtb HN878 is not driven by PGL expression. B6 and CCR2$^{-/-}$ mice (n=5) were aerosol-infected with ~100 CFU HN878 *pks1–15::hygB*. (A) Lung bacterial burden was determined by plating on 30 d.p.i. (B) Lung myeloid cell populations of AMs, RMs, monocytes and neutrophils were enumerated in B6 and CCR2$^{-/-}$ HN878 *pks1–15:hygB* infected mice using flow cytometry. (C) Pulmonary histology was assessed on FFPE lung sections stained with H&E, and inflammatory area was quantified using the morphometric tool of the Zeiss Axioplan microscope. (D-F) BMDCs, BMDMs, and C10 epithelial cells were cultured and infected with indicated *Mtb* strains at an MOI of 1 for 48 hours (n=5). Supernatants 34 were analyzed by multiplex or ELISA assay for CCL2. (G) *Ccl2* mRNA localization was determined within FFPE lung sections from B6 and CCR2$^{-/-}$ HN878-infected using RNA Scope in situ hybridization (ISH). Arrows point to *Ccl2* mRNA localization

(brown). AMs=Alveolar Macrophages, RMs=Recruited Macrophages, Monos=Monocytes, Neuts=Neutrophils. (A-C) Student's t-test. (D-F) 1-way ANOVA with Tukey's post-test.

2.3 Materials and Methods

Mice

C57BL/6J (B6), CCR2$^{-/-}$, [174] and CCL2$^{-/-}$ [309] mice on the B6 background were purchased from The Jackson Laboratory (Bar Harbor, ME). CCR2-DTR[175] and CCR2-GFP [308] were a kind gift from Drs. Robyn Klein and Marco Colonna at Washington University School of Medicine and bred in-house. Iκκ2$^{fl/fl}$ Sftpc-cre[298] were a kind gift from Dr. Pasparakis (University of Cologne). CCR2-DTR mice were administered sterile PBS or 20 ng Dtx/g body weight (VWR, Radnor, PA) approximately 500 ng/mouse in 200 μL sterile PBS, intraperitoneally (i.p.), 3 times as indicated.

All mice were maintained in the animal facility at Washington University in St. Louis and bred in-house. Experimental mice were age and sex matched and infected between the ages of 6 and 8 weeks. All mice were maintained and used in accordance with the approved Washington University in St. Louis Institutional Animal Care and Use Committee guidelines. Both male and female mice were used and to our knowledge no sex-based differences were observed.

Mtb Strains and Experimental Infections

Mtb strains H37Rv (Trudeau Institute), CDC1551, HN878, and HN563 were obtained from BEI Resources (Manassas, VA) under National Institutes of Health contract AI-75320. HN878 *pks1-15*::*hygB* was used as previously published.[225] H37Rv-GFP and HN878-GFP was transformed with the integrating EGFP expression vector pMV261.kan (provided by Dr.

Christina Stallings, Washington University in St. Louis) to generate GFP-expressing *Mtb*. Indo-Oceanic T17x strain was acquired from Dr. Karen M. Dobos, Colorado State University. All *Mtb* strains were cultured in Proskauer Beck medium supplemented with 0.05% Tween 80 and frozen at −80 °C while in mid-log phase. Mice were aerosol-infected with low doses (~100 CFU) of indicated *Mtb* strains in sterile PBS using a Glas-col nebulizer.[310] Mice were monitored and weighed as needed and lungs and spleens were harvested at described time points. *Mtb* CFU/organ was quantitated by plating serial dilutions of homogenized lung or spleen tissue on 7H11 agar plates (BD Biosciences, Franklin Lakes, NJ). Plates were incubated for 2–3 weeks at 37 °C and colonies were counted visually.

In Vitro Culture

Mouse epithelial C10 cells were cultured in complete Dulbecco's modified eagle's medium (cDMEM) to confluence for approximately 2 days. Counts from a representative well were used to calculate the concentration of C10 cells/well, performed visually by hemocytometer.

Bone marrow-derived macrophages (BMDMs) and bone marrow-derived DCs (BMDCs) were cultured from bone marrow cells as previously described.[311] Briefly, bone marrow cells from the femur and tibia of B6 and gene deficient mice were extracted, and 1×10^7 cells were plated in 10 mL of cDMEM supplemented with 20 ng/mL mouse recombinant (rm) granulocyte-macrophage colony-stimulating factor (GM-CSF) (Peprotech, Rocky Hill, NJ).[310] Cells were then cultured at 37 °C in 5% CO2. On day 3, 10 mL of cDMEM containing 20 ng/mL rmGM-CSF was added. On day 7, adherent cells were collected as macrophages and non-adherent cells were collected as DCs.

Chemotaxis Assay

BMDMs were grown as above, and plated at 2×10^6/mL and stimulated with 20 μg/mL irradiated *Mtb* HN878 (BEI) for 24 h in cDMEM at 37 °C. BMDMs were then added to the upper chamber of the 24-well transwell plate (Costar, Cambridge, CA), 1×10^5 cells/well in 100 μL of Hank's balanced salt solution containing 1% fetal bovine serum with 600 μL of indicated conditioned media beneath the transwell in a 24-well plate. These were incubated for 90 min at 37 °C, then transmigrated cells were collected from the lower chamber, stained and analyzed by flow cytometry.

In Vitro Infections

BMDMs, BMDCs, and C10 epithelial cells were infected with *Mtb* (multiplicity of infection, MOI:1) in antibiotic-free cDMEM. Cell culture supernatants were collected for analysis of cytokines 48 hours post infection.

Adoptive transfer

Lung cell suspensions were prepared as before from the lungs of donor CCR2-GFP (+/KI or KI/KI) mice on 30 d.p.i. following *Mtb* HN878 infection. $CD11c^+$ cells were enriched from the lung suspension using magnetic selection with CD11c microbeads (Miltenyi Biotec, Auburn, CA) per manufacturer's instructions, yielding a population of (>85%) $CD11c^+$ cells. These cells were resuspended at 1×10^7 cells in 500 μL sterile PBS. 50 μL (1×10^6 cells) of this suspension was administered i.t. to HN878-infected mice at 30 d.p.i. These mice were harvested on 50 d.p.i. as indicated.

BMDMs were grown as above, and plated at 2×10^6 cells/mL and stimulated with 20 μg/mL irradiated *Mtb* HN878 (BEI) for 24 hours in cDMEM at 37 °C. These cells were then harvested and resuspended at 1×10^7 cells in 500 μL sterile PBS. 50 μL (1×10^6 cells) of this suspension was administered i.t. to HN878-infected mice at 15 and 22 or 30 d.p.i. as indicated.

Flow Cytometry

For distinguishing between airway and non-airway cells, mice received 0.7 μg of V500 or PE-conjugated CD45.2 mAb (Clone 104, BD Biosciences and Biolegend, San Diego, CA), administered i.t. in 50 μL sterile PBS per mouse. Mice were rested for 15 min following which lungs were harvested. To validate the technique some mice received 50 uL of HCl in sterile water (pH 1.5) i.t. and rested for 24 hours prior to instillation of CD45.2 antibody. [313]

Lung single cell suspensions were prepared as before,[310] treated with Fc Block (CD16/CD32, 2.4G2, Tonbo Biosciences, San Diego, CA), and stained with appropriate fluorochrome-labeled specific antibodies or isotype control antibodies: CD11c (HL3, BD Biosciences), CD11b (M1/70, BD Biosciences and Tonbo Biosciences), SiglecF (E50-2440, BD Biosciences), CD64(X54-5/7.1, Biolegend), Gr-1 (RB6-8C5, BD Biosciences), CCR2 (FAB5538P, R&D Systems), CX3CR1 (SA011F11, Biolegend), Ly6C (AL21, BD Biosciences), Ly6G (1A8, BD Biosciences), CD3 (145-2C11, Tonbo Biosciences), CD4 (GK1.5, BD Biosciences), CD44 (IM7, eBioscience), IFN-γ (XMG1.2, BD Biosciences), and rat IgG1 (BD Biosciences).

Cells were processed using a Becton Dickinson FACS LSR Fortessa flow cytometer using FACSDiva software, or sorted on a Becton Dickinson FACSJazz cell sorter using BD FACS sorting software. Cells were gated based on their forward and side scatter characteristics

and the frequency of specific cell types was calculated using FlowJo (FlowJo, LLC, Ashland, OR). Neutrophils were defined as $CD11b^{+}CD11c^{-}Gr\text{-}1^{hi}$ cells, monocytes were defined as $CD11b^{+}CD11c^{-}Gr\text{-}1^{lo}$ cells, and RMs were defined as $CD11b^{+}CD11c^{-}Gr\text{-}1^{-}$ cells. mDCs were defined as $CD11b^{+}CD11c^{+}$ cells. AMs were defined as $CD11b^{lo}CD11c^{+}$ cells (Fig. 1) and subsequently as $CD11b^{lo}CD11c^{+}SiglecF^{+}$ cells. The flow cytometry gating strategy used for lung subset analysis was an approach using our i.t. labeling method to select for airway populations and a combined gating strategy from several previous publications.[114,312-315] [314–318]

For uptake experiments, lung cell suspensions were prepared from H37Rv-GFP- or HN878-GFP-infected B6 mice and stained with appropriate fluorochrome-labeled specific antibodies. Uptake was determined by the co-localization of GFP with known fluorophore-conjugated cell subset markers as measured by flow cytometry.

Bronchoalveolar Lavage (BAL)

Mice were administered i.t. CD45.2 Ab as above and ~10 min later euthanized. BAL was then performed as previously described.[172,191] Briefly, the chest cavity was opened and the sternum/ribcage was resected. The trachea was isolated and a blunt tipped needle was gently inserted into the trachea. The lungs were lavaged with ~5 (5 × 1 mL) washes with sterile 0.2 mM EDTA (Sigma-Aldrich) in PBS. Cells were collected from these lavages and analyzed by flow cytometry as above.

RNA Extraction and Quantitative Real-Time PCR (qRT-PCR)

Lung tissue was homogenized and snap-frozen in RLT buffer (Qiagen, Valencia, CA). Total RNA was extracted from lung tissue using the Qiagen RNeasy Mini kit (Qiagen). RNA

was converted to cDNA using ABI reverse transcription reagents (ABI/ThermoFisher Scientific, Carlsbad, CA) using a BioRad DNA Engine Thermal Cycler (BioRad, Hercules, CA). cDNA was then amplified using TaqMan reagents on the ABI Viia7 Real-Time PCR detection system (ThermoFisher Scientific). The primer and probe sequences for murine glyceraldehyde 3-phosphate dehydrogenase (*Gapdh*) and *Tnfα* were previously published.[316] The primers and probes for murine *Arg1*, *Ccl2*, *Ccl7*, and *Ccl12* were purchased commercially (ABI Biosystems). The primer and probe sequences for *Tgfb1* are forward 5′-TGACGTCACTGGAGTTGTACGG-3′, reverse 5′-GGTTCATGTCATGGATGGTGC-3′, probe 5′-/56-FAM/TTC AGC GCT CAC TGC TCT TGT GAC AG/3BHQ_1/-3′. Fold increase was determined over uninfected controls relative to *Gapdh* expression using the ΔΔCT calculation as previously described. [316]

RNA-Sequencing of AM Populations

AMs were sorted and RNA was extracted as described above. RNA sequencing libraries were generated using Clontech SMART-Seq v4 Ultra Low Input RNA Kit for sequencing and Illumina Nextera XT DNA Library preparation kit following the manufacturer's protocol. The cDNA libraries were validated using KAPA Biosystems primer premix kit with Illumina-compatible DNA primers and quality was examined using Agilent Tapestation 2200. The cDNA libraries were pooled at a final concentration of 1.8 pM. Cluster generation and 75 bp paired-read dual-indexed sequencing were performed on Illumina NextSeq 500. Single-ended 75 bp reads were cleaned using Trimmomatic (version 0.36) to remove adapters and quality trimmed to filter out reads <60 bp in length (after trimming). Cleaned sequence data was mapped against the mouse reference genome build GRCh38.90 (Ensembl) using the HISAT2[317] aligner (version 2.1.0) with default parameters, generating sam format alignment files. These sam files were then used as input for featureCounts (version 1.5.1), requiring a minimum mapping quality score of

10. Raw read counts were used as input for DESeq2[301] (version 1.16.1) differential expression analysis, using default settings and an FDR-adjusted *P* value threshold of 0.05 for significant differential expression. Lists of differentially expressed genes were used to test for significant enrichment among KEGG pathways[318] and Mammalian Phenotype Ontology,[319] using WebGestalt[320] (default settings, adjusted $P = 0.05$ threshold for enrichment). Heatmap clustering was performed using "hclust" in R, using Pearson distances and complete linkage, based on *Z*-scores calculated per row using Microsoft Excel.

Histology

Lung lobes were perfused with 10% neutral buffered formalin and embedded in paraffin. For immunofluorescent staining, formalin-fixed paraffin-embedded (FFPE) lung sections were cut, immersed in xylene to remove paraffin, and then sequentially hydrated in absolute ethanol, 95% ethanol, 70% ethanol, and water. Antigens were unmasked with a DakoCytomation Target Retrieval Solution (Dako, Carpinteria, CA) and nonspecific binding was blocked with 5% (v/v) normal donkey serum and Fc Block (BD Pharmingen, San Jose, CA). Endogenous biotin (Sigma-Aldrich) was neutralized by adding avidin followed by incubation with biotin.

Antibodies for Histological Identification of Lung Cells:

Rabbit anti-*Mtb* antibody, (MBS534825, MyBiosource.com)
Rabbit anti MCP-1/CCL2 (GTX37379, GeneTex, Irvine, CA)
Goat anti-human/mouse E-Cadherin (AF748, R&D Systems)
Monoclonal hamster anti-ITGAX/CD11c (N418, Lifespan Biosciences, Inc., Seattle, WA)
Polyclonal rabbit anti-Siglec 5/CD170 (LS-C97825, Lifespan Biosciences, Inc.).
Fluorescein (FITC) affinipure F(ab')2 fragment donkey anti-rabbit IgG (H+L) (711-096-152, Jackson Immunoresearch, West Grove, PA).
Biotin-SP (long spacer) affinipure F(ab')2 fragment rabbit anti-Syrian hamster IgG (H+L) (307-066-003, Jackson Immunoresearch).
Streptavidin, Alexa Fluor® 488 conjugate (S-11223, ThermoFisher Scientific).

Biotinylated goat anti-GFP (GTX26658, Genetex, Irvine, CA) was visualized with Alexa Fluor 568 donkey anti-goat IgG and Alexa Fluor 555 streptavidin. GFP stain was pseudocolored to green with the Axiovision software. Images were collected using an inverted Observer.Z1 Axioplan Zeiss Microscope with Colibri system (Zeiss, Thornwood, NY) and the Axiovision Rel 4.8. Software.

FFPE lung sections were stained with hematoxylin and eosin (H&E) and inflammatory features were evaluated by light microscopy. Inflammatory lesions were outlined with the automated tool of the Zeiss Axioplan 2 microscope (Carl Zeiss) and percentage of inflammation was calculated by dividing the inflammatory area by the total area of individual lung lobes. FFPE lung sections were stained for collagen and muscle using Masson's Trichrome 2000 stain procedure kit (#KTMTR2, American Mastertech, Lodi, CA) per the manufacturer's instructions. Trichrome stained slide images were acquired using a Hamamatsu Nanozoomer 2.0 HT system with NDP scan image acquisition software. Trichrome staining was quantified using Visiomorph image processing software (Visiopharm, Broomfield, CO). FFPE lung sections were subjected to in situ hybridization (ISH) with the mouse-Ccl2 probe using the RNAscope 2.5HD Detection Kit (Brown staining) as per the manufacturer's recommendations (Advanced Cell Diagnostics, Newark, CA). The representative pictures were taken with the Hamamatsu Nanozoomer 2.0 HT system with NDP scan image acquisition software.

Cytokine Production Quantification

Cytokine levels within cell culture supernatants were analyzed using the BD OptEIA Mouse CCL2 ELISA kit (BD Biosciences) or using Milliplex Multiplex Assays (Millipore, Billerica, MA), as per standard protocol.

Statistical Analyses

Statistical analyses were performed using GraphPad Prism 5 and Microsoft Excel. Specific analysis techniques and post tests are mentioned in figure legends. SEM error bars displayed. $*P \leq 0.05$, $**P \leq 0.01$, $***P \leq 0.001$, n.s.—not significant.

2.4 Discussion and Conclusions

In humans, polymorphisms in *Ccl2* have been associated with pulmonary TB,[288] while mouse infection studies have shown that CCR2 expression is dispensable for protective immunity to infection with aerosolized Euro-American lineage 4 *Mtb* strains.[176] Zebrafish modeling of granulomas using *M. marinum* has proposed that the CCR2–CCL2 axis through interactions with virulence factors drives the generation of permissive macrophages and promotes mycobacterial replication and pathogenesis.[144,145,176] In the current study, using murine models, we provide novel evidence that the CCR2 axis is critical for protective immunity against infection with emerging *Mtb* lineages, such as the W-Beijing family of *Mtb* strains. Our data demonstrate that AMs express CCR2 that is required for localization of AMs within the TB granulomas. In the absence of CCR2, AMs fail to localize within TB granulomas, resulting instead in accumulation of neutrophils and development of necrotic TB lesions, a characteristic

of failed immunity in TB. Additionally, we show that the requirement for CCR2 for protective immunity to *Mtb* HN878 is not solely dependent on expression of PGL and PGL-mediated modulation of this chemokine axis. Thus, our study provides novel insights by projecting that CCR2 expression, especially on AMs, is required for protective immunity against emerging *Mtb* strains.

AMs are a tissue-resident macrophage lineage that under homeostatic conditions are believed to mature during neonatal development.[312] However, under conditions of inflammation, inflammatory monocytes, perhaps through a transient lung-resident macrophage population may also give rise to AMs.[312] During *Mtb* infection, although it is widely believed that tissue-resident AMs are the primary innate cell type that are infected, the functional relevance of AMs during *Mtb* infection is unclear.[321] Utilizing the zebrafish granuloma model, it has been shown that *M. marinum* can be transported across neuroepithelial barriers by macrophages and results in CCL2-mediated recruitment of permissive monocyte-derived macrophages that mediate formation of the granuloma to enhance disease pathogenesis.[144,145] Using a murine model, our studies here show that following infection with *Mtb* HN878, bonafide AMs increase in the lung following *Mtb* infection, and they localize within the airway. As infection progresses and TB granulomas form, our results show that AMs respond to CCL2-dependent chemokine signals likely from lung epithelial cells to egress from the airways. Furthermore, adoptive transfer of $CD11c^{+}$ $SiglecF^{+}$ AMs expressing CCR2 localized within granulomas, and AMs not expressing CCR2 did not localize within granulomas, suggesting that AMs may require CCR2 expression to respond to epithelial signals and localize into granulomas. Additionally, we show that HN878 *pks1-15::hygB* infection still results in increased susceptibility in $CCR2^{-/-}$ mice. Thus, the protective versus disease-promoting features of the CCR2 axis and AMs in mycobacterial infections in

mouse versus zebrafish model may be due to (1) differences in the animal models used, (2) a specific feature of AM trafficking from airways that are not observed in zebrafish macrophages, or (3) due to the fact that *M. marinum* PGLs contain a monosaccharide while *Mtb* PGL contain a trisaccharide domain.[261]

Ligands for CCR2, namely CCL2, CCL7, and CCL12 are induced in response to *Mtb* infection in mice, non-human primates, and humans.[322-324] Despite this, studies in the last decade have shown that CCR2$^{-/-}$ mice display negligible or low susceptibility to low dose aerosolized *Mtb* infection belonging to the Euro-American lineage 4, such as H37Rv and Erdman.[176,291] Our data show that when W-Beijing family lineage 2 clinical *Mtb* strains are used, the absence of CCR2 in the CCR2$^{-/-}$ or deletion of CCR2 in CCR2-DTR mice render mice more susceptible to infection, with coincident defects in macrophage accumulation, instead promoting neutrophil accumulation, an immune cell type associated with failed immunity.[189,294-296] The influx of neutrophils may be a direct response to the tissue damage and inflammatory environment brought on by the lack of apoptotic clearance and anti-inflammatory signaling of AMs.[106] This increase in susceptibility in CCR2$^{-/-}$ mice is not just limited to lineage 2 but also to clinical isolates within the Euro-American lineage and Indo-Oceanic lineages, albeit not to the same extent as in W-Beijing family *Mtb* infection. The observation that infection with the *Mtb* HN878 mutant lacking PGLs still requires CCR2 for AM accumulation and protective immunity supports the idea that expression of other factors by emerging *Mtb* strains are likely involved. It is possible that the observed *Mtb* strain-dependent response is due to distinct cellular responses brought on by pattern recognition and phagocytic receptor interactions with *Mtb* strain-specific membrane lipids and virulence factors.[222] This is supported by published data that *Mtb*-associated membrane lipids and other virulence factors lead to differential transcriptional and

metabolic profiles in macrophages.[186,325,326]

Upon infection with Streptococcus, AMs can leave the airway to migrate to lymph nodes to transport bacteria.[141] However, whether AMs can egress from the airway and participate in immune responses locally within the lung was unknown up to this point. In our study, we find that airway AMs apart from expressing the core macrophage signature genes, also express a unique transcriptional signature. Furthermore, airway AMs upon *Mtb* infection upregulate transcriptional pathways associated with antigen presentation and phagosome maturation. Using a novel IT labeling technique, we show that $CCR2^{+}$ AMs are present within airways during early stages of *Mtb* infection. As the disease progresses, airway AMs can likely respond to chemokine signals from lung epithelial cells (and other cells such as DCs) and egress from the airway and localize within TB granulomas. Upon localization within granulomas, non-airway AMs can undergo classical activation including the production of iNOS, upregulation of genes associated with inflammation, pattern recognition receptors, and T-cell costimulation thereby providing optimal *Mtb* control. Whether the activation of non-airway AMs is due to localization within the inflammatory granulomas and dependent on signals within the granuloma is yet to be studied.

This airway labeling technique we have developed can be useful in the study of airway-localized immune cell types in the lung, including the localization of AMs, monocytes, DCs, and neutrophils in the airways versus lung tissue. While this labeling technique can be useful for tracking early cellular changes in the airways as in this study, upon formation of granulomas and disease progression to chronic stages of infection, the structural integrity of the lung airway epithelium can be compromised and may be a caveat as airway administered antibody may leak, thus also labeling non-airway cells. Furthermore, with time, fluid accumulation and scarring may occur in the airway, leading to less effective labeling of airway cells. These caveats should be

carefully considered in the use of this labeling technique during chronic stages of infection, or under conditions of loss of structural integrity or tissue scarring.

In summary, we show that CCR2 expression, while dispensable for protection against *Mtb* lineage 4 infections, is critical for protection against emerging *Mtb* strains. Together our data show that during early HN878 infection, AMs upregulate CCR2 and accumulate in the airways. As the infection progresses, some AMs remain in the airway where they likely continue to phagocytose and process TB antigen. Other $CCR2^{+}$ AMs egress in response to the production of CCL2 by epithelial cells or DCs around forming granulomas and interact with other inflammatory cells to become classically activated and potentially localize within organized granulomas to mediate *Mtb* control. Thus, our results provide novel insights into the role of AMs and the CCR2 axis in macrophage anti-microbial mechanisms of protection against *Mtb* infection.

Chapter 3: The role of IκκΒ2/NF-κB signaling in modulating AM effector functions and global pulmonary immune responses to *Mtb* infection

3.1 Introduction

Mtb, the causative agent of pulmonary TB, is one of the leading causes of death worldwide, infecting approximately one fourth of the world's human population and killing approximately 1.3 million people per year.[1] While this death toll is staggering, approximately 90-95% of infected people have LTBI, and remain mostly asymptomatic with no clinical hallmarks of disease or overt inflammation. However, approximately 5-10% of the estimated 2 billion humans infected with *Mtb* will develop ATB during their lifetime, presenting an urgent global health crisis.[1] Despite these shocking figures, we do not have an effective vaccine to treat adult pulmonary disease.

One of the greatest barriers to developing better vaccine treatments for TB is our poor understanding of the early host response mechanisms that mediate protective immunity against *Mtb* infection. Most current vaccine strategies aim to induce protective adaptive immune responses targeting helper $CD4^+$ T-cells[13,16-20] or B cells/antibodies.[170,244,286,287,327] Unfortunately, adaptive immune responses to *Mtb* are weeks slower than similar responses to other pulmonary infections. This is due to delayed interactions between pulmonary DCs and $CD4^+$ T-cells in the lung dLNs,[21,22,103,142,280] which slows peak adaptive immune responses until roughly one month after *Mtb* exposure.[23] Because of this delay, current research characterizing protective human immune responses to *Mtb* infection focus on predictive host biomarkers antecedent to ATB conversion and onset of adaptive immunity. In humans and multiple model organisms, blood biomarkers such as Type 1 IFNs[11] and S100A8/9[12,14] can be used to accurately predict conversion to ATB in LTBI individuals. These studies correlate early inflammatory mediators and protective immunity, thus suggesting a role for innate responses in early TB defense.[26-28,328]

Interestingly, an incident almost a century ago[29,30] demonstrated that in some cases

adaptive immunity may not be required for protection. In the winter of 1929-1930 at the Lübeck General Hospital in Germany, 251 infants were accidentally given a BCG vaccine course contaminated with live *Mtb*.[29,30] Approximately ⅓ of these infants succumbed to TB complications. Surprisingly, approximately ⅓ recovered after moderate to severe TB disease and the remaining ⅓ displayed only mild symptoms.[25,30] This tragedy demonstrated that innate immunity alone could variably clear high dose *Mtb* infection in the surviving 2/3 of the cohort, as human infants do not yet have robustly developed adaptive immune repertoires at this age.

Beyond the Lübeck disaster, there is a growing body of evidence suggesting that early responses driven by innate immune cells can *entirely prevent the establishment of infection*, a concept called *early clearance*.[25] Indeed, a meta-analysis of 41 human studies found that approximately 50% of highly exposed household contacts of TB patients remain uninfected long term with no evidence of adaptive immunity.[24,25] Similarly, innate immune determinates have been associated with resistance to infection.[26-28,328] Early pulmonary responses are driven by local innate immune cells, mainly airway AMs, DCs, and AECs. Interestingly, *Mtb* DNA, but not live bacteria, have been observed in AMs and AECs of otherwise histologically normal tissue,[26] suggesting the ability of these cells to clear *Mtb*. Together, these lines of evidence demonstrate a critical role for early innate responses in preventing *Mtb* establishment and early pathogenesis. These findings provide an attractive therapeutic alternative compared to current approaches of treating and controlling disease *after onset of ATB disease*.

Despite being the key initiators of the pulmonary immune response, characterizing the role of innate phagocytes like AMs during infection has proven difficult. Depletion of AMs in various pulmonary infection models have yielded mixed results.[94-99] Depletion of airway AMs and mDCs by clodronate liposomes improved disease outcomes, marked by increased T-cell

priming[100] and decreased total *Mtb* burden, pulmonary inflammation and damage.[96] In other studies, transient depletion of AMs and mDCs utilizing transgenic DTR models exacerbated inflammation and drove severe pulmonary infection with *Mtb*, *Francisella tularensis,* Influenza or RSV.[98,99,103-105] These mixed findings demonstrate that AMs may play divergent roles in pulmonary infection. To our current knowledge, *no studies have observed AMs/mDC depletion to have no effect on pulmonary immune responses,* thus demonstrating these cells are critical for the benefit of either the pathogen or the host.

Comparing the divergent roles of AMs during pulmonary infection requires examining M1 and M2 polarization, which is a useful convention for determining functional responses to a variety of infectious or inflammatory contexts.[67,109] M2 profiles are driven by mammalian target of rapamycin (mTOR) and peroxisome proliferator-activated receptor gamma (PPAR-γ), the major signaling nodes induced by type 2 cytokines IL-4 and IL-13.[329,330] These pathways are critical for M2 polarization and AM steady state development.[330-333] M2 responses are characterized by expression of *Arg1* and production of IL-10 and TGF-β,[91,334-337] which drive tissue remodeling and repair responses after large scale damage.[76,78,106-108] In pulmonary *Mtb* infection, M2 polarization drives decreased iNOS production and inhibited microbicidal function, decreased pro-inflammatory cytokine production,[110-112] and a metabolic shift to fatty acid oxidation (FAO). FAO improves nutrient availability and provides a hospitable environment for *Mtb*,[67] therefore suggesting AMs are permissive to *Mtb* replication and persistence.[67,109,121,122]

M1 polarization is induced by recognition of microbial PAMPs and inflammatory type 1 cytokines such as IFN-γ and TNF-α.[330] M1 polarization improves phagocytosis, iNOS production and microbicidal function to drive a hostile environment for *Mtb*. M1 profiles are also marked by a metabolic shift to glycolysis[67,89,109] that correlates with pro-inflammatory cytokine

production. [110-112] [338,339] Previous work demonstrated that non-airway AMs upregulated multiple functional pathways associated with M1 polarization and NF-κB,[113,126] which is the major nexus of pro-inflammatory signaling driven by pathogen sensing pathways. Interestingly, M1 polarization is negatively regulated by Iκκ2, a member of the NF-κB complex involved in enhancing activation. Using pharmacological approaches[138] and/or genetic models,[139,140] inhibiting Iκκ2 drove increased MHC-II expression and inflammatory cytokine production on macrophages, suggesting improved M1 polarization. Furthermore, NF-κB inhibition surprisingly yielded increased *Mtb* control *in vitro* in primary human macrophages,[138] also supporting this hypothesis. These studies therefore provided us with a concise target for examining M1/M2 roles of airway and non-airway AMs by focusing on Iκκ2/ NF-κB.

In the current study, we aimed to determine how the factors Iκκ2 and NF-κB specifically modulate M1 activation of migrating AMs during *Mtb* infection. We examined how these inflammatory nodes modulate effector functions of AMs and long-term disease outcomes. Establishing a link between specific inflammatory signaling components, macrophage effector functions, and disease outcomes will allow us to elucidate potential druggable targets for inducing protective host responses during pulmonary infection. Taken together with prior evidence for early clearance, we hypothesized that AMs may become M1 polarized to drive protective pro-inflammatory responses *in vivo* that can clear *Mtb* infection.[26]

3.2 Results

3.2.1 *Abrogated Iκκ2 modulates cytokine production in CD11c expressing phagocytes*

In previous studies, it was demonstrated that non-airway localized AMs upregulated M1 activation effector functions.[113,126] Several of these specific pathways and genes are directly downstream of NF-κB,[137,340] thus suggesting this key signaling node was likely involved in the bifurcation of AM effector responses during *Mtb* infection. To test this, we utilized the *ikk2*-fl/fl (Iκκ2$^{fl/fl}$) mouse[113,298] crossed to a *itgax*-cre (CD11c-cre) for CD11c^{+} expressing cells,[341,342] which specifically targets AMs and mDCs.

We validated decreased levels of Iκκ2 protein *in vitro* by measuring uninfected and *Mtb* infected cell culture lysates. We utilized either sorted lung CD11c^{+} cells, or BMDMs and BMDCs, which also highly express CD11c.[343-345] We observed approximately ~90% decreased Iκκ2 levels in infected CD11c^{+} lung cells (**Figure 8A**), and approximately ~50% and ~66% decreased Iκκ2 levels in infected BMDMs (left panel) and BMDCs (right panel), respectively (**Figure 8B**).

To examine a functional output of Iκκ2 reduction on NF-κB activity, we then quantified inflammatory cytokine output from the above culture supernatants. We observed opposite trends in the two models, with increased production of IL-6 and IL-1β in the CD11c^{+} sorted lung cells (**Figure 8C**) and decreased production of IL-6 and IL-1β in both bone marrow cell types (**Figure 8D**). These differences are likely influenced by the culture conditions and compartment of origin, which drastically alters cytokine production and function in macrophages.[343-345] Interestingly, we also observed increased cytokine production in the CD11c^{-} fraction from the lung. Though these CD11c^{-} cells are unaffected by the cre-flox system, it is likely that cellular interactions are

skewed by the altered cytokine production within AMs/mDCs, which may lead to a generally hyper-inflammatory environment at steady state. It was previously demonstrated that Iκκ2 negatively regulates M1 activation,[139,140] thus suggesting that our model may yield M1 "pre-polarized" AMs in the lung and heightened inflammation even at steady state that could have far-reaching effects on other cellular compartments.

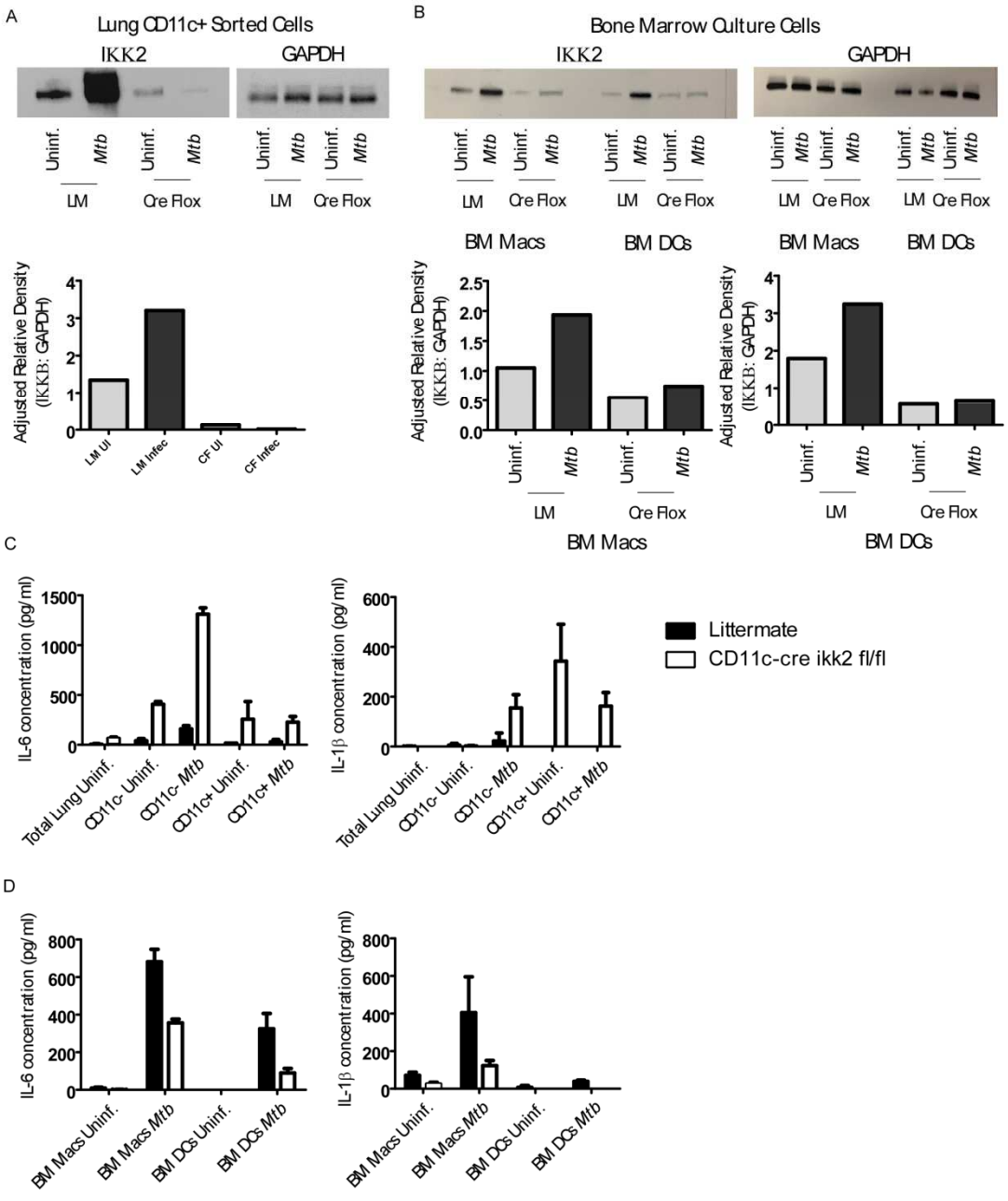

Figure 8: Abrogated Iκκ2 modulates cytokine production in CD11c expressing phagocytes. A) Magnetically sorted CD11c^{+} cells from whole lung cell suspensions from littermate or CD11c-cre Iκκ2$^{fl/fl}$ mice were infected with *Mtb* H37Rv at MOI=0.1 for 3 days. B) BMDMs and BMDCs from littermate or CD11c-cre Iκκ2$^{fl/fl}$ mice were cultured and infected with *Mtb* H37Rv at an MOI of 1 for 3 days (n=3) A&B) Western blots for Iκκ2 and GAPDH were performed on lysates from collected cells at 3 d.p.i.. Relative density of Iκκ2 over Gapdh was quantified using ImageJ analysis. C&D) Supernatants from infected cells were analyzed by ELISA assay for the indicated cytokines IL-6 and IL-1β

3.2.2 Decreased Iκκ2 in CD11c$^+$ phagocytes drives early increased inflammation and decreased Mtb burden in the lung

We then aimed to characterize the broader effects that decreased Iκκ2 expression in AMs would have on pulmonary *Mtb* infection. To do this, we infected littermate and CD11c-cre Iκκ2$^{fl/fl}$ mice with a low dose of aerosolized *Mtb* HN878. In line with the idea that Iκκ2 expression antagonizes M1 activation, we observed that CD11c-cre Iκκ2$^{fl/fl}$ mice were less susceptible to *Mtb* than littermate controls at early time points (**Figure 9A**). Similarly, we observed increased accumulation of lung resident AMs and mDCs (**Figure 9B**), and increased recruitment of inflammatory neutrophils, monocytes, and RMs (**Figure 9C**). In support of this, we observed heightened levels of most inflammatory cytokines and chemokines at 21 d.p.i. **(Figure 9D)**, and slightly increased inflammation in lung sections at baseline (left) and 21 d.p.i. (right) (**Figure 9E**). Taken together, this heightened early inflammatory milieu likely drives improved innate immune responses that at least partially contribute to the observed early protection.

To further test this hypothesis, we examined effector functions of these innate cells using expression of surface MHC-II, and our previously published airway labeling technique.[113] We observed that both AMs (left panel) and mDCs (right panel) had significantly higher expression of MHC-II at baseline in CD11c-cre Iκκ2$^{fl/fl}$ mice, (**Figure 9F**) suggesting a "primed" capability of these cells to present antigen even with abrogated Iκκ2. Furthermore, we observed increased migration of AMs out of the airway by 21 d.p.i, as measured by the decreased proportion of airway label positive cells over time in CD11c-cre Iκκ2$^{fl/fl}$ mice (**Figure 9G**). We found that at baseline and 14 d.p.i., the majority of both AMs (left) and mDCs (right) from CD11c-cre Iκκ2$^{fl/fl}$ mice were localized in the airway, as expected and previously demonstrated. However, by 21

d.p.i., the relative proportion of AMs in the airway of CD11c-cre Iκκ2$^{fl/fl}$ mice had significantly decreased when compared to littermate controls and previous time points. Airway localization of mDCs in CD11c-cre Iκκ2$^{fl/fl}$ mice remained constant throughout all early time points. This trend of increased AM migration *from the airway* around 21 d.p.i. was previously observed to correlate with AM homing into forming granulomas,[113] thus suggesting that Iκκ2 may directly inhibit this function.

Increased migration *to the airway* was observed for recruited cell types, where we found an increased proportion of airway label positive neutrophils (left), monocytes (center), and RMs (right) both at baseline and over the early time course in CD11c-cre Iκκ2$^{fl/fl}$ mice (**Figure 9H**). This "swapping" of AMs to the interstitium and neutrophils to the airway was previously observed in our studies as part of the general course of *Mtb* infection and suggests that decreased Iκκ2 in AMs and mDCs may lead to enhanced inflammatory responses within the lung tissue, but not in the airway. Increased migration of AMs *from the airway* and neutrophils *to the airway* may be indicative of specific immune functions or cellular interactions not yet characterized.

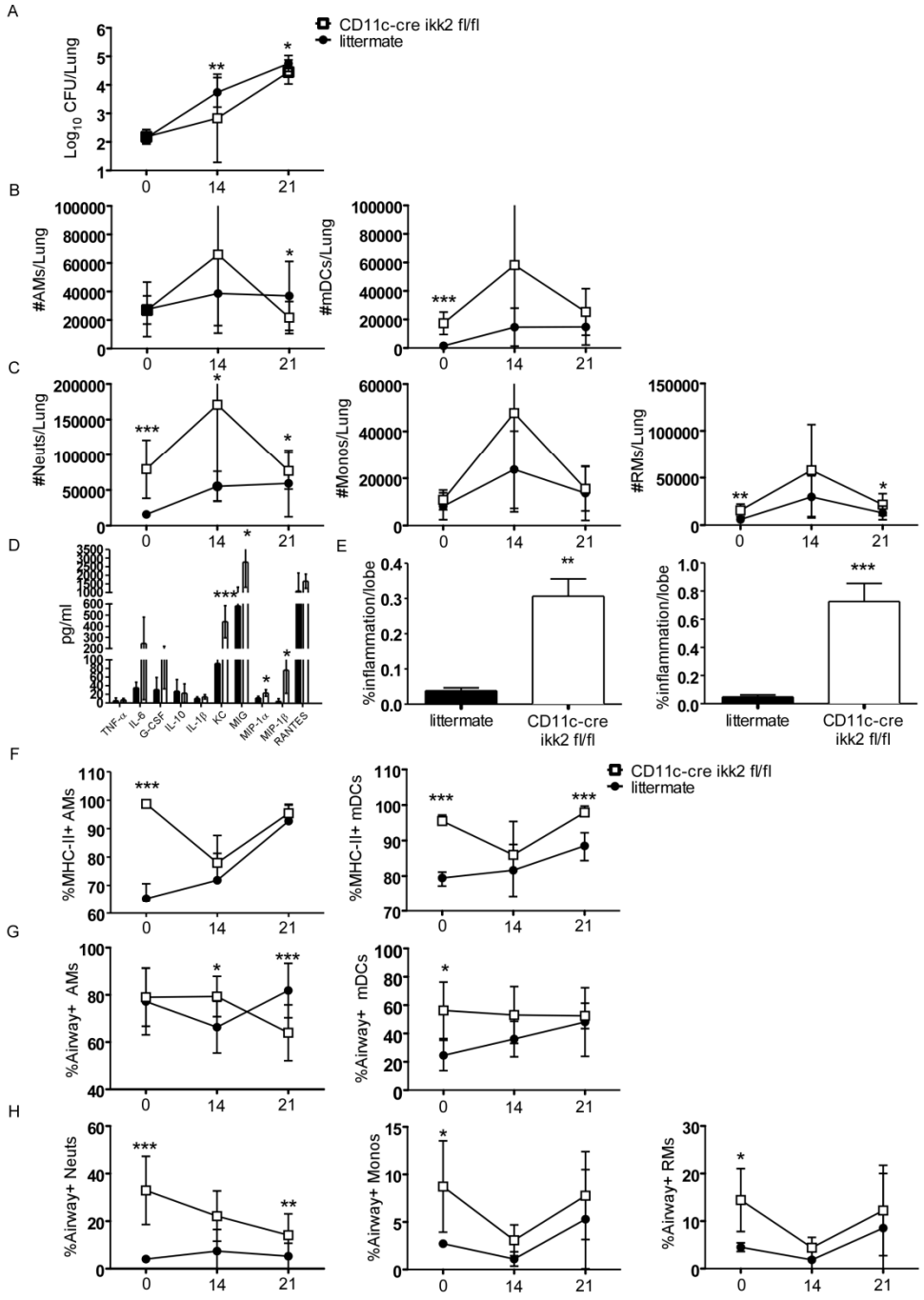

Figure 9: Decreased Iκκ2 in CD11c^{+} phagocytes drives early increased inflammation and decreased *Mtb* burden in the lung. Littermate and CD11c-cre Iκκ2$^{fl/fl}$ mice were aerosol-infected with ~100 CFU of *Mtb* HN878 (n=5 mice/group, experimental replicates=3). A) Bacterial burden in the lung was determined by serial dilution plating at indicated timepoints. B&C) Lung myeloid cell populations were enumerated in littermate and CD11c-cre Iκκ2$^{fl/fl}$ HN878-infected mice using flow cytometry at baseline or indicated d.p.i. D) Whole lung tissue homogenates were analyzed by cytokine multiplex for indicated cytokines at 21 d.p.i. E) Pulmonary histology was assessed on H&E stained FFPE lung sections from uninfected baseline and 21 d.p.i. infected littermate and CD11c-cre Iκκ2$^{fl/fl}$ mice . F)

Littermate and CD11c-cre Iκκ2$^{fl/fl}$ mice were aerosol-infected with ~100 CFU of *Mtb* HN878. (n=5 mice/group, experimental replicates=3) The percentage of MHCII^{+} AMs (left) and mDCs (right) were determined by flow cytometry. The percentage of (G) AMs (left) and mDCs (right) or (H) neutrophils (Neuts, left), monocytes (Monos, middle), and recruited macrophages (RMs, right) stained positive with airway label CD45.2 was calculated at indicated time points by flow cytometry. Littermate and CD11c-cre Iκκ2$^{fl/fl}$ mice groups (n≥5) at individual time points were compared using Student's t-test. Mean and standard deviation (SD) were plotted for each group at each indicated time point. *p<0.05, **p<0.01, ***p<0.001.

3.2.3 Decreased Iκκ2 in CD11c^{+} phagocytes maintains global decreased Mtb burden, increased inflammatory responses at later time points

To examine the long-term consequences of abrogated Iκκ2 activity in airway phagocytes, we examined later time points in our *in vivo Mtb* infection model. We selected these time points to be generally after the onset of adaptive immunity and granuloma formation.[23,64] We observed significantly decreased bacterial burden in the lungs of HN878-infected CD11c-cre Iκκ2$^{fl/fl}$ mice at 60 d.p.i., though no significant differences were observed at 30 or 75 d.p.i. (**Figure 10A**). As with the early time points, we observed general heightened inflammatory responses, characterized by increased accumulation of inflammatory cell types, most notably at 60 d.p.i. (**Figure 10B&C**). At 75 d.p.i, we observed a switch in our trends, where the littermate mice yielded higher inflammatory cell accumulation compared to CD11c-cre Iκκ2$^{fl/fl}$ mice. We further observed heightened levels of inflammatory cytokines and chemokines as before, and trends toward increased inflammation in lung sections (**Figure 10D-E**).

To determine what consequences, if any, that decreased Iκκ2 expression in airway phagocytes would have on adaptive immunity, we examined CD4^{+} and CD8^{+} T-cells at 75 d.p.i. We found that CD11c-cre Iκκ2 fl/fl mice had decreased accumulation of CD3^{+} lymphocytes in general, (**Figure 10F**) as well as decreased accumulation of activated CD4^{+} (**Figure 10G,H)** and CD8^{+} T-cells (**Figure 10J,K)**. Furthermore, less IFN-γ and IL-17 producing CD4^{+} (**Figure 10I**) and CD8^{+} (**Figure 10L**) T-cells were observed in the lungs CD11c-cre Iκκ2$^{fl/fl}$ mice, thus

suggesting dampened adaptive responses (**Figure 10I,L**). Taken together, these findings suggest that abrogated Iκκ2 on airway phagocytes has significant effects on both short and long term pulmonary immune responses, and that decreased Iκκ2 expression may detrimentally affect the induction of adaptive immunity, while maintaining slight protection against pulmonary *Mtb* infection.

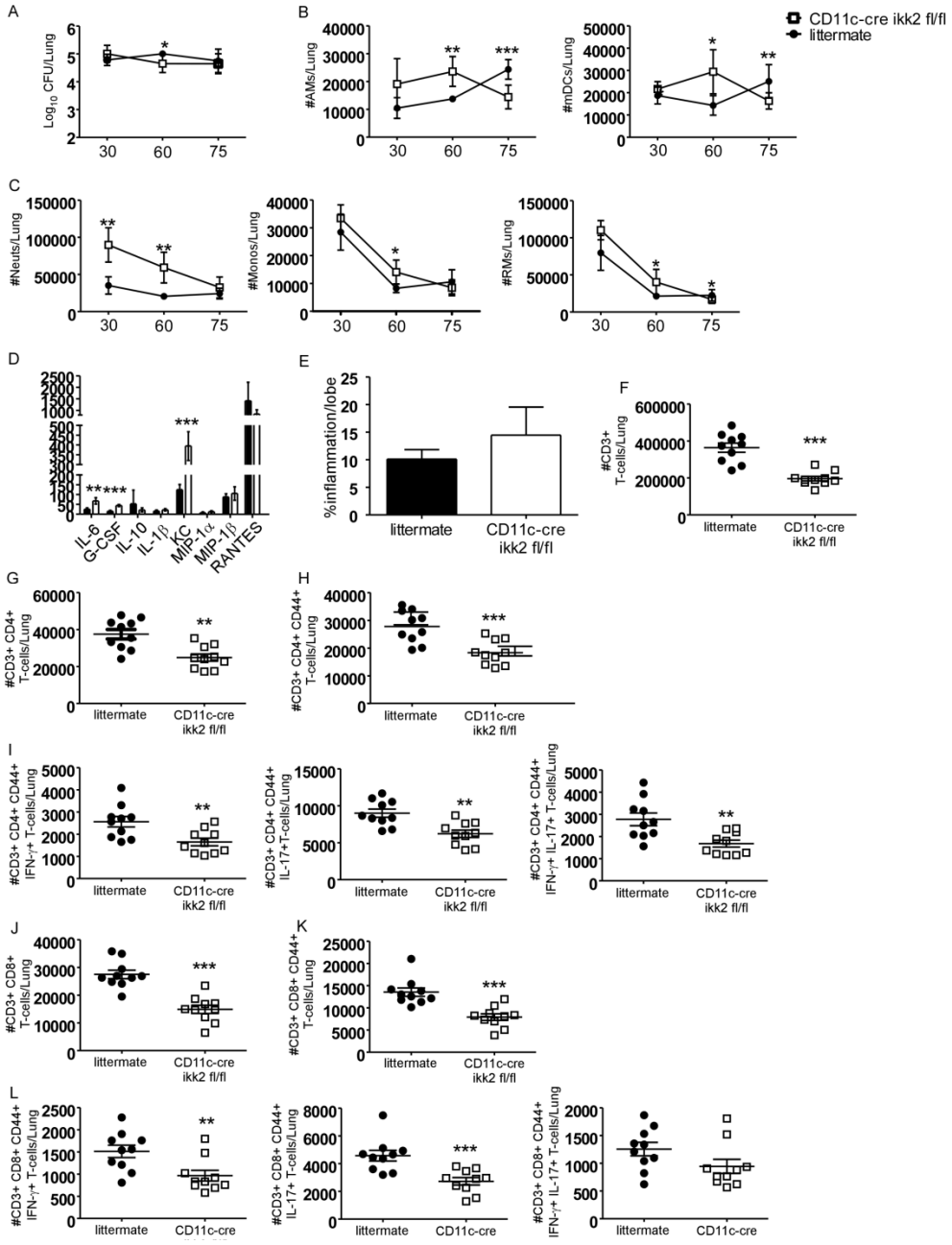

Figure 10: Decreased Iκκ2 in CD11c^{+} phagocytes maintains global decreased *Mtb* burden, increased inflammatory responses at later time points. A) Littermate and CD11c-cre Iκκ2$^{fl/fl}$ mice were aerosol-infected with ~100 CFU of *Mtb* HN878 (n=5-10 mice/group). Bacterial burden in the lung was determined by serial dilution plating at indicated timepoints. B&C) Lung myeloid cell populations were enumerated in littermate and CD11c-cre Iκκ2$^{fl/fl}$ HN878-infected mice using flow cytometry at baseline or indicated d.p.i. D) Whole lung tissue homogenates were analyzed by cytokine multiplex for indicated cytokines at 60 d.p.i. E) Pulmonary histology was assessed on H&E stained FFPE lung sections from 60 d.p.i. infected littermate and CD11c-cre Iκκ2$^{fl/fl}$ mice. F-L) Accumulation of (F)

$CD3^+$ lymphocytes, (G,H) $CD4^+$ or (J,K) $CD8^+$ T-cells expressing CD44 were determined at 75 d.p.i. by flow cytometry (n=10). (I,L) Activated CD44hi $CD4^+$ (I) or $CD8^+$ (L) T-cells producing IFN-γ, IL-17 or both were determined by flow cytometry. Littermate and CD11c-cre $I\kappa\kappa2^{fl/fl}$ mice groups ($n\geq5$) at individual time points were compared using Student's t-test. Mean and standard deviation (SD) were plotted for each group at each indicated time point. *$p<0.05$, **$p<0.01$, ***$p<0.001$.

3.3 Materials and Methods

Mice

C57BL/6J (B6) were purchased from The Jackson Laboratory (Bar Harbor, ME) and bred in house. *Itgax*-cre (CD11c-cre) mice were a kind gift from the Virgin lab at WUSM and bred in house. $I\kappa\kappa2^{fl/fl}$ (ikk2 fl/fl) were sourced and bred in house as previously described.[113,298] All mice were maintained in the animal facility at Washington University in St. Louis and bred in-house. Experimental mice were age and sex matched and infected between the ages of 6 and 8 weeks. All mice were maintained and used in accordance with the approved Washington University in St. Louis Institutional Animal Care and Use Committee (IACUC) guidelines. Both male and female mice were used and to our knowledge no sex-based differences were observed.

Mtb Strains and Experimental Infections

Mtb strains H37Rv (Trudeau Institute), and HN878 were obtained from BEI Resources (Manassas, VA) under National Institutes of Health contract AI-75320 as previously described.[113] H37Rv-GFP and HN878-GFP were transformed with the integrating EGFP expression vector pMV261.kan (provided by Dr. Christina Stallings, Washington University in St. Louis) to generate GFP-expressing *Mtb* as previously described.[113]

Proskauer Beck medium supplemented with 0.05% Tween 80 and frozen at −80 °C while in mid-log phase. Prior to infection, frozen stocks were thawed and placed in a solution of sterile

PBS. Mice were aerosol-infected at tested low doses (~100 CFU) of indicated *Mtb* strains using a Glas-col nebulizer.[310] Mice were monitored and weighed as needed. At the indicated time points mice were sacrificed via carbon dioxide narcosis and lungs and spleens were harvested. *Mtb* CFU/organ was quantitated by plating 10-fold serial dilutions of homogenized lung or spleen tissue on 7H11 agar plates (BD Biosciences, Franklin Lakes, NJ). Plates were incubated for 2–3 weeks at 37 °C and colonies were counted visually.

In Vitro Culture, Stimulation, and Infection

Mouse lung epithelial cell line C10 cells were cultured to confluence in 24 well plates in complete Dulbecco's modified eagle's medium (cDMEM) to confluence for approximately 2 days. Prior to *in vitro* infection hemocytometer counts from a representative well were used to calculate multiplicity of infection (MOI). C10 cells were washed once with sterile PBS and then either stimulated or infected as described previously.[113,192] Briefly, cells were either stimulated with indicated conditioned media or infected with *Mtb* at an MOI of 1 in cDMEM without antibiotics and in both cases incubated at 37°C, 7.5% CO_2 for indicated time points. Supernatants were collected and stored at −80°C. Cells were collected by tryspinization and stained as per manufacturer's protocol.

Primary B6 mouse BMDMs and BMDCs were prepared as previously described.[113,192,310] Briefly, bone marrow was harvested from the femur and tibia of B6 and gene deficient mice were extracted, in a solution of serum free DMEM and then passed through a 70 μm screen, spun down and then resuspended in red blood cell lysis solution. 1×10^7 cells were plated in 10 mL of cDMEM supplemented with 3% (30 ng/mL) mouse recombinant (rm) granulocyte-macrophage colony-stimulating factor (GM-CSF) (Peprotech, Rocky Hill, NJ) for ~7 days total at 37 °C in

5% CO2.[310] On day 3, cultures were supplemented with an additional 10 mL of cDMEM + rmGM-CSF. At harvest, adherent cells were collected as BMDMs, and floating cells were collected as BMDCs, gently washed with cDMEM via centrifugation (1,200 rpm, 6 min at 4°C), resuspended and then plated at 1×10^6 cells per ml.

BMDMs, BMDCs, and C10 epithelial cells were infected with *Mtb* at indicated multiplicity of infection (MOI) in antibiotic-free cDMEM. Cell culture supernatants were collected for analysis of cytokines at indicated timepoints post infection.

Flow Cytometry

Flow cytometry was conducted on single cell preparations derived from infected and uninfected lungs using fluorochrome conjugated antibodies. For distinguishing between airway and non-airway cells, mice received 0.7 µg of BV605-conjugated CD45.2 mAb (Clone 104, BD Biosciences and Biolegend, San Diego, CA), administered i.t. in 50 µL sterile PBS per mouse as described previously.[113] Mice were rested for 15 min following which lungs were harvested. Lung single cell suspensions were prepared as before, [113,192,310] treated with Fc Block (CD16/CD32, 2.4G2, Tonbo Biosciences, San Diego, CA), and stained with appropriate fluorochrome-labeled specific antibodies or isotype control antibodies:

Myeloid antigen presenting cell panel:[113,192] CD11b (M1/70, BD Biosciences and Tonbo Biosciences), CD11c (HL3, BD Biosciences), Gr-1 (RB6-8C5, BD Biosciences), Siglec-F (E50-2440, BD Biosciences), Ly6G (1A8,BD Biosciences), Ly6C (AL-21,BD Biosciences), CD64 (X54-5/7.1,Biolegend), CX3CR1 (SA011F11, Biolegend), MHC-II (M5/114.15.2, Tonbo Biosciences and eBiosciences).

Cells were defined as: AMs: $CD11b^-$, $CD11c^+$, $Siglec\text{-}F^+$, $CD64^+$, and/or $Gr\text{-}1^-$. mDCs:

$CD11b^+$, $CD11c^+$, $MHC\text{-}II^+$. Neutrophils: $CD11b^+$, $CD11c^-$, $Gr\text{-}1^{hi}$. Monocytes: $CD11b^+$ $CD11c^-$ $Gr\text{-}1^{int}$ and/or $Ly6C^+$. Recruited macrophages: $CD11b^+$ $CD11c^-$, $Gr\text{-}1^{lo}$, $CD64^{+/-}$, $Ly6C^{+/-}$, $MHC\text{-}II^{+/-}$.

Activated lymphocyte panel:[21,172] CD3ε (500A2 or 145-2C11, Tonbo Biosciences), CD4 (GK1.5 or RM4-5, BD Biosciences), CD8α (53-6.7, BD Biosciences), CD44 (IM7, eBioscience), IFN-γ (XMG1.2, BD Biosciences) and rat IgG1 (BD Biosciences).

Live, apoptotic, or dead cell panel:[113] Annexin V (PE) and 7-AAD (PerCP-Cy5.5) from the BD Pharmingen Apoptosis Detection kit were utilized and cell percentages were quantified by flow cytometry as per manufacturer's suggested protocol (BD Biosciences). The percentage of cells were defined as live (Annexin V^-, 7-AAD^-), apoptotic (Annexin V^+, 7-AAD^-), and dead (Annexin V^+, 7-AAD^+).

Data collection and analysis were conducted on the BD LSR Fortessa, Fortessa-X20 Cytometers or the FACSJazz Cell Sorter, all with FACS Diva software and post-acquisition analysis conducted on FlowJo.

Western Blotting

Western blot analysis to determine protein content was carried out as previously described.[346] Briefly, whole-cell extracts were prepared using radioimmunoprecipitation assay (RIPA) cell lysis buffer supplemented with PMSF, and other protease and phosphatase inhibitors. Samples were normalized for equal amounts of proteins using a Bicinchoninic acid (BCA) protein assay kit (Thermofisher Scientific, Waltham, MA). Proteins were resolved by electrophoresis on 10% SDS-PAGE and transferred to nitrocellulose membrane (Biorad, Hercules, CA). Membranes were blocked with 5% nonfat milk in TBST buffer and incubated

with Ικκβ (Ικκ2, ikk2) primary antibody (rabbit monoclonal Ικκβ antibody, Cell Signaling Technology, Danvers, MA; 1:500) or the loading control antibody (rabbit polyclonal Gapdh, Thermofisher scientific; 1:1000) overnight at 4C. Peroxidase-conjugated goat anti-rabbit IgG (ThermoFisher Scientific; 1:10,000) was used as a secondary antibody and protein detection was accomplished using the Pierce ECL western blotting detection kit (Thermofisher Scientific). Densitometry was performed on scanned western blots using ImageJ software (NIH, Bethesda, Maryland). The results presented are the mean Ικκβ (Ικκ2) band intensity, relative to control Gapdh band intensity.

Histology

All histological processing, visualization and analysis was performed as previously described.[113,192] Briefly, lung lobes were perfused with 10% neutral buffered formalin and embedded in paraffin. For immunofluorescent staining, formalin-fixed paraffin-embedded (FFPE) lung sections were cut, immersed in xylene to remove paraffin, and then sequentially hydrated in absolute ethanol, 95% ethanol, 70% ethanol, and water. Antigens were unmasked with a DakoCytomation Target Retrieval Solution (Dako, Carpinteria, CA) and nonspecific binding was blocked with 5% (v/v) normal donkey serum and Fc Block (BD Pharmingen, San Jose, CA). Endogenous biotin (Sigma-Aldrich) was neutralized by adding avidin followed by incubation with biotin.

For inflammatory quantification, FFPE lung sections were stained with hematoxylin and eosin (H&E) and inflammatory features/pathology were evaluated by light microscopy. Features were assessed digitally using the automated tool of the Zeiss Axioplan 2 microscope (Carl Zeiss) of H&E stained slides to quantify inflammation and immunofluorescence labeled slides B220,

CD3 and counter stained with DAPI in order to assess lymphoid follicle area.

Cytokine Production Quantification

Cytokine/chemokine production was analyzed in lung homogenates from infected mice or cell culture supernatants via Luminex Multiplex assays (Millipore-Sigma) or indicated ELISA (R&D) as per standard protocol.

Statistical Analysis

Data analysis was conducted in GraphPad Prism 5 (La Jolla, CA) using unpaired two tailed Student's *t*-test for comparison between two groups or one-way analysis of variance for multiple comparisons. Significance is denoted as: $*p < 0.05$, $**p < 0.01$, $***p < 0.001$, not detected, ND.

3.4 Discussion and Conclusions

Even though *Mtb* is the leading cause of infectious disease related deaths worldwide, the initial steps in preventing establishment of pulmonary infection remain poorly understood. A large body of evidence suggests that the innate immune system has the capacity to entirely clear *Mtb* infection in some individuals prior to onset of adaptive immunity.[24,25] Furthermore, recent work to characterize host correlates of protection has implicated innate immunity and early inflammatory responses in the conserved protective response across species.[11,12,14,15,347] Despite this strong evidence in support of early clearance by innate immunity, determining the concise role airway resident AMs and mDCs play in these responses has proven difficult. Depletion of

AMs and mDCs by clodronate liposomes yielded improved disease outcomes during *Mtb* infection, as marked by improved T-cell priming,[100] and decreased pulmonary inflammation, gross lung damage, and total *Mtb* burden.[96] In other studies, transient DTR depletion of AMs and mDCs yielded exacerbated inflammation and more severe *Mtb* burden.[98,99,103-105] These mixed findings reflect the complex nature of balancing inflammation during pulmonary infection, and suggest multiple roles for macrophages during pulmonary infection depending on context.

In this study, we sought to concisely isolate and characterize the contrasting roles of AMs during *Mtb* infection. In previous work we and others found that non-airway localized AMs highly upregulated genes and pathways associated with M1 functions and NF-κB activation.[113,126] We therefore aimed to separate early M1/M2 macrophage polarization and effector functions by targeting NF-κB activation. Furthermore, we sought to determine how these effector roles skew disease severity and mediate both short- and long-term protective responses. In order to model these distinct airway and non-airway signatures, we developed a mouse model targeting Iκκ2 of the NF-κB complex in CD11c expressing AMs and mDCs.

Using this CD11c-cre $I\kappa\kappa2^{fl/fl}$ mouse model to abrogate Iκκ2 in airway phagocytes, we aimed to separate the airway and non-airway phenotypes to concisely determine their contributions to early protective immunity. We found that decreased Iκκ2 activity drove increased inflammatory cytokine production in isolated $CD11c^{+}$ cells. We observed this same hyperinflammatory phenotype at early time points during *in vivo Mtb* infection, which were marked by increased production of inflammatory cytokines and accumulation of innate immune cells at all time points prior to granuloma formation. Indeed, previous studies show a role for Iκκ2 in antagonizing M1 activation,[139,140] and inhibition of NF-κB improves *Mtb* killing *in vitro* in human macrophages.[138] Protective M1 roles are generally attributed to monocyte derived

macrophages recruited from the bone marrow, and AMs are generally regarded as permissive.[67,89,109] Our findings suggest that the CD11c-cre Iκκ2$^{fl/fl}$ model may yield pre-polarized M1 AMs and may be a suitable model for understanding protective early pulmonary responses.

When examining CD11c-cre Iκκ2$^{fl/fl}$ mice *in vivo*, we observed a mixture of phenotypes when compared to the aforementioned depletion models. We found CD11c-cre Iκκ2$^{fl/fl}$ mice to yield decreased *Mtb* burden but increased inflammatory responses and decreased T-cell priming. The differences observed in our model compared to these previous studies are likely due to heightened pro-inflammatory responses driven by NF-κB/Iκκ2 inhibition, which skews towards M1 polarization. While increased M1 polarization yields direct improved killing of *Mtb* by macrophages, it also drives overt inflammation and tissue damage.[139] Furthermore, the timing/nature of depletion and the strain of *Mtb* used likely affects the differential overall outcomes observed.

We found that this hyperinflammation correlated with protection and decreased *Mtb* bacterial burden at most time points examined, even after granuloma formation and induction of adaptive immunity. It is important to note that genetic knockout mouse models rarely yield protective phenotypes during pulmonary *Mtb* infection,[11,348,349] making these findings noteworthy. We found that even at later time points after induction of adaptive immunity, the hyperinflammatory effects of our model were still maintained. We found increased accumulation of innate immune cells and inflammatory cytokines around the time of granuloma formation, as well as later time points.

When we examined recruited lymphocytes, we shockingly observed decreased accumulation of activated CD4$^+$ and CD8$^+$ T-cells at 75 d.p.i. This was contrary to our

hypothesis, as we expected that heightened M1 activity in the model would drive improved T-cell interactions and therefore improved adaptive immunity. It is possible that decreased *Mtb* burden across time points can explain the abrogated T-cell responses we observed. It is also likely that differential effects of the CD11c-cre Iκκ2$^{fl/fl}$ model separately on AMs and mDCs could also play a significant role. While this model drives improved M1 polarization of AMs, it is likely that abrogation of NF-κB in DCs affects cellular migration[137] and expression of costimulatory markers,[350,351] thus abrogating T-cell priming and activation. Indeed, we observed that around half of mDCs remained in the airway through 21 d.p.i. in CD11c-cre Iκκ2$^{fl/fl}$ mice, which was significantly higher than littermate controls. Future work will attempt to further isolate the distinct roles of AMs and mDCs with more specific targeting, so as to prevent confounding effects such as these.

Many factors can alter macrophage phenotype and effector function, suggesting that the M1/M2 dogma should be redefined as more of a spectrum of responses across various contexts.[123,124] Recent findings demonstrate that cellular microenvironment and inflammatory milieu play a key role in determining macrophage polarization, and the timing, context, location, and magnitude of M1/M2 responses can determine overall outcomes.[20,51] taken with previous work, these findings suggest that AMs may play protective roles in some contexts,[25,26] and may not always be permissive as previously thought. Our work further highlights a key role for AM inflammatory signaling throughout infection, not just at the onset of pathogenesis. These data suggest that AMs contribute to host responses and have broad effects on inflammation and host defense, even well after the onset of adaptive immunity. These findings have key implications for our knowledge of bridging innate and adaptive responses and provide support for directing preventative strategies at pulmonary innate immunity.

Taken together, this study suggests that targeting Ikκ2 as a therapeutic approach may have protective effects during pulmonary *Mtb* infection. As reliable drugs are already available to researchers for targeting and abrogating Ikκ2 activity, this approach may prove a promising strategy for priming innate immunity to entirely prevent *Mtb* establishment and infection.

Chapter 4: Examining the role of *Mtb*-specific lipid factors in modulating early lung immune interactions and long-term susceptibility

This chapter is excerpted from the following manuscript:

Dunlap & Prince et al. Formation of lung inducible Bronchus Associated Lymphoid Tissue is regulated by Mycobacterium tuberculosis expressed determinants. *Front Immunol.* (2020) PMID: 31010841

Please refer to the above publication for supplemental data referenced in this chapter

4.1 Introduction

The first interactions between *Mtb* and the host happen in the lung airways immediately after inhalation of *Mtb* bacilli. These early interactions involve AMs,[352] DCs,[103,353] and AECs lining the airway[35,60] and have the potential to drive immune responses. As a result of initiation of immune responses, the tubercle granuloma is formed, which is a hallmark immune structure formed during TB.[179] We have previously shown that protective granulomas that are formed during latent TB are associated with the formation of B-cell containing lymphoid follicles.[172] During severe ATB, granulomas that do not effectively contain *Mtb* are comprised predominantly of neutrophils[190,191] and permissive monocytes,[354] which have been implicated in general tissue destruction, thus skewing responses toward disease progression. Non-protective granulomas are hallmarked by the formation of hypoxic, necrotic cores that do not prevent *Mtb* growth and eventually lead to dissemination to other organs and tissues.[191] The earliest mechanism(s) which determine the nature and outcome of granulomas during infection remains elusive, and are a focus of this work.

In this study, we aimed to determine the *Mtb* and host specific factors that drive the formation of iBALT during TB. To examine the *Mtb* specific factors involved, we utilized an *Mtb* transposon mutant library to screen the induction of lymphoid follicles using the Non-Human Primate (NHP) model of pulmonary TB. This screen allowed us to identify *Mtb* genes which when mutated led to increased induction of iBALT within granulomas. The NHP model exhibits characteristics associated with human TB including the pulmonary cellular and acellular lesions.[355-357] We found an over-representation of *Mtb* cell wall mutants within iBALT containing granulomas and further characterized the role of one such mutant using the mouse model of TB. The *Mmpl7* inner membrane protein is best known for the transport of PDIM to the

free fatty acid layer of the MOM.[226,227] The role of lipid presentation in the MOM is well-documented in modulating various host responses,[265,266,358] suggesting that MOM lipids contact with host cells in the lung plays a role in disease progression.

In light of these observations, we aimed to understand how the *Mtb* Δ*mmpl7* cell wall mutant identified in our screen modulates early epithelial signaling and myeloid recruitment in order to coordinate granuloma structure and the formation of iBALT. In this study we found that in the mouse model, infection with the Δ*mmpl7* mutant drives decreased bacterial burden and increased formation of iBALT, as was observed in NHPs. Furthermore, the Δ*mmpl7* mutant also drove decreased inflammatory cytokine and chemokine production *in vitro* and *in vivo*, along with decreased accumulation of myeloid and lymphoid immune cells. We demonstrate that the Δ*mmpl7* mutant overexpresses diacyl trehaloses (DATs), a *Mtb* cell wall lipid, which can drive the observed decreased inflammatory cytokines and chemokine production by *in vitro* macrophages and also yields increased production of IL-10.

4.2 Results

4.2.1 *Identification of Mtb genes associated with formation of protective lymphoid follicles*

TB granulomas contain distinct iBALT structures which are protective in mice and macaques.[23,172] NHPs infected with *Mtb* exhibit the spectrum of disease severity observed clinically during human TB, with a diverse array of granuloma structures reflected by differences in immune cell recruitment and disease outcome.[355,356] Thus, we used the NHP model to probe the early host-*Mtb* interactions that mediate the signaling events that initiate the induction of iBALT within TB granulomas. NHPs were infected with $1x10^5$ CFU of *Mtb* (H37Rv) mutants

from the himar1 transposon mutagenesis site hybridization (TraSH) library.[359,360] Four to six weeks post-infection, the animals were humanely euthanized due to TB disease. At this time, macaque lungs demonstrated a wide distribution of caseous and follicular granulomatous structures (**Figure 11**), with follicular granulomas featuring prominent cellular structure. In combination with mesodissection, DNA sequencing analysis of separate B cell follicle containing granulomas, seeded by *Mtb* mutants,[361,362] identified nine *Mtb* single mutants that were highly represented within distinct iBALT containing TB granulomas in macaques (**Figure 11 and Table 4**). Of the *Mtb* mutants represented within these "protective" granulomas, two members of the mycobacterial membrane protein large family (*Mmpl2* and *Mmpl7*), were well reflected. *Mmpl2* is a putative inner membrane transporter protein with unknown substrate, while *Mmpl7* is an inner membrane protein associated with PDIM transport to the MOM.[226,227] The NAD dehydrogenase, *NdhA* is a nonessential protein found in the inner mycobacterial membrane associated with NADH mediated electron transfer to the electron transport chain.[363] *EccD5* is an essential inner membrane protein that makes up part of the type VII secretion system, the absence of which results in sensitivity to detergents and killing by macrophage.[364] *ClpB* and *Acr2* are both heat stress molecular chaperones regulated by the alternative sigma factors *SigH* and *SigE*, respectively.[365] Of the two, only *ClpB* is essential for *in vitro* growth. The non-redundant glutamine synthetases *GlnA2* and *GlnA4* are involved in nitrogen metabolism but are not associated with any loss of virulence *in vivo*.[366] *Cmtr* is a cytosolic sensor of cadmium Cd(II) and lead Pb(II)[367,368] which are trace metal contaminants found in the lung (**Table 4**).

Taken together, the *Mtb* transposon screen conducted in NHPs has identified a novel set of *Mtb* genes involved in generation of lymphoid follicles within the lung, that appear to control *Mtb* metabolism and inner membrane lipid transport. In this study, we chose to mainly focus on

the interaction driven by *Mtb Mmpl7* that mediates formation of the granuloma.

Table 4: Identification of *Mtb* genes associated with formation of protective lymphoid follicles	
Mtb genes identified from NHP transposon screen	Putative Function
mmpL2 (Rv0507) 106 kDa	Fatty acid transport
mmpL7 (Rv2942) 95 kDa	Fatty acid transport
ndhA (Rv0392c) 50 kDa	Electron transport
eccD5 (Rv1795) 53 kDa	Type VII secretion (*)
clpB (Rv0384c)	Molecular chaperone (*)
acr2 (Rv0251c)	Molecular chaperone
glnA2 (Rv2222c)	Glutamine biosynthesis
glnA4 (Rv2860c)	Glutamine biosynthesis
cmtR (Rv1994c)	Metal sensor, transcriptional regulator

Table 4: Identification of *Mtb* genes associated with formation of protective lymphoid follicles. Transposon site hybridization library (TraSH) using the himar1 transposon mutagenesis strategy was employed to create a *Mtb* mutant library for the specific discovery of *Mtb* genes influencing the progression of lymphoid follicle containing granulomas in NHPs. NHPs were infected with $1x10^5$ CFU of *Mtb* H37Rv mutants and lung sections were harvested 4-6 weeks after infection. In combination with mesodissection, the analysis of >1,200 lesions identified 9 *Mtb* mutants that were highly represented within protective iBALT containing TB granulomas in macaques. *=essential gene.

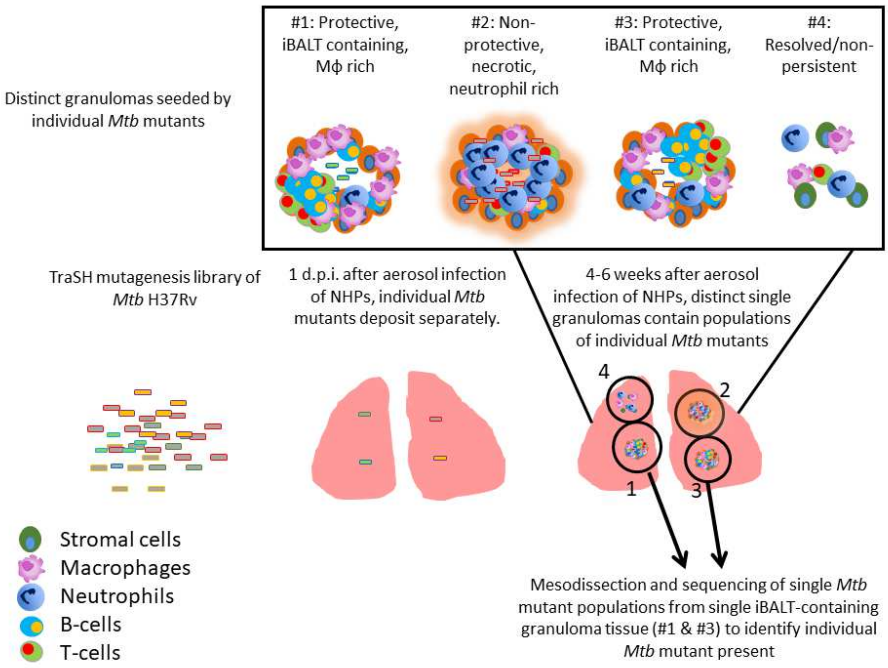

Figure 11: Identification of *Mtb* genes associated with formation of protective lymphoid follicles. Transposon site hybridization library (TraSH) using the himar1 transposon mutagenesis strategy was employed to create a *Mtb* mutant library for the specific discovery of *Mtb* genes influencing the progression of lymphoid follicle containing granulomas in NHPs. NHPs were infected with 100,000 CFU of *Mtb* mutants and lung sections were harvested 4-6 weeks after infection. In combination with mesodissection, the analysis of >1200 separate lesions identified nine *Mtb* single mutants that were highly represented within protective iBALT containing TB granulomas in macaques. Single *Mtb* mutants were isolated from single granulomas.

4.2.2 Δmmpl7 mutant drives Mtb enhanced B cell follicle containing iBALT formation in the mouse model

To determine the functional role of *Mtb Mmpl7* in modulating iBALT generation *in vivo*, we infected B6 with 100 CFU *Mtb* Erdman or the *Δmmpl7* mutant Erdman strain and characterized immune recruitment and induction of iBALT features in the lung. As previously shown, infection with the *Δmmpl7* mutant resulted in early decreased *Mtb* CFU which recovered by 40 d.p.i. in the lung and spleen (**Figure 12A**). At a time when *Mtb* CFU was comparable between the WT and mutant strains, we observed that the total inflammation observed in the lungs of the *Δmmpl7* mutant infected mice was significantly decreased (**Figure 12B-C**).

However, despite significantly decreased overall inflammation, infection with the *Δmmpl7* mutant resulted in increased formation of B cell lymphoid follicle containing area, reflecting iBALT areas (**Figure 12D-E**). Furthermore, by 40 d.p.i., T-cells were well able to infiltrate within iBALT containing granulomas, as the area of T cell cuffing around the granulomas was decreased in *Δmmpl7* mutant infected mice (**Figure 12D-E**). Together, these findings suggest that *Mtb* lacking the *Mmpl7* gene induces improved induction of iBALT and decreased inflammation, suggesting that *Mtb* actively shuts down iBALT formation utilizing virulence factors such as PDIM, or alternatively, the reduced early *Mtb* growth in the *Mmpl7* mutant in vivo propagates iBALT containing granulomas.

It has been shown previously that the *Δmmpl7* mutant lacks the ability to transport PDIMs, an important Mtb structural lipid and virulence factor, to the MOM, leading to an early growth defect *in vivo* when mice are infected intravenously.[226,227] Thus, to specifically address if the early decrease in *Mtb* CFU burden in the mutant infection was responsible for increased iBALT formation, we infected mice with a 5-fold higher dose (500 CFU) of *Mtb Δmmpl7* to directly compare the ability of *Δmmpl7* mutant to induce iBALT when compared to low dose (100 CFU) infection with wildtype (WT) *Mtb* Erdman (**Supplemental Figure 6, Appendix**). Using the higher dose model, our data show that *Δmmpl7* mutant still had early defects in *Mtb* CFU *in vivo* in the lung and spleen as previously shown, but at 40 d.p.i. showed comparable CFU to WT *Mtb* and similar overall inflammation (**Supplemental Figure 6A-B, Appendix**). Importantly, the higher dose model maintained the observed increased iBALT formation (**Supplemental Figure 6C, Appendix**). Whether this phenotype was due partially or entirely to the lack of PDIMs on the MOM or due to other changes in the *Δmmpl7* mutant was further evaluated in this study.

Furthermore, by 40 d.p.i., no differences in bacterial burden were observed in the lung or spleen between WT Erdman and *Δmmpl7* mutant, which is more likely due to increased control of WT Erdman while *Δmmpl7* mutant CFU levels were maintained. These findings demonstrate that our 5-fold higher CFU dose aerosol infection used to compensate for the growth defect in the *Δmmpl7* mutant still recapitulates the *in vivo* phenotype observed with low dose infection. These data suggest that the observed phenotype of increased iBALT formation in the *Δmmpl7* mutant infection is likely not an artifact of abrogated *Mtb* growth.

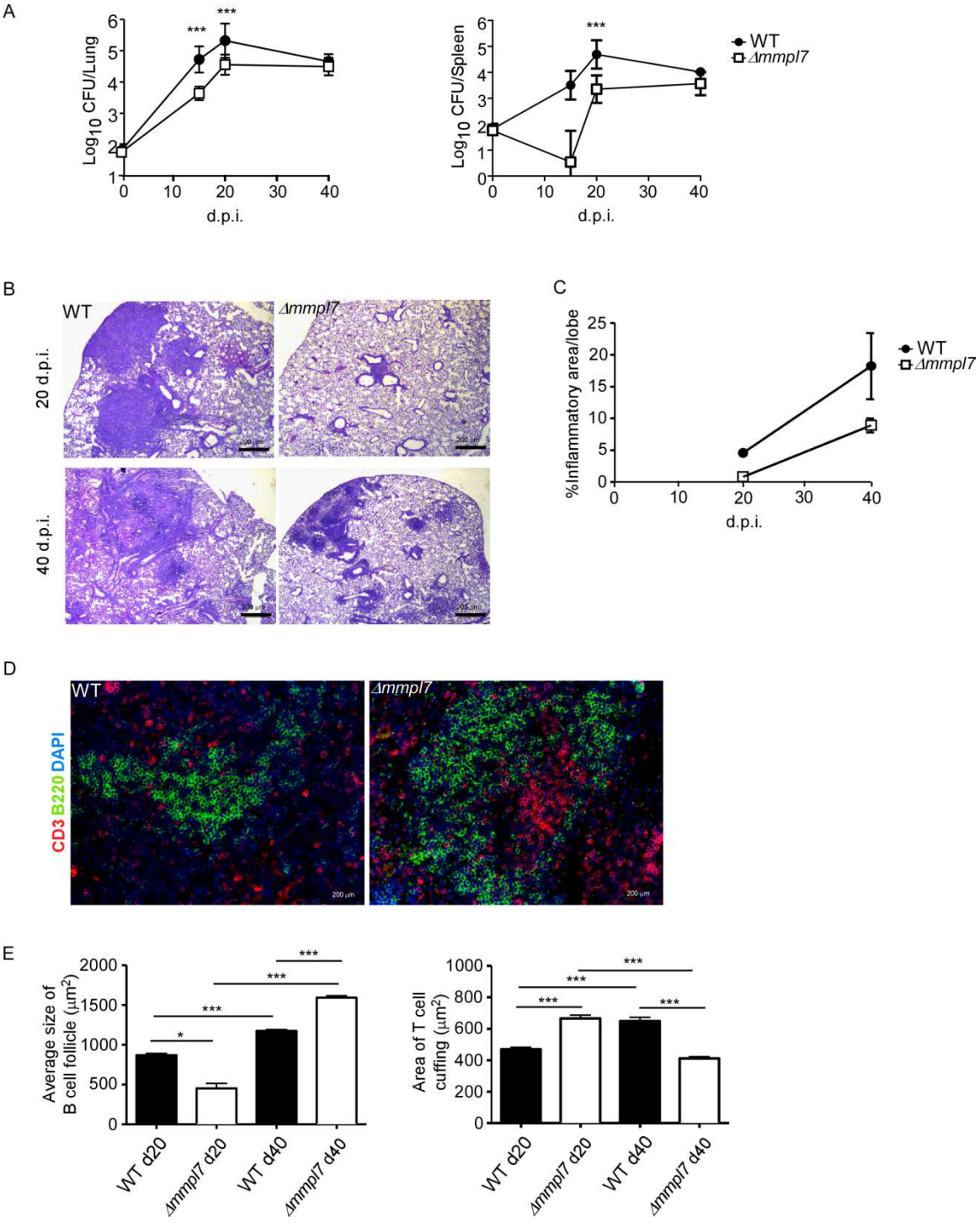

Figure 12: *Δmmpl7* mutant drives *Mtb* enhanced B cell follicle formation in mouse model. Sex and age matched C57BL/6 mice were infected with 100 CFU of *Mtb* Erdman WT or *Δmmpl7*. A) Lung and spleen homogenates were used to determine *Mtb* CFU counts at indicated time points. B-C) Lungs from *Mtb*-infected mice at 20 (top) and 40 (bottom) d.p.i. were formalin fixed, embedded in paraffin and used for H&E staining and inflammation was quantified by tracing areas. D-E) B cell follicles present within lung sections were visualized by confocal microscopy. Slides were visualized and quantified by outlining the lesions using the automated tool of the Zeiss Axioplan 2 microscope. Infected groups (n≥5) comparing WT Erdman and *Δmmpl7 Mtb* strains at individual time points were compared using

Student's t-test. Mean and standard deviation (SD) were plotted for each group at each indicated time point. *p<0.05, **p<0.01, ***p<0.001.

4.2.3 Δmmpl7 mutant Mtb limits early myeloid cell accumulation in the Mtb-infected lung

To examine the early immune events that occur in the lung that mediate differences in iBALT formation, we infected mice with 100 CFU wildtype *Mtb* Erdman or 5-fold higher CFU (500 CFU) of the *Δmmpl7* mutant and characterized myeloid and T cell accumulation in the lung. Upon infection with the *Δmmpl7* mutant, we observed decreased neutrophils, monocytes and RMs at early time points as well as decreased accumulation of AMs and mDCs when compared with accumulation in WT *Mtb* infected lungs (**Figure 13A-B**). We saw similar decreases in accumulation of total $CD3^+$ T-cells (**Figure 13C**), activated and IFN-γ producing $CD4^+$ (**Figure 13D**) and $CD8^+$ T-cells (**Figure 13E**) at later time points.

These cellular changes coincided with early decreased production of inflammatory cytokines, such as IL-6, G-CSF and IL-17, and chemokines, such as MIP-2 (CXCL2), and IP-10 (CXCL10) that are associated with myeloid recruitment in *Mtb Δmmpl7* infected mice, (**Figure 13F-J**). Interestingly, this coincided with an early increased induction of IL-10 at 15 d.p.i., though this effect was abolished by the later time points (**Figure 13K**). As IL-10 is a known mediator of anti-inflammatory responses,[162,369] these findings suggest a potential mechanism for the decrease in pro-inflammatory cytokines and lung inflammation. Taken together, these data demonstrate an overall "dampening" of the immune response during early infection with the *Δmmpl7* mutant, suggesting that decreased inflammation and decreased neutrophilia may improve the formation of protective iBALT containing granulomas, thus improving TB disease.

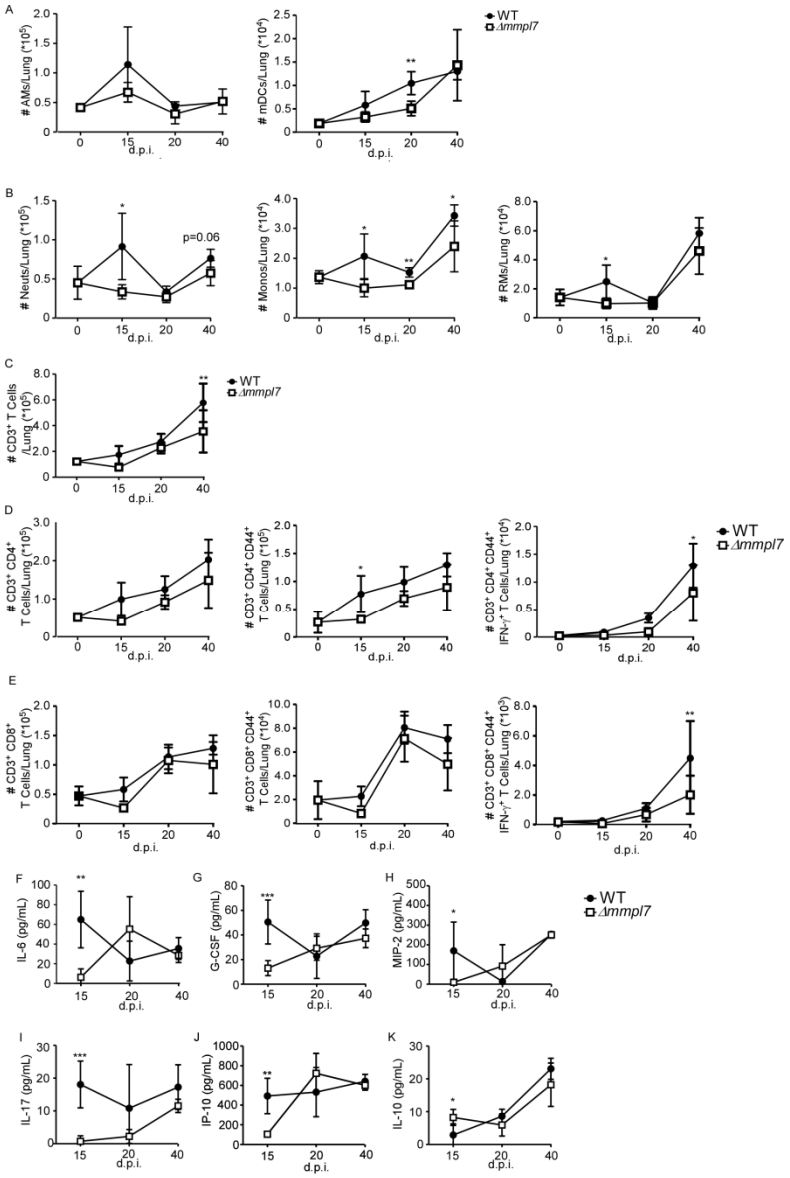

Figure 13: *Δmmpl7* mutant *Mtb* limits myeloid cell accumulation in the lung. Sex and age matched C57BL/6 mice were infected with 100 CFU *Mtb* Erdman WT or 500 CFU *Δmmpl7*. Single cell suspensions were processed from infected lungs and immune cell subsets were analyzed by flow cytometry. A) tissue resident myeloid and B) recruited myeloid cell accumulation in the *Mtb*-infected lungs was determined at indicated time points. C) $CD3^+$ lymphocytes, D) $CD4^+$ or E) $CD8^+$ T-cells were determined using flow cytometry. F-K) Protein levels of inflammatory cytokine and chemokines IL-6, G-CSF, MIP-2(CXCL2), IL-17, IP-10 (CXCL10), and IL-10 were determined in lung homogenates at indicated time points. Infected groups (n=5) comparing WT Erdman and *Δmmpl7 Mtb* strains at individual time points were compared using Student's t-test. Individual time points within the same group were compared using 2-way ANOVA with Bonferroni post-tests. Mean and standard deviation (SD) were plotted for each group at each indicated time point. *p<0.05, **p<0.01, ***p<0.001.

4.2.4 Δmmpl7 mutant Mtb overexpresses DATs and limits cytokine production in lung epithelial cells

Having observed abrogated recruitment of myeloid cells after infection with the *Mtb Δmmpl7* mutant and decreased cytokine/chemokine production *in vivo* (**Figure 13**), we hypothesized that the *Δmmpl7* mutant was specifically modulating inflammatory molecule production and subsequent recruitment of immune cells. Increased early IL-10 production and decreased neutrophilia and inflammation observed after infection with the *Δmmpl7* mutant likely skewed the immune response towards protective iBALT containing granulomas. Alternatively, increased neutrophil accumulation and increased pro-inflammatory cytokines, including G-CSF and IL-6, are induced in response to WT *Mtb* infection and drive non-protective, necrotic granulomas.[190,191,370]

To address if G-CSF was a marker of ATB disease in humans, we measured levels in individuals with ATB or LTBI in two human cohorts. We observed that G-CSF production was increased in ATB individuals when compared with LTBI or house contacts (HCs) (**Figure 14A**). Furthermore, it was previously demonstrated that individuals with ATB also have increased serum levels of IL-6.[371,372] As such, both G-CSF and IL-6 were used as cytokine indicators of inflammatory response severity for the remainder of this study.

To further test this hypothesis in our model, we examined mouse lung epithelial cells *in vitro*, which are a key source of G-CSF, and other inflammatory cytokines in the context of lung infection.[34-36,52,60,190,299,373] We assayed epithelial cell derived G-CSF production *in vitro* after infection with either WT *Mtb* Erdman or *Δmmpl7* mutant. Firstly, we found that epithelial cells infected with WT *Mtb* induced significant G-CSF in a time-dependent manner. In contrast, infection of epithelial cells with *Δmmpl7* mutant resulted in significantly decreased G-CSF production when compared to WT Erdman infection (**Figure 14B**). When performing

coinfection with varying ratios of WT Erdman and *Δmmpl7* mutant, we observed that even 3 times the presence of WT Mtb did not reverse the abrogated G-CSF production observed upon *Δmmpl7* mutant infection (**Figure 14C**). Furthermore, we observed a significant decrease in G-CSF production even when WT Erdman infected epithelial cells were co-administered heat-killed (HK) *Δmmpl7* mutant, suggesting that the inhibition of G-CSF was dependent on a factor expressed by *Mtb Δmmpl7* and did not depend on the viability or infectivity of the bacteria (**Figure 14D**). These data together suggest that a molecular factor present in the *Δmmpl7* mutant is likely limiting G-CSF expression *in vitro* and *in vivo*.

From these data, we hypothesized that a lack of *Mmpl7* in *Mtb* led to changes in the lipid profile of the MOM beyond the reported loss of PDIMs,[226,227,268] thus inducing the presence of other lipids and virulence factors than those present on WT *Mtb* Erdman.[201,374] We hypothesized that these lipids may decrease the production of G-CSF, IL-6 and other inflammatory cytokines, thus driving decreased myeloid recruitment and increased iBALT formation upon infection. To test this, we freshly grew *Mtb* WT and *Δmmpl7* mutant bacteria three independent times, normalized by bacteria weight, and extracted and characterized their total lipid content by 1 and 2 dimensional thin layer chromatography (1D or 2D TLC) (**Figure 14E and Supplemental Figure 7, Appendix**), using different solvents systems allowing us to fully screen the wide range of lipids present on the mycobacterial cell envelope. We found that while SLs, TDMs, and TMMs were present at similar levels, DATs were expressed at higher levels in the cell envelope of the *Δmmpl7* mutant *Mtb* (11.5% of total lipid) when compared to WT Erdman (6.8% of total lipid) (**Figure 14E and Supplemental Figure 7, Appendix, black arrows**). DATs are heterogeneous glycolipids (>30 molecular species described) composed of a trehalose sugar structure with two acyl chains, where the trehalose moiety is thought to bind to the macrophage-

inducible C-type lectin Mincle.[262-264] DATs have been previously shown to negatively regulate the pro-inflammatory response of the host, thus promoting *Mtb* survival.[265,266] Thus, these findings suggested that increased presence of DATs in the *Δmmpl7* mutant could be linked to the decreased production of inflammatory molecules like G-CSF and IL-6 and the dampened pulmonary inflammatory response observed *in vitro* and *in vivo*.[265]

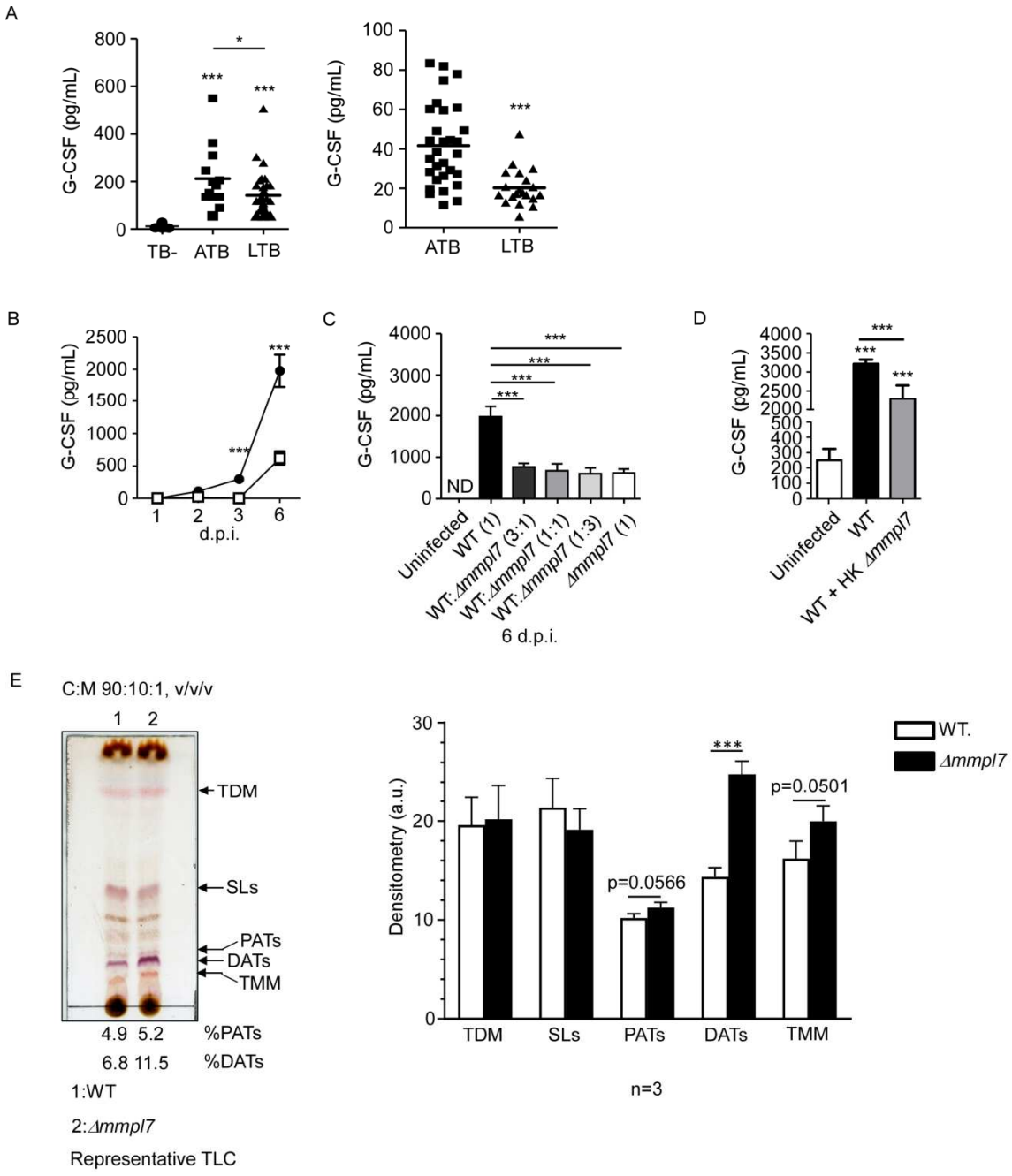

Figure 14: *Δmmpl7* mutant *Mtb* overexpresses DATs and limits cytokine production in lung epithelial cells. A) Serum samples from human active TB patients and controls (Left Panel: Mexico (TB- n=30; ATB n=13; LTB n=33), Right Panel: South Africa (ATB n=30; LTB n=20) were analyzed for G-CSF levels. Mouse lung epithelial cells (n≥4 per group) were infected with *Mtb* Erdman WT or *Δmmpl7* at B) MOI=1 or MOI=5, respectively, for indicated time points. C) Mouse lung epithelial cells (n=4) were infected with *Mtb* Erdman WT and/or *Δmmpl7* at indicated ratios for a constant total MOI=1. D) Mouse lung epithelial cells (n=4) were infected with *Mtb* Erdman WT with or without the addition of heat-killed (HK) *Δmmpl7*. A-D) Supernatants were collected and G-CSF concentration was quantified by ELISA. E) Total lipids from *Mtb* Erdman WT or *Δmmpl7* were obtained from freshly grown bacteria (3 independent times) and extracted with chloroform:methanol (2:1, v/v/) after normalization by total bacterial number. Total lipids (100 mg) were analyzed by TLC using as a solvent system (chloroform:methanol:water, 90:10:1, v/v/v) and 10% sulfuric acid in ethanol as a developer to visualize total lipid contents (representative experiment shown).

Densitometry analyses of the observed lipids were performed using the NIH software ImageJ, n=3 (where each value corresponds to independent extractions from freshly grown bacteria and TLCs). Human cohort study groups were compared by 1-way ANOVA with Tukey's post-test, or unpaired Student's t-test, respectively. Infected groups comparing WT Erdman and *Δmmpl7 Mtb* strains under indicated conditions at individual time points were compared using 1-way ANOVA with Tukey's post-test or unpaired Student's t-test. TLC densitometry was analyzed by unpaired Student's t-test. *p<0.05, **p<0.01, ***p<0.001.

4.2.5 DAT administration drives decreased inflammatory molecule production in epithelial and myeloid cells.

We next hypothesized that the increased expression of DATs could abrogate production of cytokines, especially G-CSF, in epithelial cells,[60,375] similar to what we observed with infection with the *Δmmpl7* mutant. To demonstrate this, we infected lung epithelial cells with *Mtb* Erdman and co-treated them with DATs. Our results show that co-treatment with DATs limited the production of G-CSF and IL-6 by WT *Mtb* infected epithelial cells (**Figure 15A**), similar to the responses observed when *Δmmpl7* mutant single infection and coinfections were carried out (**Figure 14**). Additionally, the inhibitory effect observed was dose dependent, thus confirming that the overexpression of DATs was one factor that was skewing the induction of cytokines upon infection with the *Δmmpl7* mutant. This effect was likely not due to DAT-induced cell death, as levels of total live, apoptotic, and dead cells were only slightly altered after addition of DATs (**Supplemental Figure 8A, Appendix**). IL-10 production within this culture was below the limits of detection of the assay for all groups, even with addition of DATs, thus suggesting that epithelial cells are likely not a significant source of anti-inflammatory signals in this phenomenon.

We next aimed to determine if this phenotype was specific to epithelial cells or if the *Δmmpl7* mutant also regulated cytokine expression in myeloid phagocytes, and if the presence of DATs modulated these responses as previously shown.[265] Therefore, we infected macrophages and DCs with WT and *Δmmpl7* mutant (**Figure 15B-E**). We found that while *Δmmpl7* mutant

abrogated IL-1β and IL-6 expression in both macrophages and DCs (**Figure 15C,E**), the *Δmmpl7* mutant surprisingly induced increased IL-10 expression in both cell types when compared to WT *Mtb* (**Figure 15B,D**). Furthermore, no differences in cell death were observed between WT *Mtb* and the *Δmmpl7* mutant (**Supplemental Figure 8B-C, Appendix**), thus suggesting that this finding is due to specific regulation of cytokine production, not apoptosis induced abrogation. The decreased production of IL-1β and IL-6 in phagocytes was likely not only due to active inhibition by DAT alone, as co-treatment with DAT-coated beads did not decrease production of these cytokines during WT infection when compared to control beads. However, in BMDMs the increased induction of IL-10 driven by the *Δmmpl7* mutant *Mtb* over WT Erdman was recapitulated by addition of DATs to WT Erdman infection (**Figure 15B**), thus suggesting that DAT overexpression on *Δmmpl7* mutant *Mtb* actively induced expression of anti-inflammatory IL-10 produced by macrophages. The increased production of anti-inflammatory IL-10 by lung macrophages may explain the early increased IL-10 observed *in vivo* in lung homogenates. These early anti-inflammatory signals may abrogate the production of inflammatory cytokines and pulmonary neutrophilia, thus skewing the immune response away from neutrophil rich, non-protective granulomas, and towards iBALT containing protective granulomas.

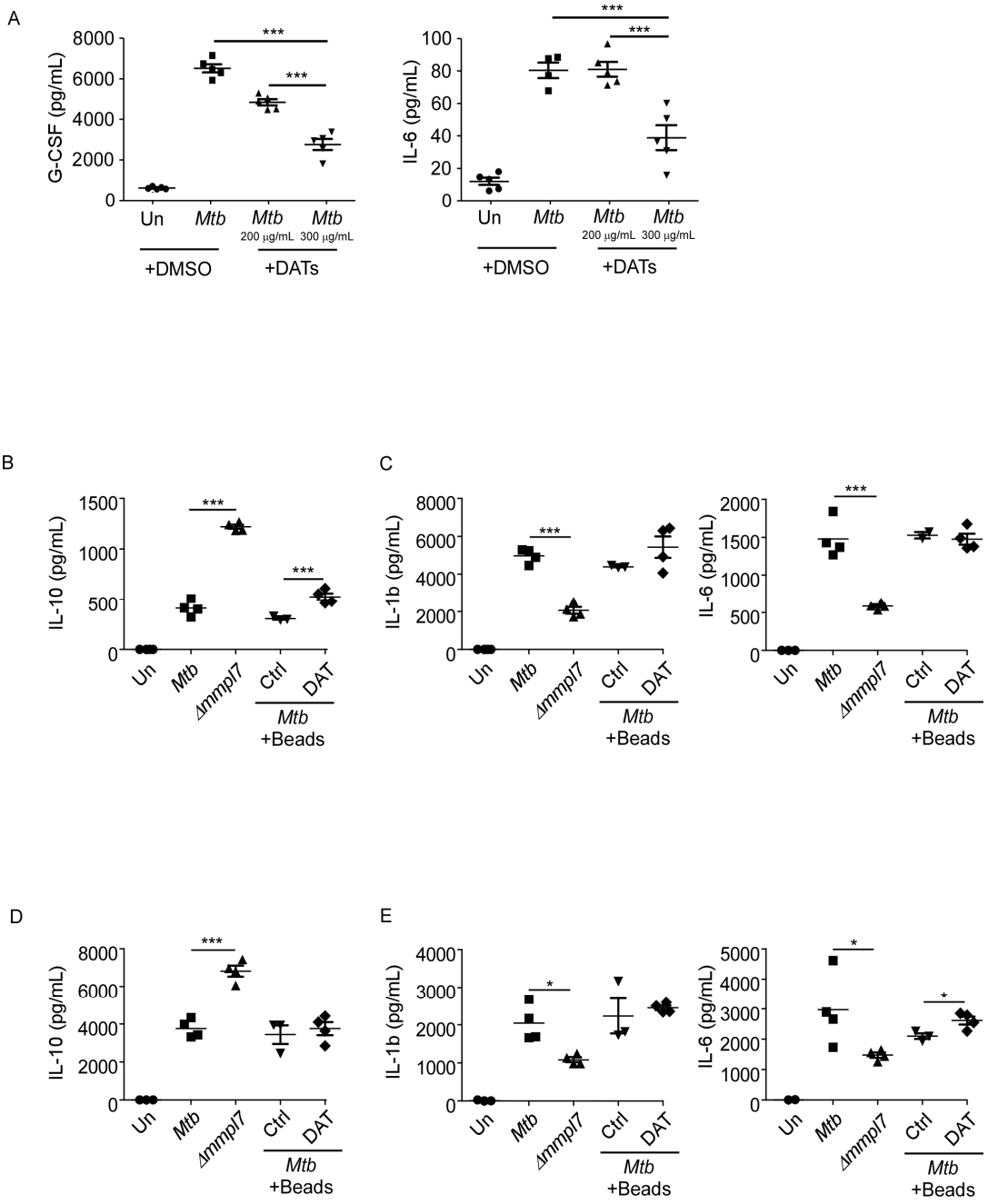

Figure 15: DAT administration drives decreased inflammatory molecule production in epithelial and myeloid cells. A) Mouse lung epithelial cells (n=5) were infected with *Mtb* Erdman WT with or without the addition of raw DATs at MOI=1 for 6 days. Mouse bone-marrow derived B-C) macrophages (BMDMs) (n=5) or D-E) dendritic cells (BMDCs) (n=5) were infected with *Mtb* Erdman WT with or without the addition of DAT coated agarose beads, or *Δmmpl7* for 3 days. Supernatants were collected and the concentrations of cytokines G-CSF, IL-6, IL-1β and IL-10 were quantified by multiplex assays. Multiple groups were compared by 1-way ANOVA with Tukey's post-tests. *p<0.05, **p<0.01, ***p<0.001.

4.3 Materials and Methods

Non-Human Primate Infection

An *Mtb* (H37Rv) transposon site hybridization mutants (TraSH) library (kind gift of Dr. Chris Sassetti) was delivered high dose (≥100,000) CFU via bronchoscopic procedure into the lungs of triplicate Indian rhesus macaques. Delivery of bacteria to the lower lungs was confirmed via dilution plating and *Mtb* infection was confirmed by direct observation of the clinical signs of TB and concurrent positive tuberculin skin test. NHPs were humanely euthanized after being held 4–6 weeks due to development of disease using prespecified criteria.[187,376,377] Lungs from infected animals were harvested and processed for mesodissection as previously described.[378,379] Briefly, lung sections were removed, formalin fixed and paraffin embedded. A series of unstained and H&E slides were then made and used with the mesodissection instrument and 2iD Imaging software. The H&E guide slide is used to direct the consumable mill bit to dissect the unstained slide and harvest the nuclear material for downstream upscaling and identification. By staining of B cells, iBALT associated lesions were first identified. The appropriate sections from H&E slides were then dissected and used for sequencing as previously described[380] to identify the single *Mtb* mutant associated with each individual lesion.[361,362]

Mice

B6 mice used were 6–8 weeks old and sex matched. All treatments and conditions used to handle study animals are in accordance with the approved Institutional Animal Care and Use Committee (IACUC) guidelines at Washington University in St. Louis.

Bacterial Strains, Infection and Instillation

Mtb (Erdman) and Δ*mmpl7* mutant (MJM39)[226] were stocked in Proskauer-Beck with 0.05% tween 80 and stored at −80°C. Prior to infection, frozen stocks were thawed and placed in a solution of sterile PBS for loading into the Glas-col nebulizer. Mice were infected with aerosolized *Mtb* in the above Glas-col nebulizer at tested doses of ~100 CFU (low) or ~500 CFU (5-fold higher) of *Mtb* per mouse. At the indicated time points mice were sacrificed via carbon dioxide narcosis and lungs and spleens were harvested.

Microscopy and Inflammation, B Cell Quantification

Lung pathology from formalin fixed paraffin embedded lungs was assessed digitally using the automated tool of the Zeiss Axioplan 2 microscope (Carl Zeiss) of H&E stained slides to quantify inflammation and immunofluorescence labeled slides B220, CD3 and counter stained with DAPI in order to assess lymphoid follicle area.

Bacterial Culture and Cytokine Analysis

Bacterial burden was assessed using serial 10-fold dilutions of lung or spleen and plated on 7H11 supplemented with OADC (oleic acid, bovine albumin, dextrose, and catalase). After 2–3 weeks incubation colonies were counted visually. Cytokine/chemokine expression was analyzed in lung homogenates from infected mice via Luminex (Millipore-Sigma) or ELISA (R&D).

Flow Cytometry

Flow cytometry was conducted on single cell preparations derived from infected and uninfected lungs using fluorochrome conjugated antibodies:

Myeloid antigen presenting cell panel[113] : CD11b (M1/70), CD11c (HL3), Gr-1 (RB6-8C5), Siglec-F (E50-2440), Ly6G (1A8), Ly6C (AL-21), CD64 (X54-5/7.1), MHC-II (M5/114.15.2). Cells were defined as: AMs: $CD11b^{-}$, $CD11c^{+}$, $Siglec\text{-}F^{+}$, $CD64^{+}$. mDCs: $CD11b^{+}CD11c^{+}$, $MHC\text{-}II^{+}$. Neutrophils: $CD11b^{+}$, $CD11c^{-}$, $Gr\text{-}1^{hi}$. Monocytes: $CD11b^{+}$ $CD11c^{-}$ $Gr\text{-}1^{int}$ and/or $Ly6C^{+}$. Recruited macrophages: $CD11b^{+}$ $CD11c^{-}$, $Gr\text{-}1^{lo}$, $CD64^{+/-}$, $Ly6C^{+/-}$, $MHC\text{-}II^{+/-}$.

Activated lymphocyte panel[21,172]: CD3ε (500A2), CD4 (RM4-5), CB8α (53-6.7), CD44 (IM7), IFN-γ (XMG1.2).

Live, apoptotic, or dead cell panel[113]: Annexin V (PE) and 7-AAD (PerCP-Cy5.5) from the BD Pharmingen Apoptosis Detection kit were utilized and cell percentages were quantified by flow cytometry as per manufacturer's suggested protocol (BD Biosciences). The percentage of cells were defined as live (Annexin V^{-}, $7\text{-}AAD^{-}$), apoptotic (Annexin V^{+}, $7\text{-}AAD^{-}$), and dead (Annexin V^{+}, $7\text{-}AAD^{+}$).

Data collection and analysis were conducted on the BD LSR Fortessa, Fortessa-X20 Cytometers or the FACSJazz Cell Sorter, all with FACS Diva software and post-acquisition analysis conducted on FlowJo.

Human Serum Collection and Analysis

Human samples were collected on approval from the Ethics Committee of the National Institute for Respiratory Diseases, KwaZulu-Natal Research Institute for TB and HIV, Durban, South Africa; and The American British Cowdray Medical Center, Mexico City, Mexico on a protocol approved by the Ethics Committee of the National Institute for Respiratory Diseases (INER), KwaZulu-Natal Research Institute for TB and HIV (Currently renamed AHRI), South

Africa and The American British Cowdray Medical Center. All subjects were of similar socioeconomic status and unrelated to the third generation as determined by a questionnaire. TB cases had symptoms (weight loss >10 kg, cough, fever, night sweats for >1 month, or cervical or axillary lymphadenopathy) and chest radiographic findings consistent with recent pulmonary TB, a positive sputum acid-fast smear and culture confirmed for *Mtb*. Fresh blood samples from active pulmonary TB patients were obtained from patients recruited to the Tuberculosis Outpatient Clinic, INER, Mexico, or the KwaZulu-Natal Research Institute for TB and HIV, South Africa. Serum samples from all patients with active TB were collected prior to anti-*Mtb* treatment and did not present comorbidities such as diabetes, HIV, cancer, and COPD. LTBI patients were defined as asymptomatic individuals who had positive IGRA test results as previously described.[191] We simultaneously recruited a group of HCs and these individuals were negative for IGRA tests at collection sites.

In Vitro Culture, Isolation, Stimulation, and Infection

Mouse lung epithelial cell line C10 cells were cultured to confluence in 24 well plates in DMEM. Prior to *in vitro* infection hemocytometer counts from a representative well were used to calculate multiplicity of infection (MOI). C10 cells were washed once with sterile PBS and then infected with *Mtb* or *Mtb* mutant at an MOI of 1 in DMEM without antibiotics and incubated at 37°C, 7.5% CO2. Supernatants from the infection was collected and stored at −80°C. Cells were collected by tryspinization and stained as per manufacturer's protocol.

Primary B6 mouse BMDMs and BMDCs were prepared as previously described.[113] Briefly, bone marrow was harvested in a solution of serum free DMEM and then passed through a 70 μm screen, spun down and then resuspended in red blood cell lysis solution. Equal volume

of cDMEM was added and again spun down. The single cell suspension was plated at 1×10^6 cells per ml and supplemented with 4% GM-CSF for 7 days. At harvest, adherent cells were collected as BMDMs, and floating cells were collected as BMDCs, gently washed with CDMEM via centrifugation (1,200 rpm, 6 min at 4°C), resuspended and then plated at 1×10^6 cells per ml.

Indicated cell types were stimulated with either DATs resuspended in DMSO, or BSA-control or DAT-coated beads suspended in PBS as indicated at 200 μg/mL. Briefly, beads (1.5×10^9 Polybead polystyrene beads) were washed twice in 0.05 M carbonate-bicarbonate buffer (pH 9.6) and then incubated with 50 μg of DATs or buffer alone for 1 h at 37°C. Beads were then blocked with 5% BSA, washed repeatedly in 0.5% BSA, and finally adjusted to 4.0×10^8/ml in 0.5% BSA before being used. [388]

Lipid Extraction and Analysis

Mtb bacterial pellets normalized by bacterial numbers (counted by microscopy, 1×10^{10}) were extracted with chloroform:methanol (2:1, v/v) following the previously published method.[358] Dried total lipids extracts were analyzed (loaded 100 μg by weight) by thin layer chromatography using chloroform:methanol:water (90:10:1, v/v/v) as the mobile phase, and 10% sulfuric acid in ethanol as a developer as described.[381] Densitometry using NIH ImageJ software was used to quantify all the spots/lipids per lane in each TLC, and to calculate the percentage of total DATs and total PATs per lane. Densitometry analyses of each spot/lipids were also calculated as using NIH ImageJ software ($n = 3$, where each value corresponds to independent extractions and TLCs). DATs were purified by preparative TLC as previously described for other *Mtb* cell envelope lipids,[381] and used for *in vitro* studies at the indicated concentrations, resuspended in DMSO.

Statistical Analysis

Data analysis was conducted in GraphPad Prism 5 (La Jolla, CA) using unpaired two tailed Student's *t*-test for comparison between two groups or one-way analysis of variance for multiple comparisons. Significance is denoted as: $*p < 0.05$, $**p < 0.01$, $***p < 0.001$, not detected, ND.

4.4 Discussion and Conclusions

Although pulmonary *Mtb* infection is the leading cause of death by an infectious agent worldwide, the initial steps in pathogenesis that govern the induction of iBALT formation within granulomas remain unknown. In this study, using a transposon library in the NHP pulmonary infection model, we have identified *Mtb* drivers of B cell-containing iBALT formation. Our work here demonstrates that murine infection with the Δ*mmpl7* mutant induces increased iBALT formation by dampening early innate immune responses. The Δ*mmpl7* mutant overexpressed DATs in the cell wall, which drove abrogated inflammatory molecule production and increased IL-10 in the lung, thus leading to decreased cellular recruitment. This study provides novel evidence for a critical role for *Mtb* specific factors in skewing the earliest host pathogen interactions that drive protective or detrimental disease outcomes.

Although significant advances have been made in understanding the factors that aid in the intracellular survival of *Mtb* and their potential as therapeutic targets using *in vitro* approaches and the mouse model, it is unclear if these factors play important roles in human tubercle formation. Furthermore, most physiological events cannot be modeled by targeting a single gene or its substrates, as interaction and/or compensation among several genes/pathways underpin complex outcomes. Thus, in this study we have examined the *Mtb* determinants that mediate

granulomas by using the well-established preclinical model of NHP TB infection. The macaque model replicates many facets of clinically observed *Mtb* infection, thus providing relevance to identification of *Mtb* determinants that drive or limit granuloma and iBALT formation. By infecting NHPs with an *Mtb* mutant transposon library we have identified a novel subset of *Mtb* genes associated with protective iBALT containing granulomas that correspond with effective *Mtb* control. Although the gene subsets identified using this approach did not fall into any specific pathway, they were interrelated in that they were predominantly involved in mycobacterial growth and survival via responses to stress (*Acr2, ClpB, Gln4, NdhA*, and *Cmtr*) or the synthesis/translocation of virulence components including lipids and proteins (*Mmpl2, Mmpl7, EccD5*).

Among the two heat stress molecular chaperones identified in our study *ClpB* has already been established as essential for the *in vitro* growth of *Mtb*,[365] however the importance of *Acr2* is yet to be established. *Acr2* is the most up-regulated gene following phagocytosis of *Mtb* by macrophages[365,382] and is under the control of the master regulator *PhoP*.[383] Wilkinson et al. found that *Acr2* was strongly expressed in response to heat shock protein (HSP) *Rv0251c* and appears to play a role in early immune responses.[384] HSPs assist in *Mtb* survival but also act as signaling agents to the host inflammatory mechanisms. While the role of *Acr2* in *Mtb* virulence in humans is not clear, it remains essential for virulence in a murine model of TB.[384] To our knowledge this is the first study to report on the association of absence of *Acr2* with protective granulomas in the NHP model.

Until recently *NdhA* was considered a non-essential protein found in the inner mycobacterial membrane associated with nicotinamide adenine dinucleotide (NADH) mediated electron transfer to the electron transport chain.[363] Recent studies by Vilcheze et al. concluded

that when *NdhA* is the only type I NADH dehydrogenase present in *Mtb* it affects *Mtb* growth and renders it susceptible to oxidative stress.[385] Likewise, while *GlnA2* and *GlnA4* are not associated with *Mtb* virulence *in vivo* another member of this family *GlnA1* was found to contribute to *Mtb* virulence in a guinea pig model.[386] Also, while a direct role for *Cmtr* in *Mtb* virulence is yet to be established, a transcriptional survey of intracellular mycobacteria and their host macrophages revealed signatures of heavy metal poisoning and an associated strong induction of *Cmtr* and *Csor* which are known to encode metal responsive transcriptional regulators.[387]

The *Mtb* cell wall expresses a variety of virulence factors that contribute to bacterial survival and intrinsic drug resistance. Identification of genes that regulate uptake and secretion machinery across the membrane is critical to characterizing the corresponding secretory products and thus the pathogenesis of *Mtb*. *EccD5* has been identified as being associated with protective granulomas. *EccD5* as part of the ESX-5 system is involved in the translocation of Proline-Proline Glutamate (PPE) proteins and its disruption affects cell wall integrity leading to strong attenuation of the pathogen in a mouse model.[364] But the impact of *EccD5* in human *Mtb* infection or in NHPs is not known. Lastly, we also identified *Mmpl2* and *Mmpl7* to be associated with protective granulomas in the NHP model. Sequencing of the *Mtb* genome revealed 12 membrane proteins that were primarily involved in transport of *Mtb* lipids. *Mmpl*-mediated lipid secretion impacts both the innate ability of the pathogen to survive intracellularly and also the host-pathogen interactions that determine the disease outcome. It has been previously established that only *Mmpl4* and the well-characterized *Mmpl7*, which transports PDIM to the MOM, have both impaired growth kinetics and impaired lethality.[388] In summary, our *Mtb* mutant transposon library infection model in the NHPs has identified for the first time several unique *Mtb* genes

whose roles in *Mtb* virulence were previously considered as redundant.

Since *Mmpl7* is the most well-characterized of all *Mmpl* genes being the known transporter of the virulence lipid PDIM, and as the substrate for *Mmpl2* is currently not known,[389] we decided to focus our further studies utilizing the *Mmpl7* mutant strain (Δ*mmpl7*). Beyond reduced expression of PDIM, the Δ*mmpl7* mutant also has an established *in vivo* growth defect in the lung, spleen, and liver of mice, which we compensated for in our study by infecting with higher doses of the mutant compared to wild type. The decreased CFU in the lungs of Δ*mmpl7* mutant infected mice that we observed is similar to previous findings by Cox et al. and others,[390] but the decreased dissemination to the spleen was not previously observed. This is likely due to the use of different background *Mtb* strains and routes of infection in our study. Furthermore, our higher dose aerosol infection recapitulates a similar phenotype in increased iBALT formation as the standard low dose aerosol infection. Thus, our findings suggest that the improved TB disease outcomes observed is likely not simply due to the absence of PDIMs or a growth defect of the mutant, but that the observed increased iBALT formation is likely driven specifically by the Δ*mmpl7* mutant and overexpression of DATs.

Despite using a higher dose of the Δ*mmpl7* mutant in our infection studies, we observed enhanced iBALT formation and abrogated inflammatory molecule production and cellular recruitment, including both myeloid and lymphoid cell types. As T-cells are required for the formation of iBALT, it would seem that slightly decreased T cell accumulation should also yield decreased iBALT, which was not the case. However, our main observed differences in cellular recruitment involved decreased early neutrophil associated responses, specifically abrogated cytokines like IL-6 and G-CSF, and increased IL-10. It is known that neutrophils are overrepresented in non-protective, necrotic granulomas that do not control or contain *Mtb*, and

that neutrophil counts in peripheral blood, as well as IL-6 levels, correlate with ATB disease.[191,370,371]

Our study confirms these findings with heightened blood levels of G-CSF in people with active TB when compared to LTBI, and as such we used these two inflammatory cytokines as readouts for response severity for our *in vitro* experiments. Thus, these data suggest that a lack of IL-6 and G-CSF and decreased neutrophils may be skewing toward a dampened immune response, potentially mediated by increased early IL-10, that allows for the enhanced formation of iBALT containing granulomas as opposed to necrotic, neutrophil containing lesions. This hypothesis is also supported by our findings *in vitro*, which show decreased IL-6 and G-CSF in lung epithelial cells, a key source of inflammatory molecules, after Δ*mmpl7* mutant infection.

Importantly, we observed increased IL-10 production in macrophages and DCs after Δ*mmpl7* mutant infection. It is known that IL-10 antagonizes IL-17 production, and thus downstream G-CSF production,[64] suggesting a potential mechanism for our observed dampened immune responses and improved outcomes. Indeed, *Mtb* is capable of dampening immune responses mediated by PRRs, and not just stimulating heightened inflammatory responses by interactions with these receptors.

Mmpl7 is colocalized with genes involved in polyketide biosynthesis (*pks* genes) and genes involved in lipid metabolism (*PapA, FadD*) suggesting that it is involved in complex lipid transport involving more than one substrate in *Mtb*.[391,392] Therefore, we aimed to determine if there were any other differences in the lipid profile of *Mtb* beyond the loss of PDIM that could explain the observed abrogated cytokine responses *in vivo* and *in vitro*. We found that DATs are overrepresented in the Δ*mmpl7* mutant, validated by both 1D and 2D thin layer chromatography (TLC). *Mmpl10* is considered to be the putative agent responsible for the transport of DAT

across the plasma membrane.[389] Hence, it is likely that the absence of *Mmpl7* during infection could be compensated by *Mmpl10* function accounting for the observed accumulation of DATs. The addition of DATs during WT *Mtb* infection recapitulated our findings of decreased inflammatory cytokine production in epithelial cells and yielded increased IL-10 production by macrophages, both supporting what was observed in Δ*mmpl7* mutant infection *in vivo*. These findings suggest distinct mechanisms for driving dampened immune responses depending on cell types, with likely interactions of IL-10 sourced from macrophages driving decreased production of inflammatory cytokines by epithelial cells. DATs likely do not act in isolation, as addition of DATs to WT *Mtb* Erdman infection did not fully recapitulate all aspects of Δ*mmpl7* mutant infection *in vitro* in these model systems.

Mycobacterial lipid virulence factors such as PDIMs are known to mask PAMPs and the resultant downstream PRR signaling.[268] Lipid virulence factors are also known to directly act as TLR antagonists.[393] Apart from TLRs, other surface receptors including Mincle, that recognizes trehalose moieties,[262-264] are likely involved in this phenomenon as BMDMs from Mincle deficient mice reportedly produce less G-CSF and TNF in response to *Mtb* infection.[394] Moreover, the expression of TLRs is also known to vary between different phagocytic cell types.[245] Hence these separate responses are likely due to differences in PRR expression and signaling by these cell types. Interestingly, previous studies have shown DAT dependent abrogation of inflammatory cytokine production in monocytes and macrophages *in vitro*.[265] This study was performed using several different human phagocyte models without abrogating the expression of Mincle. While Mincle is established to interact with trehalose moieties, this study validates our claim that DATs can drive abrogated inflammatory cytokine production, independent of any manipulation of the expression of Mincle, suggesting a separate mechanism.

It is likely that the interactions and modulated cytokine/chemokine production we have observed involves other PRRs and *Mtb* lipid factors, beyond the singular interaction between DATs and Mincle.[264]

While the various immune cells and cytokine/chemokine signals that contribute to iBALT formation are well-established in a variety of disease contexts,[51] the *Mtb* specific factors that drive these protective responses, and the mechanism of those interactions, are poorly understood. This study demonstrates that a single *Mtb* specific lipid factor can differentially affect the ability of various cell types to produce inflammatory and anti-inflammatory cytokines, all of which contribute in different aspects to the milieu that fosters conditions beneficial to iBALT formation. In the context of an immune structure as complex as iBALT, where multiple coordinated and regulated signals and cell types are required, future work will likely need to use a similar approach across several *in vivo* and *in vitro* model systems examining multiple cell types in order to elucidate the concise contribution of a specific *Mtb* factor and PRR interactions. Future work may also need to examine not only multiple cell types, but also locational and temporal cellular interactions throughout the course of infection, as a single *Mtb* factor is likely neither necessary nor sufficient in isolation to drive iBALT by interactions with a single cell type at one specific time point.

While this study was not exhaustive in analyzing all potential lipid factors involved, it provides a framework for determining the contributions of the other *Mtb* genes and potential candidate lipids in skewing toward protective outcomes. We acknowledge that the role of any specific lipid in skewing iBALT formation is not an isolated phenomenon, as *Mtb* mutants knocking out certain lipids inevitably drive compensatory overexpression of others. Furthermore, we expect that the increased iBALT formation we have observed is likely due to a combination

of a lack of PDIM along with increased DATs, with the possibility of other lipids being involved that we did not identify or assay for.

Our novel findings demonstrate that genes associated with *Mtb* cell wall lipids are critical to the initial interactions between *Mtb* and the host and suggest that *Mtb* specific lipids are key determinants of the early immune response that skews toward formation of iBALT. Our findings further provide a list of *Mtb* gene candidates for future work examining conditions needed for protective iBALT formation, specifically aimed at early responses that determine these outcomes. We have also demonstrated for the first time a panel of novel *Mtb* genes that are associated with *enhanced formation of protective iBALT containing granulomas and improved disease outcomes*, while most work on this topic examines genes involved in detrimental host outcomes and loss of protection. This study thus provides a framework for future attenuated vaccine candidates and mechanistic studies across model systems.

Chapter 5: Perspectives and Conclusions

5.1 Discussion and Future Directions

My doctoral dissertation work focuses on early innate immunity during pulmonary *Mtb* infection, specifically in characterizing the contribution of lung resident AMs to both early inflammatory responses and long-term disease outcomes. These connections between innate and adaptive immunity are generally attributed to DCs, though my work demonstrates that AMs play crucial roles in cytokine production, immune cell recruitment, granuloma and iBALT formation. My studies focused on how AM specific signaling and effector functions were altered by *Mtb* strains and cellular location within the lung, and further examined the implications these modulations had on broader disease phenotypes during both early and later *Mtb* infection. Another major goal of this work aimed to characterize how *Mtb* cell wall lipids can directly modulate macrophage behavior and effector functions. Several cell wall lipids were studied in this body of work and were found to have divergent effects on protective immunity in a variety of contexts. These key interactions have durable effects on immune responses, and further elucidating how to target both AM effector functions and *Mtb* specific lipids for advantageous host responses remains a subject of ongoing study.

Lipid factors that modulate early immunity

Mtb strains and specific lipid factors drive critical interactions that modulate cytokine and chemokine production by host cells, thus skewing the fundamental type of immune response generated.[23,64] Furthermore, *Mtb* specific determinants can alter host cell effector functions, as we observed in multiple studies. For example, in **Aim 1** we observed *Mtb* strain specific induction of the CCR2:CCL2 axis during hypervirulent *Mtb* HN878 infection, and this drove the

novel AM migration phenotype from the airways we reported.[113] We found that CCR2 was required for AM migration from the airways into granulomas in response to a specific induction of CCL2 within and around granulomas. Interestingly, we show that susceptibility of $CCR2^{-/-}$ mice to hypervirulent HN878 is not entirely due to expression of PGLs, a *Mtb* lipid factor known to induce and exploit CCL2 production.[144,145] We found that $CCR2^{-/-}$ mice were even more susceptible to an HN878 pks gene mutant when compared to wildtype HN878, suggesting that other lipid factors are at play that make HN878 potentially even more inflammatory in the absence of the PKS gene family. As previously discussed, many *Mtb* lipid virulence factors are regulated by PKS genes, and the compensatory mechanism of hyperinflammation we observed could be due to one or multiple of these candidates. In future work we will examine how the known and unknown lipid targets of PKS genes are involved in hypervirulence and driving overt inflammation.

In both **Aims 1 & 3**, we also show that alteration of *Mtb* lipid factor, such as PGLs, DATs, and PDIM, can have effects on formation of granulomas and iBALT. We observed that overexpression of DATs, as a compensatory mechanism for decreased expression of PDIM on the MOM, drove dampened inflammatory responses in macrophages and epithelial cells that improved iBALT formation and overall disease outcomes.[192] We furthermore provide a framework for examining the contribution of individual lipids to these processes, which can be applied to other *Mtb* mutants and lipid virulence factors of interest. These findings suggest that future research should involve comparison of multiple *Mtb* strains in order to properly examine any cellular mechanism or host disease phenotype. Furthermore, a robust database to compare the lipidome of various catalogued *Mtb* strains would be a useful reference tool for researchers, allowing specific phenotypes and mechanisms to be properly attributed to specific *Mtb* lipid

factor interactions with host determinants. Significantly, determining the concise contribution of specific *Mtb* lipid factors such as PGLs, PDIM, and DATs examined in my work, will pave the way for use of these lipids as components or adjuvants in future vaccine formulations, or potential targets for *Mtb* neutralization strategies.

While my studies did not cover this topic, another key facet of future work should examine how host cell metabolism is affected by *Mtb* lipids. Characterizing how functional roles of immune cell types are directly affected by the presence or absence of individual *Mtb* lipids would provide specific targets for future therapeutic strategies aimed at either neutralizing *Mtb* lipids or inducing/abrogating specific cellular effector functions. Specifically driving beneficial cellular processes while inhibiting damaging or detrimental processes would allow for more rapid clearing of infection with less damaging inflammation. Similarly, host directed therapeutic strategies do not run the same risk of developing resistance as antibiotic courses do, demonstrating an attractive alternative to the current standard of care.

Host factors and signaling that drive AM compartmental migration and effector function

In my previous work, we correlated AM migration from the airway to the formation of protective granuloma structures, but the contributions of specific cytokines and chemokines beyond the CCR2 axis were not examined. It is likely that, similar to migration phenotypes previously observed in T-cells, that multiple chemokine axes contribute to AM migration into granulomas. It is also likely that distinct chemokine axes are involved in airway homing of neutrophils and other inflammatory cells, so a concise, targeted approach at inducing or abrogating cellular migration will be challenging.

AMs do not perform their effector functions in a vacuum; therefore mDCs, neutrophils,

T-cells, and lung epithelial cells were also examined in my studies, though not to the same depth and extent. Future work will characterize concise interactions between AMs and these other cell types individually, specifically using co-culture approaches and targeted genetic manipulation to characterize beneficial components. Understanding the bystander cell specific factors that drive the differential AM effector functions will allow us to characterize additional correlates of protection against *Mtb*. It is known that epithelial cells and AMs drive mutual signal amplification during *Mtb* infection, inducing production of inflammatory cytokines that then in turn further activate neighboring cells.[33] This key early interaction likely drives the phenotypes we have observed across my studies, and determining the specific contributions of PRRs, cytokines, and *Mtb* specific factors to AM priming and activation will be a general theme of applied future work.

Targeting M1 polarization as a tool for priming innate immunity

From our RNA-seq data presented in Chapter 2, we observed that many of the differentially expressed genes and pathways upregulated in the non-airway AMs were mediated by NF-κB. This suggested a key signaling target to further parse out the previously unknown non-airway phenotype of AMs. Furthermore, NF-κB and the subunit Iκκ2 are considered critical to *Mtb* immune responses, though activation of this nexus drives overt, damaging inflammation that is detrimental to the host. Concurrent studies recapitulated our AM migration phenotype, and demonstrated a dependence on IL-1β/IL1R signaling and the inflammasome for this function.[126] Furthermore, other work has demonstrated compartmentally distinct functions for lung macrophages, though identification of specific macrophage subsets was less robust.[67,109] Taken together, these studies support a link between M1 polarization, NF-κB signaling, and the

IL-1β/inflammasome pathway in driving compartmentally distinct functions for AMs

In future work, we will further examine the AM specific requirements for driving compartmental migration of AMs, and determine if this function is advantageous for therapeutic targeting. Future studies will characterize AM specific genes and specific cellular interactions and/or cytokine/chemokine signals required for migration to granulomas, coordinating inflammation, and *Mtb* killing. Considering several of these pathways have been rigorously studied in a variety of contexts for decades, robust genetic models and effective drugs can be used to specifically examine the contribution of individual axes in the protective or detrimental mechanisms at play. If migration of M1 polarized AMs into granulomas is indeed protective, targeting this functionality to therapeutically induce interstitial localization could be a major milestone in utilizing early clearance to combat pulmonary *Mtb* infection.

5.2 Closing Remarks

Taken together, my dissertation research demonstrates the consequential role of early innate immunity in determining host outcomes to pulmonary *Mtb* infection. We examine specific factors involved in the earliest interactions between *Mtb* and the host, and present evidence that these early interactions have long term protective or detrimental consequences for disease outcomes. These studies together elucidate the earliest mechanisms of protective innate immunity and shed new light on the critical primary interactions between macrophages, *Mtb* and epithelial cells that drive short- and long-term disease outcomes in pulmonary TB.

References:

1 World Health, O. *Global Tuberculosis Report 2019*. (2019).

2 Reid, M. J. A. *et al.* Building a tuberculosis-free world: The Lancet Commission on tuberculosis. *Lancet* **393**, 1331-1384, doi:10.1016/S0140-6736(19)30024-8 (2019).

3 Burki, T. K. The global cost of tuberculosis. *The Lancet Respiratory Medicine* **6**, 13, doi:10.1016/s2213-2600(17)30468-x (2018).

4 Schiller, I. *et al.* Bovine Tuberculosis: A Review of Current and Emerging Diagnostic Techniques in View of their Relevance for Disease Control and Eradication. *Transboundary and Emerging Diseases*, no-no, doi:10.1111/j.1865-1682.2010.01148.x (2010).

5 Buddle, B. M., Parlane, N. A., Chambers, M. A. & Gortázar, C. Vaccination of domestic and wild animals against tuberculosis. *Bovine tuberculosis*, 206-224, doi:10.1079/9781786391520.0206.

6 Waters, W. R., Palmer, M. V., Buddle, B. M. & Vordermeier, H. M. Bovine tuberculosis vaccine research: historical perspectives and recent advances. *Vaccine* **30**, 2611-2622, doi:10.1016/j.vaccine.2012.02.018 (2012).

7 Hershkovitz, I. *et al.* Detection and Molecular Characterization of 9000-Year-Old Mycobacterium tuberculosis from a Neolithic Settlement in the Eastern Mediterranean. *PLoS ONE* **3**, e3426, doi:10.1371/journal.pone.0003426 (2008).

8 Wirth, T. *et al.* Origin, spread and demography of the Mycobacterium tuberculosis complex. *PLoS Pathog.* **4**, e1000160, doi:10.1371/journal.ppat.1000160 (2008).

9 World Health, O. *Guidelines for Treatment of Drug-Susceptible Tuberculosis and Patient Care: 2017 Update*. (2017).

10 Falzon, D. *et al.* World Health Organization treatment guidelines for drug-resistant tuberculosis, 2016 update. *Eur. Respir. J.* **49**, doi:10.1183/13993003.02308-2016 (2017).

11 Ahmed, M. *et al.* Immune correlates of tuberculosis disease and risk translate across species. *Sci. Transl. Med.* **12**, doi:10.1126/scitranslmed.aay0233 (2020).

12 Zak, D. E. *et al.* A blood RNA signature for tuberculosis disease risk: a prospective cohort study. *Lancet* **387**, 2312-2322, doi:10.1016/S0140-6736(15)01316-1 (2016).

13 Ottenhoff, T. H. M. & Kaufmann, S. H. E. State of the art in vaccine development against TB. *Tuberculosis*, 59-71, doi:10.1183/1025448x.10015912 (2012).

14 Scott, N. R. *et al.* S100A8/A9 regulates CD11b expression and neutrophil recruitment during chronic tuberculosis. *J. Clin. Invest.*, doi:10.1172/JCI130546 (2020).

15 Mendelsohn, S. C., Mbandi, S. K., Hatherill, M. & Scriba, T. J. Blood transcriptional signatures for tuberculosis testing. *Lancet Respir Med* **8**, 330-331, doi:10.1016/S2213-2600(20)30045-X (2020).

16 Ottenhoff, T. H. M. *et al.* First in humans: a new molecularly defined vaccine shows excellent safety and strong induction of long-lived Mycobacterium tuberculosis-specific Th1-cell like responses. *Hum. Vaccin.* **6**, 1007-1015, doi:10.4161/hv.6.12.13143 (2010).

17 Day, C. L. *et al.* Induction and regulation of T-cell immunity by the novel tuberculosis vaccine M72/AS01 in South African adults. *Am. J. Respir. Crit. Care Med.* **188**, 492-502, doi:10.1164/rccm.201208-1385OC (2013).

18 Leroux-Roels, I. *et al.* Improved CD4 T cell responses to Mycobacterium tuberculosis in PPD-negative adults by M72/AS01 as compared to the M72/AS02 and Mtb72F/AS02 tuberculosis candidate vaccine formulations: A randomized trial. *Vaccine* **31**, 2196-2206, doi:10.1016/j.vaccine.2012.05.035 (2013).

19 Méndez-Samperio, P. Development of tuberculosis vaccines in clinical trials: Current status. *Scandinavian Journal of Immunology* **88**, e12710, doi:10.1111/sji.12710 (2018).
20 Orme, I. M., Robinson, R. T. & Cooper, A. M. The balance between protective and pathogenic immune responses in the TB-infected lung. *Nat. Immunol.* **16**, 57-63, doi:10.1038/ni.3048 (2015).
21 Griffiths, K. L. *et al.* Targeting dendritic cells to accelerate T-cell activation overcomes a bottleneck in tuberculosis vaccine efficacy. *Nature Communications* **7**, doi:10.1038/ncomms13894 (2016).
22 Wolf, A. J. *et al.* Mycobacterium tuberculosis infects dendritic cells with high frequency and impairs their function in vivo. *J. Immunol.* **179**, 2509-2519 (2007).
23 Slight, S. R. & Khader, S. A. Chemokines shape the immune responses to tuberculosis. *Cytokine & Growth Factor Reviews* **24**, 105-113, doi:10.1016/j.cytogfr.2012.10.002 (2013).
24 Morrison, J., Pai, M. & Hopewell, P. C. Tuberculosis and latent tuberculosis infection in close contacts of people with pulmonary tuberculosis in low-income and middle-income countries: a systematic review and meta-analysis. *Lancet Infect. Dis.* **8**, 359-368, doi:10.1016/S1473-3099(08)70071-9 (2008).
25 Verrall, A. J., Netea, M. G., Alisjahbana, B., Hill, P. C. & van Crevel, R. Early clearance of Mycobacterium tuberculosis: a new frontier in prevention. *Immunology* **141**, 506-513, doi:10.1111/imm.12223 (2014).
26 Arriaga, A. K., Orozco, E. H., Aguilar, L. D., Rook, G. A. W. & Hernández Pando, R. Immunological and pathological comparative analysis between experimental latent tuberculous infection and progressive pulmonary tuberculosis. *Clin. Exp. Immunol.* **128**, 229-237, doi:10.1046/j.1365-2249.2002.01832.x (2002).
27 Cobat, A. *et al.* Tuberculin skin test reactivity is dependent on host genetic background in Colombian tuberculosis household contacts. *Clin. Infect. Dis.* **54**, 968-971, doi:10.1093/cid/cir972 (2012).
28 Cobat, A. *et al.* Two loci control tuberculin skin test reactivity in an area hyperendemic for tuberculosis. *J. Exp. Med.* **206**, 2583-2591, doi:10.1084/jem.20090892 (2009).
29 THE LUBECK CATASTROPHE: A GENERAL REVIEW. *Br. Med. J.* **1**, 986-988 (1931).
30 Fox, G. J., Orlova, M. & Schurr, E. Tuberculosis in Newborns: The Lessons of the "Lübeck Disaster" (1929-1933). *PLoS Pathog.* **12**, e1005271, doi:10.1371/journal.ppat.1005271 (2016).
31 Patel, B., Gupta, N. & Ahsan, F. Particle engineering to enhance or lessen particle uptake by alveolar macrophages and to influence the therapeutic outcome. *Eur. J. Pharm. Biopharm.* **89**, 163-174, doi:10.1016/j.ejpb.2014.12.001 (2015).
32 Schiller, H. B. *et al.* The Human Lung Cell Atlas: A High-Resolution Reference Map of the Human Lung in Health and Disease. *American Journal of Respiratory Cell and Molecular Biology* **61**, 31-41, doi:10.1165/rcmb.2018-0416tr (2019).
33 Allard, B., Panariti, A. & Martin, J. G. Alveolar Macrophages in the Resolution of Inflammation, Tissue Repair, and Tolerance to Infection. *Front. Immunol.* **9**, 1777, doi:10.3389/fimmu.2018.01777 (2018).
34 Li, Y., Wang, Y. & Liu, X. The Role of Airway Epithelial Cells in Response to Mycobacteria Infection. *Clinical and Developmental Immunology* **2012**, 1-11, doi:10.1155/2012/791392 (2012).

35 Reuschl, A.-K. *et al.* Innate activation of human primary epithelial cells broadens the host response to Mycobacterium tuberculosis in the airways. *PLoS Pathog.* **13**, e1006577, doi:10.1371/journal.ppat.1006577 (2017).
36 Scordo, J. M. *et al.* The human lung mucosa drives differential Mycobacterium tuberculosis infection outcome in the alveolar epithelium. *Mucosal Immunol.* **12**, 795-804, doi:10.1038/s41385-019-0156-2 (2019).
37 Holt, P. G. Alveolar macrophages. I. a simple technique for the preparation of high numbers of viable alveolar macrophages from small laboratory animals. *Journal of Immunological Methods* **27**, 189-198, doi:10.1016/0022-1759(79)90264-3 (1979).
38 Herbert, J. A. *et al.* β2 integrin LFA1 mediates airway damage following neutrophil trans-epithelial migration during RSV infection. *Eur. Respir. J.*, doi:10.1183/13993003.02216-2019 (2020).
39 Weng, Q. *et al.* Early recruited neutrophils promote asthmatic inflammation exacerbation by release of neutrophil elastase. *Cell. Immunol.*, 104101, doi:10.1016/j.cellimm.2020.104101 (2020).
40 Tenland, E. *et al.* Innate Immune Responses after Airway Epithelial Stimulation with Mycobacterium bovis Bacille-Calmette Guérin. *PLoS One* **11**, e0164431, doi:10.1371/journal.pone.0164431 (2016).
41 Mishra, B. B. *et al.* Nitric oxide prevents a pathogen-permissive granulocytic inflammation during tuberculosis. *Nat Microbiol* **2**, 17072, doi:10.1038/nmicrobiol.2017.72 (2017).
42 Silver, R. F. *et al.* Diversity of Human and Macaque Airway Immune Cells at Baseline and during Tuberculosis Infection. *Am. J. Respir. Cell Mol. Biol.* **55**, 899-908, doi:10.1165/rcmb.2016-0122OC (2016).
43 Okamoto, M., Takeda, K., Joetham, A., Han, J. & Gelfand, E. W. IL-6 from Dendritic Cells Regulates Airway Hyperresponsiveness and Inflammation by Controlling the Fate of CD4 T Cells. *D22. MODULATORS OF INFLAMMATORY PATHWAYS IN AIRWAY DISEASE*, doi:10.1164/ajrccm-conference.2009.179.1_meetingabstracts.a5463 (2009).
44 Ballke, C., Gran, E., Baekkevold, E. S. & Jahnsen, F. L. Characterization of Regulatory T-Cell Markers in CD4 T Cells of the Upper Airway Mucosa. *PLOS ONE* **11**, e0148826, doi:10.1371/journal.pone.0148826 (2016).
45 Jarvela, J. *et al.* -Induced Bronchoalveolar Lavage Gene Expression Signature in Latent Tuberculosis Infection Is Dominated by Pleiotropic Effects of CD4 T Cell-Dependent IFN-γ Production despite the Presence of Polyfunctional T Cells within the Airways. *J. Immunol.* **203**, 2194-2209, doi:10.4049/jimmunol.1900230 (2019).
46 Wolber, F. M. *et al.* Lymphocyte recruitment and the kinetics of adhesion receptor expression during the pulmonary immune response to particulate antigen. *Am. J. Pathol.* **151**, 1715-1727 (1997).
47 Kraneveld, A. D. *et al.* Antibody to very late activation antigen 4 prevents interleukin-5-induced airway hyperresponsiveness and eosinophil infiltration in the airways of guinea pigs. *J. Allergy Clin. Immunol.* **100**, 242-250, doi:10.1016/s0091-6749(97)70231-8 (1997).
48 Anderson, K. G. *et al.* Intravascular staining for discrimination of vascular and tissue leukocytes. *Nat. Protoc.* **9**, 209-222, doi:10.1038/nprot.2014.005 (2014).

49 Osier, M. & Oberörster, G. Intratracheal Inhalation vs Intratracheal Instillation: Differences in Particle Effects. *Toxicological Sciences* **40**, 220-227, doi:10.1093/toxsci/40.2.220 (1997).
50 Khader, S. A. *et al.* In a Murine Tuberculosis Model, the Absence of Homeostatic Chemokines Delays Granuloma Formation and Protective Immunity. *The Journal of Immunology* **183**, 8004-8014, doi:10.4049/jimmunol.0901937 (2009).
51 Marin, N. D., Dunlap, M. D., Kaushal, D. & Khader, S. A. Friend or Foe: The Protective and Pathological Roles of Inducible Bronchus-Associated Lymphoid Tissue in Pulmonary Diseases. *J. Immunol.* **202**, 2519-2526, doi:10.4049/jimmunol.1801135 (2019).
52 Scordo, J. M., Knoell, D. L. & Torrelles, J. B. Alveolar Epithelial Cells in Mycobacterium tuberculosis Infection: Active Players or Innocent Bystanders? *J. Innate Immun.* **8**, 3-14, doi:10.1159/000439275 (2016).
53 Galkina, E. Preferential migration of effector CD8 T cells into the interstitium of the normal lung. *Journal of Clinical Investigation* **115**, 3473-3483, doi:10.1172/jci24482 (2005).
54 Gern, B. H. *et al.* Tgfβ Restricts T Cell Function and Bacterial Control within the Tuberculous Granuloma. *SSRN Electronic Journal*, doi:10.2139/ssrn.3541366.
55 Fennelly, K. P. & Jones-López, E. C. Quantity and Quality of Inhaled Dose Predicts Immunopathology in Tuberculosis. *Front. Immunol.* **6**, 313, doi:10.3389/fimmu.2015.00313 (2015).
56 Fennelly, K. P. *et al.* Cough-generated aerosols of Mycobacterium tuberculosis: a new method to study infectiousness. *Am. J. Respir. Crit. Care Med.* **169**, 604-609, doi:10.1164/rccm.200308-1101OC (2004).
57 Shiloh, M. U. Mechanisms of mycobacterial transmission: how does Mycobacterium tuberculosis enter and escape from the human host. *Future Microbiol.* **11**, 1503-1506, doi:10.2217/fmb-2016-0185 (2016).
58 Ruhl, C. R. *et al.* Mycobacterium tuberculosis Sulfolipid-1 Activates Nociceptive Neurons and Induces Cough. *Cell* **181**, 293-305.e211, doi:10.1016/j.cell.2020.02.026 (2020).
59 Stamm, C. E., Collins, A. C. & Shiloh, M. U. Sensing of Mycobacterium tuberculosis and consequences to both host and bacillus. *Immunol. Rev.* **264**, 204-219, doi:10.1111/imr.12263 (2015).
60 Arcos, J. *et al.* Mycobacterium tuberculosis cell wall released fragments by the action of the human lung mucosa modulate macrophages to control infection in an IL-10-dependent manner. *Mucosal Immunol.* **10**, 1248-1258, doi:10.1038/mi.2016.115 (2017).
61 Polverino, M. *et al.* Anatomy and neuro-pathophysiology of the cough reflex arc. *Multidiscip. Respir. Med.* **7**, 5, doi:10.1186/2049-6958-7-5 (2012).
62 Kaltreider, H. B. & Benfer Kaltreider, H. Alveolar Macrophages. *Chest* **82**, 261-262, doi:10.1378/chest.82.3.261 (1982).
63 Schiller, E. Alveolar Macrophages. *Free Radicals and Inhalation Pathology*, 237-389, doi:10.1007/978-3-642-18619-6_9 (2004).
64 Monin, L. & Khader, S. A. Chemokines in tuberculosis: the good, the bad and the ugly. *Semin. Immunol.* **26**, 552-558, doi:10.1016/j.smim.2014.09.004 (2014).

65 Srivastava, S., Ernst, J. D. & Desvignes, L. Beyond macrophages: the diversity of mononuclear cells in tuberculosis. *Immunol. Rev.* **262**, 179-192, doi:10.1111/imr.12217 (2014).
66 Armstrong, J. A. & Hart, P. D. Phagosome-lysosome interactions in cultured macrophages infected with virulent tubercle bacilli. Reversal of the usual nonfusion pattern and observations on bacterial survival. *The Journal of Experimental Medicine* **142**, 1-16, doi:10.1084/jem.142.1.1 (1975).
67 Huang, L., Nazarova, E. V., Tan, S., Liu, Y. & Russell, D. G. Growth of Mycobacterium tuberculosis in vivo segregates with host macrophage metabolism and ontogeny. *The Journal of Experimental Medicine* **215**, 1135-1152, doi:10.1084/jem.20172020 (2018).
68 Rook, G. A. Macrophages and Mycobacterium tuberculosis: the key to pathogenesis. *Immunol. Ser.* **60**, 249-261 (1994).
69 Dannenberg, A. M. Immunopathogenesis of Pulmonary Tuberculosis. *Hospital Practice* **28**, 51-58, doi:10.1080/21548331.1993.11442738 (1993).
70 Lurie, M. B., Abramson, S. & Heppleston, A. G. On the response of genetically resistant and susceptible rabbits to the quantitative inhalation of human type tubercle bacilli and the nature of resistance to tuberculosis. *J. Exp. Med.* **95**, 119-134, doi:10.1084/jem.95.2.119 (1952).
71 Kang, P. B. *et al.* The human macrophage mannose receptor directs Mycobacterium tuberculosis lipoarabinomannan-mediated phagosome biogenesis. *Journal of Experimental Medicine* **202**, 987-999, doi:10.1084/jem.20051239 (2005).
72 Astarie-Dequeker, C. *et al.* The Mannose Receptor Mediates Uptake of Pathogenic and Nonpathogenic Mycobacteria and Bypasses Bactericidal Responses in Human Macrophages. *Infection and Immunity* **67**, 469-477, doi:10.1128/iai.67.2.469-477.1999 (1999).
73 Yadav, M. & Schorey, J. S. The beta-glucan receptor dectin-1 functions together with TLR2 to mediate macrophage activation by mycobacteria. *Blood* **108**, 3168-3175, doi:10.1182/blood-2006-05-024406 (2006).
74 Cywes, C., Hoppe, H. C., Daffé, M. & Ehlers, M. R. Nonopsonic binding of Mycobacterium tuberculosis to complement receptor type 3 is mediated by capsular polysaccharides and is strain dependent. *Infection and immunity* **65**, 4258-4266, doi:10.1128/iai.65.10.4258-4266.1997 (1997).
75 Melo, M. D., Catchpole, I. R., Haggar, G. & Stokes, R. W. Utilization of CD11b knockout mice to characterize the role of complement receptor 3 (CR3, CD11b/CD18) in the growth of Mycobacterium tuberculosis in macrophages. *Cell. Immunol.* **205**, 13-23, doi:10.1006/cimm.2000.1710 (2000).
76 Guirado, E., Schlesinger, L. S. & Kaplan, G. Macrophages in tuberculosis: friend or foe. *Semin. Immunopathol.* **35**, 563-583, doi:10.1007/s00281-013-0388-2 (2013).
77 Schlesinger, L. S. *et al.* Determinants of Phagocytosis, Phagosome Biogenesis and Autophagy forMycobacterium tuberculosis. *Handbook of Tuberculosis*, 1-22, doi:10.1002/9783527611614.ch18 (2017).
78 Rajaram, M. V. S. *et al.* Mycobacterium tuberculosis activates human macrophage peroxisome proliferator-activated receptor gamma linking mannose receptor recognition to regulation of immune responses. *J. Immunol.* **185**, 929-942, doi:10.4049/jimmunol.1000866 (2010).

79 Pauwels, A.-M., Trost, M., Beyaert, R. & Hoffmann, E. Patterns, Receptors, and Signals: Regulation of Phagosome Maturation. *Trends Immunol.* **38**, 407-422, doi:10.1016/j.it.2017.03.006 (2017).
80 Bogdan, C. Nitric oxide and the immune response. *Nat. Immunol.* **2**, 907-916, doi:10.1038/ni1001-907 (2001).
81 Kwon, O. J. The role of nitric oxide in the immune response of tuberculosis. *Journal of Korean Medical Science* **12**, 481, doi:10.3346/jkms.1997.12.6.481 (1997).
82 Miller, B. H. *et al.* Mycobacteria inhibit nitric oxide synthase recruitment to phagosomes during macrophage infection. *Infect. Immun.* **72**, 2872-2878, doi:10.1128/iai.72.5.2872-2878.2004 (2004).
83 Coates, B. M. *et al.* Inhibition of the NOD-Like Receptor Protein 3 Inflammasome Is Protective in Juvenile Influenza A Virus Infection. *Front. Immunol.* **8**, 782, doi:10.3389/fimmu.2017.00782 (2017).
84 Russell, D. G. & Yates, R. M. Toll-like receptors and phagosome maturation. *Nature Immunology* **8**, 217-217, doi:10.1038/ni0307-217a (2007).
85 Yates, R. M., Hermetter, A. & Russell, D. G. The Kinetics of Phagosome Maturation as a Function of Phagosome/Lysosome Fusion and Acquisition of Hydrolytic Activity. *Traffic* **6**, 413-420, doi:10.1111/j.1600-0854.2005.00284.x (2005).
86 Kotsias, F., Hoffmann, E., Amigorena, S. & Savina, A. Reactive Oxygen Species Production in the Phagosome: Impact on Antigen Presentation in Dendritic Cells. *Antioxidants & Redox Signaling* **18**, 714-729, doi:10.1089/ars.2012.4557 (2013).
87 Campbell-Valois, F.-X. *et al.* Quantitative Proteomics Reveals That Only a Subset of the Endoplasmic Reticulum Contributes to the Phagosome. *Molecular & Cellular Proteomics* **11**, M111.016378, doi:10.1074/mcp.m111.016378 (2012).
88 Gagnon, E. *et al.* Endoplasmic Reticulum-Mediated Phagocytosis Is a Mechanism of Entry into Macrophages. *Cell* **110**, 119-131, doi:10.1016/s0092-8674(02)00797-3 (2002).
89 Russell, D. G., Huang, L. & VanderVen, B. C. Immunometabolism at the interface between macrophages and pathogens. *Nat. Rev. Immunol.* **19**, 291-304, doi:10.1038/s41577-019-0124-9 (2019).
90 Cumming, B. M., Addicott, K. W., Adamson, J. H. & Steyn, A. J. C. Mycobacterium tuberculosis induces decelerated bioenergetic metabolism in human macrophages. *eLife* **7**, doi:10.7554/elife.39169 (2018).
91 Mills, C. D., Kincaid, K., Alt, J. M., Heilman, M. J. & Hill, A. M. M-1/M-2 macrophages and the Th1/Th2 paradigm. *J. Immunol.* **164**, 6166-6173, doi:10.4049/jimmunol.164.12.6166 (2000).
92 He, Y., Li, W., Liao, G. & Xie, J. Mycobacterium tuberculosis-Specific Phagosome Proteome and Underlying Signaling Pathways. *Journal of Proteome Research* **11**, 2635-2643, doi:10.1021/pr300125t (2012).
93 Savina, A. & Amigorena, S. Phagocytosis and antigen presentation in dendritic cells. *Immunological Reviews* **219**, 143-156, doi:10.1111/j.1600-065x.2007.00552.x (2007).
94 Steiner, D. J., Furuya, Y., Jordan, M. B. & Metzger, D. W. Protective Role for Macrophages in Respiratory Francisella tularensis Infection. *Infect. Immun.* **85**, doi:10.1128/IAI.00064-17 (2017).
95 Leemans, J. C. *et al.* Macrophages play a dual role during pulmonary tuberculosis in mice. *J. Infect. Dis.* **191**, 65-74, doi:10.1086/426395 (2005).

96 Leemans, J. C. *et al.* Depletion of alveolar macrophages exerts protective effects in pulmonary tuberculosis in mice. *J. Immunol.* **166**, 4604-4611 (2001).
97 Borthwick, L. A. *et al.* Macrophages are critical to the maintenance of IL-13-dependent lung inflammation and fibrosis. *Mucosal Immunol.* **9**, 38-55, doi:10.1038/mi.2015.34 (2016).
98 Oh, D. S., Oh, J. E., Jung, H. E. & Lee, H. K. Transient Depletion of CD169(+) Cells Contributes to Impaired Early Protection and Effector CD8(+) T Cell Recruitment against Mucosal Respiratory Syncytial Virus Infection. *Front. Immunol.* **8**, 819, doi:10.3389/fimmu.2017.00819 (2017).
99 van Rijt, L. S. *et al.* In vivo depletion of lung CD11c dendritic cells during allergen challenge abrogates the characteristic features of asthma. *J. Exp. Med.* **201**, 981-991, doi:10.1084/jem.20042311 (2005).
100 Samstein, M. *et al.* Essential yet limited role for $CCR2^+$ inflammatory monocytes during Mycobacterium tuberculosis-specific T cell priming. *Elife* **2**, e01086, doi:10.7554/eLife.01086 (2013).
101 Divangahi, M., Desjardins, D., Nunes-Alves, C., Remold, H. G. & Behar, S. M. Eicosanoid pathways regulate adaptive immunity to Mycobacterium tuberculosis. *Nat. Immunol.* **11**, 751-758, doi:10.1038/ni.1904 (2010).
102 Rigaux, P., Killoran, K. E., Qiu, Z. & Rosenberg, H. F. Depletion of alveolar macrophages prolongs survival in response to acute pneumovirus infection. *Virology* **422**, 338-345, doi:10.1016/j.virol.2011.10.031 (2012).
103 Tian, T., Woodworth, J., Sköld, M. & Behar, S. M. In vivo depletion of CD11c+ cells delays the CD4+ T cell response to Mycobacterium tuberculosis and exacerbates the outcome of infection. *J. Immunol.* **175**, 3268-3272 (2005).
104 Roberts, L. M. *et al.* Depletion of alveolar macrophages in CD11c diphtheria toxin receptor mice produces an inflammatory response. *Immunity, Inflammation and Disease* **3**, 71-81, doi:10.1002/iid3.51 (2015).
105 Purnama, C. *et al.* Transient ablation of alveolar macrophages leads to massive pathology of influenza infection without affecting cellular adaptive immunity. *Eur. J. Immunol.* **44**, 2003-2012, doi:10.1002/eji.201344359 (2014).
106 Hussell, T. & Bell, T. J. Alveolar macrophages: plasticity in a tissue-specific context. *Nature Reviews Immunology* **14**, 81-93, doi:10.1038/nri3600 (2014).
107 Rajaram, M. V. S., Ni, B., Dodd, C. E. & Schlesinger, L. S. Macrophage immunoregulatory pathways in tuberculosis. *Semin. Immunol.* **26**, 471-485, doi:10.1016/j.smim.2014.09.010 (2014).
108 Rothchild, A. C. *et al.* Alveolar macrophages generate a noncanonical NRF2-driven transcriptional response to Mycobacterium tuberculosis in vivo. *Science Immunology* **4**, eaaw6693, doi:10.1126/sciimmunol.aaw6693 (2019).
109 Pisu, D., Huang, L., Grenier, J. K. & Russell, D. G. Dual RNA-Seq of Mtb-Infected Macrophages In Vivo Reveals Ontologically Distinct Host-Pathogen Interactions. *Cell Reports* **30**, 335-350.e334, doi:10.1016/j.celrep.2019.12.033 (2020).
110 Redente, E. F. *et al.* Differential polarization of alveolar macrophages and bone marrow-derived monocytes following chemically and pathogen-induced chronic lung inflammation. *J. Leukoc. Biol.* **88**, 159-168, doi:10.1189/jlb.0609378 (2010).
111 Gordon, S. Alternative activation of macrophages. *Nature Reviews Immunology* **3**, 23-35, doi:10.1038/nri978 (2003).

112 Mantovani, A. *et al.* The chemokine system in diverse forms of macrophage activation and polarization. *Trends in Immunology* **25**, 677-686, doi:10.1016/j.it.2004.09.015 (2004).
113 Dunlap, M. D. *et al.* A novel role for C-C motif chemokine receptor 2 during infection with hypervirulent Mycobacterium tuberculosis. *Mucosal Immunol.* **11**, 1727-1742, doi:10.1038/s41385-018-0071-y (2018).
114 Misharin, A. V., Morales-Nebreda, L., Mutlu, G. M., Scott Budinger, G. R. & Perlman, H. Flow Cytometric Analysis of Macrophages and Dendritic Cell Subsets in the Mouse Lung. *American Journal of Respiratory Cell and Molecular Biology* **49**, 503-510, doi:10.1165/rcmb.2013-0086ma (2013).
115 Misharin, A. V. *et al.* Monocyte-derived alveolar macrophages drive lung fibrosis and persist in the lung over the life span. *J. Exp. Med.* **214**, 2387-2404, doi:10.1084/jem.20162152 (2017).
116 Gibbings, S. L. & Jakubzick, C. V. Isolation and Characterization of Mononuclear Phagocytes in the Mouse Lung and Lymph Nodes. *Methods Mol. Biol.* **1809**, 33-44, doi:10.1007/978-1-4939-8570-8_3 (2018).
117 Landsman, L. & Jung, S. Lung macrophages serve as obligatory intermediate between blood monocytes and alveolar macrophages. *J. Immunol.* **179**, 3488-3494, doi:10.4049/jimmunol.179.6.3488 (2007).
118 Guilliams, M. *et al.* Alveolar macrophages develop from fetal monocytes that differentiate into long-lived cells in the first week of life via GM-CSF. *J. Exp. Med.* **210**, 1977-1992, doi:10.1084/jem.20131199 (2013).
119 Guilliams, M., Lambrecht, B. N. & Hammad, H. Division of labor between lung dendritic cells and macrophages in the defense against pulmonary infections. *Mucosal Immunology* **6**, 464-473, doi:10.1038/mi.2013.14 (2013).
120 Tan, S. Y. S. & Krasnow, M. A. Developmental origin of lung macrophage diversity. *Development* **143**, 1318-1327, doi:10.1242/dev.129122 (2016).
121 Philips, J. A. & Ernst, J. D. Tuberculosis Pathogenesis and Immunity. *Annu. Rev. Pathol.: Mech. Dis.* **7**, 353-384, doi:10.1146/annurev-pathol-011811-132458 (2012).
122 Murray, P. J. & Wynn, T. A. Protective and pathogenic functions of macrophage subsets. *Nat. Rev. Immunol.* **11**, 723-737, doi:10.1038/nri3073 (2011).
123 Fonseca, G. J., Seidman, J. S. & Glass, C. K. Genome-Wide Approaches to Defining Macrophage Identity and Function. *Microbiology Spectrum* **4**, doi:10.1128/microbiolspec.mchd-0039-2016 (2016).
124 Hume, D. A., Summers, K. M. & Rehli, M. Transcriptional Regulation and Macrophage Differentiation. *Microbiology Spectrum* **4**, doi:10.1128/microbiolspec.mchd-0024-2015 (2016).
125 Howard, N. C. *et al.* Publisher Correction: Mycobacterium tuberculosis carrying a rifampicin drug resistance mutation reprograms macrophage metabolism through cell wall lipid changes. *Nat Microbiol* **3**, 1327, doi:10.1038/s41564-018-0281-9 (2018).
126 Cohen, S. B. *et al.* Alveolar Macrophages Provide an Early Mycobacterium tuberculosis Niche and Initiate Dissemination. *Cell Host Microbe* **24**, 439-446.e434, doi:10.1016/j.chom.2018.08.001 (2018).
127 Briken, V., Ahlbrand, S. E. & Shah, S. Mycobacterium tuberculosis and the host cell inflammasome: a complex relationship. *Front. Cell. Infect. Microbiol.* **3**, 62, doi:10.3389/fcimb.2013.00062 (2013).

128 Liu, C. H., Liu, H. & Ge, B. Innate immunity in tuberculosis: host defense vs pathogen evasion. *Cellular & Molecular Immunology* **14**, 963-975, doi:10.1038/cmi.2017.88 (2017).
129 Mishra, B. B. *et al.* Mycobacterium tuberculosis protein ESAT-6 is a potent activator of the NLRP3/ASC inflammasome. *Cell. Microbiol.* **12**, 1046-1063, doi:10.1111/j.1462-5822.2010.01450.x (2010).
130 Mohanty, S., Padhi, A. & Sonawane, A. A novel mechanism of host cell death by ESAT-6 like protein of Mycobacterium tuberculosis. *International Journal of Infectious Diseases* **21**, 356, doi:10.1016/j.ijid.2014.03.1155 (2014).
131 Welin, A., Eklund, D., Stendahl, O. & Lerm, M. Human macrophages infected with a high burden of ESAT-6-expressing M. tuberculosis undergo caspase-1- and cathepsin B-independent necrosis. *PLoS One* **6**, e20302, doi:10.1371/journal.pone.0020302 (2011).
132 TeKippe, E. M. *et al.* Granuloma Formation and Host Defense in Chronic Mycobacterium tuberculosis Infection Requires PYCARD/ASC but Not NLRP3 or Caspase-1. *PLoS ONE* **5**, e12320, doi:10.1371/journal.pone.0012320 (2010).
133 Zhang, Q. *et al.* MCL Plays an Anti-Inflammatory Role inMycobacterium tuberculosis-Induced Immune Response by Inhibiting NF-κB and NLRP3 Inflammasome Activation. *Mediators of Inflammation* **2017**, 1-12, doi:10.1155/2017/2432904 (2017).
134 Coll, R. C. & O'Neill, L. A. J. Correction: The Cytokine Release Inhibitory Drug CRID3 Targets ASC Oligomerisation in the NLRP3 and AIM2 Inflammasomes. *PLoS ONE* **8**, doi:10.1371/annotation/9f221489-155d-4978-a36d-30c51853e438 (2013).
135 Subbarao, S., Sanchez-Garrido, J., Krishnan, N., Shenoy, A. R. & Robertson, B. D. Genetic and pharmacological inhibition of inflammasomes reduces the survival of Mycobacterium tuberculosis strains in macrophages. *Sci. Rep.* **10**, 3709, doi:10.1038/s41598-020-60560-y (2020).
136 Wong, K.-W. & Jacobs, W. R., Jr. Critical role for NLRP3 in necrotic death triggered by Mycobacterium tuberculosis. *Cellular Microbiology* **13**, 1371-1384, doi:10.1111/j.1462-5822.2011.01625.x (2011).
137 Liu, T., Zhang, L., Joo, D. & Sun, S.-C. NF-κB signaling in inflammation. *Signal Transduction and Targeted Therapy* **2**, doi:10.1038/sigtrans.2017.23 (2017).
138 Bai, X. *et al.* Inhibition of nuclear factor-kappa B activation decreases survival of Mycobacterium tuberculosis in human macrophages. *PLoS One* **8**, e61925, doi:10.1371/journal.pone.0061925 (2013).
139 Fong, C. H. Y. *et al.* An antiinflammatory role for IKKβ through the inhibition of "classical" macrophage activation. *The Journal of Experimental Medicine* **205**, 1269-1276, doi:10.1084/jem.20080124 (2008).
140 Greten, F. R. *et al.* NF-κB Is a Negative Regulator of IL-1β Secretion as Revealed by Genetic and Pharmacological Inhibition of IKKβ. *Cell* **130**, 918-931, doi:10.1016/j.cell.2007.07.009 (2007).
141 Kirby, A. C., Coles, M. C. & Kaye, P. M. Alveolar macrophages transport pathogens to lung draining lymph nodes. *J. Immunol.* **183**, 1983-1989, doi:10.4049/jimmunol.0901089 (2009).
142 Wolf, A. J. *et al.* Initiation of the adaptive immune response to Mycobacterium tuberculosis depends on antigen production in the local lymph node, not the lungs. *J. Exp. Med.* **205**, 105-115, doi:10.1084/jem.20071367 (2008).

143 Domingo-Gonzalez, R., Prince, O., Cooper, A. & Khader, S. A. Cytokines and Chemokines in Mycobacterium tuberculosis Infection. *Microbiol Spectr* **4**, doi:10.1128/microbiolspec.TBTB2-0018-2016 (2016).
144 Cambier, C. J., O'Leary, S. M., O'Sullivan, M. P., Keane, J. & Ramakrishnan, L. Phenolic Glycolipid Facilitates Mycobacterial Escape from Microbicidal Tissue-Resident Macrophages. *Immunity* **47**, 552-565.e554, doi:10.1016/j.immuni.2017.08.003 (2017).
145 Cambier, C. J. *et al.* Mycobacteria manipulate macrophage recruitment through coordinated use of membrane lipids. *Nature* **505**, 218-222, doi:10.1038/nature12799 (2014).
146 Annunziato, F., Romagnani, C. & Romagnani, S. The 3 major types of innate and adaptive cell-mediated effector immunity. *The Journal of allergy and clinical immunology* **135**, 626-635, doi:10.1016/j.jaci.2014.11.001 (2015).
147 Khader, S. A. & Cooper, A. M. IL-23 and IL-17 in tuberculosis. *Cytokine* **41**, 79-83, doi:10.1016/j.cyto.2007.11.022 (2008).
148 Khader, S. A., Gaffen, S. L. & Kolls, J. K. Th17 cells at the crossroads of innate and adaptive immunity against infectious diseases at the mucosa. *Mucosal Immunology* **2**, 403-411, doi:10.1038/mi.2009.100 (2009).
149 Kolls, J. K. & Khader, S. A. TH17 Cytokines in Primary Mucosal Immunity. *TH17 Cells in Health and Disease*, 243-256, doi:10.1007/978-1-4419-9371-7_13 (2011).
150 Lin, Y., Slight, S. R. & Khader, S. A. Th17 cytokines and vaccine-induced immunity. *Seminars in Immunopathology* **32**, 79-90, doi:10.1007/s00281-009-0191-2 (2010).
151 Monin, L. *et al.* Immune requirements for protective Th17 recall responses to Mycobacterium tuberculosis challenge. *Mucosal Immunol.* **8**, 1099-1109, doi:10.1038/mi.2014.136 (2015).
152 Torrado, E. & Cooper, A. M. IL-17 and Th17 cells in tuberculosis. *Cytokine & Growth Factor Reviews* **21**, 455-462, doi:10.1016/j.cytogfr.2010.10.004 (2010).
153 Divangahi, M., King, I. L. & Pernet, E. Alveolar macrophages and type I IFN in airway homeostasis and immunity. *Trends Immunol.* **36**, 307-314, doi:10.1016/j.it.2015.03.005 (2015).
154 Cole, S. T., Eisenach, K. D., McMurray, D. N. & Jacobs, J., William R.,. *Tuberculosis and the Tubercle Bacillus*. (American Society of Microbiology, 2005).
155 Abebe, F. Synergy between Th1 and Th2 responses during Mycobacterium tuberculosis infection: A review of current understanding. *International Reviews of Immunology* **38**, 172-179, doi:10.1080/08830185.2019.1632842 (2019).
156 Salgame, P. Host innate and Th1 responses and the bacterial factors that control Mycobacterium tuberculosis infection. *Current Opinion in Immunology* **17**, 374-380, doi:10.1016/j.coi.2005.06.006 (2005).
157 Bai, X., Wilson, S. E., Chmura, K., Feldman, N. E. & Chan, E. D. Morphometric analysis of Th1 and Th2 cytokine expression in human pulmonary tuberculosis. *Tuberculosis* **84**, 375-385, doi:10.1016/j.tube.2004.05.001 (2004).
158 Vesosky, B., Flaherty, D. K. & Turner, J. Th1 Cytokines Facilitate CD8-T-Cell-Mediated Early Resistance to Infection with Mycobacterium tuberculosis in Old Mice. *Infection and Immunity* **74**, 3314-3324, doi:10.1128/iai.01475-05 (2006).
159 Rakshit, S. *et al.* BCG revaccination boosts adaptive polyfunctional Th1/Th17 and innate effectors in IGRA+ and IGRA- Indian adults. *JCI Insight* **4**, doi:10.1172/jci.insight.130540 (2019).

160 Su, H., Peng, B., Zhang, Z., Liu, Z. & Zhang, Z. The Mycobacterium tuberculosis glycoprotein Rv1016c protein inhibits dendritic cell maturation, and impairs Th1 /Th17 responses during mycobacteria infection. *Mol. Immunol.* **109**, 58-70, doi:10.1016/j.molimm.2019.02.021 (2019).
161 Fillatreau, S. & O'Garra, A. *Interleukin-10 in Health and Disease*. (Springer, 2014).
162 Ouyang, W. & O'Garra, A. IL-10 Family Cytokines IL-10 and IL-22: from Basic Science to Clinical Translation. *Immunity* **50**, 871-891, doi:10.1016/j.immuni.2019.03.020 (2019).
163 Srivastava, S. & Ernst, J. D. Cutting edge: Direct recognition of infected cells by CD4 T cells is required for control of intracellular Mycobacterium tuberculosis in vivo. *J. Immunol.* **191**, 1016-1020, doi:10.4049/jimmunol.1301236 (2013).
164 Sakai, S. *et al.* Cutting edge: control of Mycobacterium tuberculosis infection by a subset of lung parenchyma-homing CD4 T cells. *J. Immunol.* **192**, 2965-2969, doi:10.4049/jimmunol.1400019 (2014).
165 Sallin, M. A. *et al.* Th1 Differentiation Drives the Accumulation of Intravascular, Non-protective CD4 T Cells during Tuberculosis. *Cell Rep.* **18**, 3091-3104, doi:10.1016/j.celrep.2017.03.007 (2017).
166 Hall, J. D. *et al.* The impact of chemokine receptor CX3CR1 deficiency during respiratory infections with Mycobacterium tuberculosis or Francisella tularensis. *Clin. Exp. Immunol.* **156**, 278-284, doi:10.1111/j.1365-2249.2009.03882.x (2009).
167 Kauffman, K. D. *et al.* Defective positioning in granulomas but not lung-homing limits CD4 T-cell interactions with Mycobacterium tuberculosis-infected macrophages in rhesus macaques. *Mucosal Immunol.* **11**, 462-473, doi:10.1038/mi.2017.60 (2018).
168 Hoft, S. G. *et al.* The Rate of CD4 T Cell Entry into the Lungs during Mycobacterium tuberculosis Infection Is Determined by Partial and Opposing Effects of Multiple Chemokine Receptors. *Infect. Immun.* **87**, doi:10.1128/IAI.00841-18 (2019).
169 Srivastava, M. *et al.* Mediator responses of alveolar macrophages and kinetics of mononuclear phagocyte subset recruitment during acute primary and secondary mycobacterial infections in the lungs of mice. *Cell. Microbiol.* **9**, 738-752, doi:10.1111/j.1462-5822.2006.00824.x (2007).
170 Phuah, J. Y., Mattila, J. T., Lin, P. L. & Flynn, J. L. Activated B cells in the granulomas of nonhuman primates infected with Mycobacterium tuberculosis. *Am. J. Pathol.* **181**, 508-514, doi:10.1016/j.ajpath.2012.05.009 (2012).
171 Ardain, A. *et al.* Group 3 innate lymphoid cells mediate early protective immunity against tuberculosis. *Nature* **570**, 528-532, doi:10.1038/s41586-019-1276-2 (2019).
172 Slight, S. R. *et al.* CXCR5+ T helper cells mediate protective immunity against tuberculosis. *The Journal of Clinical Investigation* **123**, 712-726, doi:10.1172/JCI65728 (2013).
173 Gopal, R. *et al.* Interleukin-17-dependent CXCL13 mediates mucosal vaccine–induced immunity against tuberculosis. *Mucosal Immunology* **6**, 972-984, doi:10.1038/mi.2012.135 (2013).
174 Peters, W. *et al.* Chemokine receptor 2 serves an early and essential role in resistance to Mycobacterium tuberculosis. *Proc. Natl. Acad. Sci. U. S. A.* **98**, 7958-7963, doi:10.1073/pnas.131207398 (2001).
175 Hohl, T. M. *et al.* Inflammatory monocytes facilitate adaptive CD4 T cell responses during respiratory fungal infection. *Cell Host Microbe* **6**, 470-481, doi:10.1016/j.chom.2009.10.007 (2009).

176 Scott, H. M. & Flynn, J. L. Mycobacterium tuberculosis in Chemokine Receptor 2-Deficient Mice: Influence of Dose on Disease Progression. *Infect. Immun.* **70**, 5946-5954, doi:10.1128/iai.70.11.5946-5954.2002 (2002).
177 Ramos-Martinez, A. G. *et al.* Variability in the virulence of specific Mycobacterium tuberculosis clinical isolates alters the capacity of human dendritic cells to signal for T cells. *Mem. Inst. Oswaldo Cruz* **114**, e190102, doi:10.1590/0074-02760190102 (2019).
178 McShane, H. Protective Immunity against Mycobacterium tuberculosis Induced by Dendritic Cells Pulsed with both CD8 - and CD4 -T-Cell Epitopes from Antigen 85A. *Infection and Immunity* **70**, 1623-1626, doi:10.1128/iai.70.3.1623-1626.2002 (2002).
179 Ehlers, S. & Schaible, U. E. The granuloma in tuberculosis: dynamics of a host-pathogen collusion. *Front. Immunol.* **3**, 411, doi:10.3389/fimmu.2012.00411 (2012).
180 Flynn, J. L. & Ernst, J. D. Immune responses in tuberculosis. *Current Opinion in Immunology* **12**, 432-436, doi:10.1016/s0952-7915(00)00116-3 (2000).
181 Ernst, J. D. The immunological life cycle of tuberculosis. *Nature Reviews Immunology* **12**, 581-591, doi:10.1038/nri3259 (2012).
182 Leong, F., Eum, S., Via, L. & Barry, C. Pathology of Tuberculosis in the Human Lung. *A Color Atlas of Comparative Pathology of Pulmonary Tuberculosis*, 53-81, doi:10.1201/ebk1439835272-8 (2010).
183 Davis, J. M., Muse Davis, J. & Ramakrishnan, L. The Role of the Granuloma in Expansion and Dissemination of Early Tuberculous Infection. *Cell* **136**, 37-49, doi:10.1016/j.cell.2008.11.014 (2009).
184 Ehlers, S. TB or not TB? Fishing for Molecules Making Permissive granulomas. *Cell Host Microbe* **7**, 6-8, doi:10.1016/j.chom.2009.12.010 (2010).
185 Volkman, H. E. *et al.* Tuberculous granuloma induction via interaction of a bacterial secreted protein with host epithelium. *Science* **327**, 466-469, doi:10.1126/science.1179663 (2010).
186 Cumming, B. M. *et al.* Mycobacterium tuberculosis arrests host cycle at the G1/S transition to establish long term infection. *PLOS Pathogens* **13**, e1006389, doi:10.1371/journal.ppat.1006389 (2017).
187 Kaushal, D. *et al.* Mucosal vaccination with attenuated Mycobacterium tuberculosis induces strong central memory responses and protects against tuberculosis. *Nat. Commun.* **6**, 8533, doi:10.1038/ncomms9533 (2015).
188 Khader, S. A. Th17 cytokines: The good, the bad, and the unknown. *Cytokine & Growth Factor Reviews* **21**, 403-404, doi:10.1016/j.cytogfr.2010.10.008 (2010).
189 Yeremeev, V., Linge, I., Kondratieva, T. & Apt, A. Neutrophils exacerbate tuberculosis infection in genetically susceptible mice. *Tuberculosis* **95**, 447-451, doi:10.1016/j.tube.2015.03.007 (2015).
190 Nouailles, G. *et al.* CXCL5-secreting pulmonary epithelial cells drive destructive neutrophilic inflammation in tuberculosis. *J. Clin. Invest.* **124**, 1268-1282, doi:10.1172/JCI72030 (2014).
191 Gopal, R. *et al.* S100A8/A9 proteins mediate neutrophilic inflammation and lung pathology during tuberculosis. *Am. J. Respir. Crit. Care Med.* **188**, 1137-1146, doi:10.1164/rccm.201304-0803OC (2013).
192 Dunlap, M. D. *et al.* Formation of Lung Inducible Bronchus Associated Lymphoid Tissue Is Regulated by Mycobacterium tuberculosis Expressed Determinants. *Frontiers in Immunology* **11**, doi:10.3389/fimmu.2020.01325 (2020).

193 Guenin-Macé, L., Siméone, R. & Demangel, C. Lipids of Pathogenic Mycobacteria: Contributions to Virulence and Host Immune Suppression. *Transboundary and Emerging Diseases* **56**, 255-268, doi:10.1111/j.1865-1682.2009.01072.x (2009).
194 Bansal-Mutalik, R. & Nikaido, H. Mycobacterial outer membrane is a lipid bilayer and the inner membrane is unusually rich in diacyl phosphatidylinositol dimannosides. *Proc. Natl. Acad. Sci. U. S. A.* **111**, 4958-4963, doi:10.1073/pnas.1403078111 (2014).
195 Daffé, M. & Draper, P. The envelope layers of mycobacteria with reference to their pathogenicity. *Adv. Microb. Physiol.* **39**, 131-203, doi:10.1016/s0065-2911(08)60016-8 (1998).
196 Daffé, M. & Reyrat, J.-M. *The Mycobacterial Cell Envelope*. (Amer Society for Microbiology, 2008).
197 Fu, L. M. & Fu-Liu, C. S. Is Mycobacterium tuberculosis a closer relative to Gram-positive or Gram–negative bacterial pathogens? *Tuberculosis* **82**, 85-90, doi:10.1054/tube.2002.0328 (2002).
198 Prasanna, A. N. & Mehra, S. Comparative phylogenomics of pathogenic and non-pathogenic mycobacterium. *PLoS One* **8**, e71248, doi:10.1371/journal.pone.0071248 (2013).
199 Malhotra, S., Vedithi, S. C. & Blundell, T. L. Decoding the similarities and differences among mycobacterial species. *PLoS Negl. Trop. Dis.* **11**, e0005883, doi:10.1371/journal.pntd.0005883 (2017).
200 Kalscheuer, R. *et al.* The Mycobacterium tuberculosis capsule: a cell structure with key implications in pathogenesis. *Biochemical Journal* **476**, 1995-2016, doi:10.1042/bcj20190324 (2019).
201 Angala, S. K., Belardinelli, J. M., Huc-Claustre, E., Wheat, W. H. & Jackson, M. The cell envelope glycoconjugates of Mycobacterium tuberculosis. *Crit. Rev. Biochem. Mol. Biol.* **49**, 361-399, doi:10.3109/10409238.2014.925420 (2014).
202 Jankute, M., Cox, J. A. G., Harrison, J. & Besra, G. S. Assembly of the Mycobacterial Cell Wall. *Annu. Rev. Microbiol.* **69**, 405-423, doi:10.1146/annurev-micro-091014-104121 (2015).
203 Alderwick, L. J., Harrison, J., Lloyd, G. S. & Birch, H. L. The Mycobacterial Cell Wall—Peptidoglycan and Arabinogalactan. *Cold Spring Harbor Perspectives in Medicine* **5**, a021113, doi:10.1101/cshperspect.a021113 (2015).
204 Barry, C. E., 3rd *et al.* Mycolic acids: structure, biosynthesis and physiological functions. *Prog. Lipid Res.* **37**, 143-179, doi:10.1016/s0163-7827(98)00008-3 (1998).
205 Liu, J., Barry, C. E., 3rd, Besra, G. S. & Nikaido, H. Mycolic acid structure determines the fluidity of the mycobacterial cell wall. *J. Biol. Chem.* **271**, 29545-29551, doi:10.1074/jbc.271.47.29545 (1996).
206 Linde, C. M., Hoffner, S. E., Refai, E. & Andersson, M. In vitro activity of PR-39, a proline-arginine-rich peptide, against susceptible and multi-drug-resistant Mycobacterium tuberculosis. *J. Antimicrob. Chemother.* **47**, 575-580, doi:10.1093/jac/47.5.575 (2001).
207 Moxon, E. R. & Kroll, J. S. The role of bacterial polysaccharide capsules as virulence factors. *Curr. Top. Microbiol. Immunol.* **150**, 65-85, doi:10.1007/978-3-642-74694-9_4 (1990).

208 Stokes, R. W., Thorson, L. M. & Speert, D. P. Nonopsonic and opsonic association of Mycobacterium tuberculosis with resident alveolar macrophages is inefficient. *J. Immunol.* **160**, 5514-5521 (1998).
209 Brennan, P. J. & Crick, D. C. The cell-wall core of Mycobacterium tuberculosis in the context of drug discovery. *Curr. Top. Med. Chem.* **7**, 475-488, doi:10.2174/156802607780059763 (2007).
210 Constant, P. *et al.* Role of the pks15/1 gene in the biosynthesis of phenolglycolipids in the Mycobacterium tuberculosis complex. Evidence that all strains synthesize glycosylated p-hydroxybenzoic methyl esters and that strains devoid of phenolglycolipids harbor a frameshift mutation in the pks15/1 gene. *J. Biol. Chem.* **277**, 38148-38158, doi:10.1074/jbc.M206538200 (2002).
211 Keating, T. A. & Walsh, C. T. Initiation, elongation, and termination strategies in polyketide and polypeptide antibiotic biosynthesis. *Current Opinion in Chemical Biology* **3**, 598-606, doi:10.1016/s1367-5931(99)00015-0 (1999).
212 Gavalda, S. *et al.* The Polyketide Synthase Pks13 Catalyzes a Novel Mechanism of Lipid Transfer in Mycobacteria. *Chemistry & Biology* **21**, 1660-1669, doi:10.1016/j.chembiol.2014.10.011 (2014).
213 Portevin, D. *et al.* A polyketide synthase catalyzes the last condensation step of mycolic acid biosynthesis in mycobacteria and related organisms. *Proc. Natl. Acad. Sci. U. S. A.* **101**, 314-319, doi:10.1073/pnas.0305439101 (2004).
214 Dubey, V. S., Sirakova, T. D. & Kolattukudy, P. E. Disruption of msl3 abolishes the synthesis of mycolipanoic and mycolipenic acids required for polyacyltrehalose synthesis in Mycobacterium tuberculosis H37Rv and causes cell aggregation. *Molecular Microbiology* **45**, 1451-1459, doi:10.1046/j.1365-2958.2002.03119.x (2002).
215 Rainwater, D. L. & Kolattukudy, P. E. Fatty acid biosynthesis in Mycobacterium tuberculosis var. bovis Bacillus Calmette-Guérin. Purification and characterization of a novel fatty acid synthase, mycocerosic acid synthase, which elongates n-fatty acyl-CoA with methylmalonyl-CoA. *J. Biol. Chem.* **260**, 616-623 (1985).
216 Sirakova, T. D., Thirumala, A. K., Dubey, V. S., Sprecher, H. & Kolattukudy, P. E. The Mycobacterium tuberculosis pks2 gene encodes the synthase for the hepta- and octamethyl-branched fatty acids required for sulfolipid synthesis. *J. Biol. Chem.* **276**, 16833-16839, doi:10.1074/jbc.M011468200 (2001).
217 Rousseau, C. *et al.* Virulence attenuation of two Mas-like polyketide synthase mutants of Mycobacterium tuberculosis. *Microbiology* **149**, 1837-1847, doi:10.1099/mic.0.26278-0 (2003).
218 Tsenova, L. *et al.* Virulence of selected Mycobacterium tuberculosis clinical isolates in the rabbit model of meningitis is dependent on phenolic glycolipid produced by the bacilli. *J. Infect. Dis.* **192**, 98-106, doi:10.1086/430614 (2005).
219 Gonzalo Asensio, J. *et al.* The virulence-associated two-component PhoP-PhoR system controls the biosynthesis of polyketide-derived lipids in Mycobacterium tuberculosis. *J. Biol. Chem.* **281**, 1313-1316, doi:10.1074/jbc.C500388200 (2006).
220 Prados-Rosales, R. *et al.* Enhanced control of Mycobacterium tuberculosis extrapulmonary dissemination in mice by an arabinomannan-protein conjugate vaccine. *PLoS Pathog.* **13**, e1006250, doi:10.1371/journal.ppat.1006250 (2017).

221 Ortalo-Magné, A. *et al.* Identification of the surface-exposed lipids on the cell envelopes of Mycobacterium tuberculosis and other mycobacterial species. *J. Bacteriol.* **178**, 456-461, doi:10.1128/jb.178.2.456-461.1996 (1996).
222 Domingo-Gonzalez, R. *et al.* Interleukin-17 limits hypoxia-inducible factor 1α and development of hypoxic granulomas during tuberculosis. *JCI Insight* **2**, doi:10.1172/jci.insight.92973 (2017).
223 Sinsimer, D. *et al.* The phenolic glycolipid of Mycobacterium tuberculosis differentially modulates the early host cytokine response but does not in itself confer hypervirulence. *Infect. Immun.* **76**, 3027-3036, doi:10.1128/IAI.01663-07 (2008).
224 Manca, C. *et al.* Differential Monocyte Activation Underlies Strain-Specific Mycobacterium tuberculosis Pathogenesis. *Infection and Immunity* **72**, 5511-5514, doi:10.1128/iai.72.9.5511-5514.2004 (2004).
225 Reed, M. B. *et al.* A glycolipid of hypervirulent tuberculosis strains that inhibits the innate immune response. *Nature* **431**, 84-87, doi:10.1038/nature02837 (2004).
226 Cox, J. S., Chen, B., McNeil, M. & Jacobs, W. R., Jr. Complex lipid determines tissue-specific replication of Mycobacterium tuberculosis in mice. *Nature* **402**, 79-83, doi:10.1038/47042 (1999).
227 Jain, M. & Cox, J. S. Interaction between polyketide synthase and transporter suggests coupled synthesis and export of virulence lipid in M. tuberculosis. *PLoS Pathog.* **1**, e2, doi:10.1371/journal.ppat.0010002 (2005).
228 Viljoen, A. *et al.* The diverse family of MmpL transporters in mycobacteria: from regulation to antimicrobial developments. *Molecular Microbiology* **104**, 889-904, doi:10.1111/mmi.13675 (2017).
229 Torrelles, J. B. & Schlesinger, L. S. Integrating Lung Physiology, Immunology, and Tuberculosis. *Trends Microbiol.* **25**, 688-697, doi:10.1016/j.tim.2017.03.007 (2017).
230 Cambi, A. & Figdor, C. G. Levels of complexity in pathogen recognition by C-type lectins. *Curr. Opin. Immunol.* **17**, 345-351, doi:10.1016/j.coi.2005.05.011 (2005).
231 Arbués, A. *et al.* Trisaccharides of Phenolic Glycolipids Confer Advantages to Pathogenic Mycobacteria through Manipulation of Host-Cell Pattern-Recognition Receptors. *ACS Chem. Biol.* **11**, 2865-2875, doi:10.1021/acschembio.6b00568 (2016).
232 Cywes, C. *et al.* Nonopsonic binding of Mycobacterium tuberculosis to human complement receptor type 3 expressed in Chinese hamster ovary cells. *Infect. Immun.* **64**, 5373-5383 (1996).
233 Hu, C., Mayadas-Norton, T., Tanaka, K., Chan, J. & Salgame, P. Mycobacterium tuberculosis infection in complement receptor 3-deficient mice. *J. Immunol.* **165**, 2596-2602, doi:10.4049/jimmunol.165.5.2596 (2000).
234 Oldenburg, R. & Demangel, C. Pathogenic and immunosuppressive properties of mycobacterial phenolic glycolipids. *Biochimie* **141**, 3-8, doi:10.1016/j.biochi.2017.03.012 (2017).
235 Rooyakkers, A. W. J. & Stokes, R. W. Absence of complement receptor 3 results in reduced binding and ingestion of Mycobacterium tuberculosis but has no significant effect on the induction of reactive oxygen and nitrogen intermediates or on the survival of the bacteria in resident and interferon-gamma activated macrophages. *Microb. Pathog.* **39**, 57-67, doi:10.1016/j.micpath.2005.05.001 (2005).

236 Tailleux, L. *et al.* DC-SIGN induction in alveolar macrophages defines privileged target host cells for mycobacteria in patients with tuberculosis. *PLoS Med.* **2**, e381, doi:10.1371/journal.pmed.0020381 (2005).
237 Tailleux, L. *et al.* DC-SIGN is the major Mycobacterium tuberculosis receptor on human dendritic cells. *J. Exp. Med.* **197**, 121-127, doi:10.1084/jem.20021468 (2003).
238 Geurtsen, J. *et al.* Identification of Mycobacterial α-Glucan As a Novel Ligand for DC-SIGN: Involvement of Mycobacterial Capsular Polysaccharides in Host Immune Modulation. *The Journal of Immunology* **183**, 5221-5231, doi:10.4049/jimmunol.0900768 (2009).
239 Ehlers, S. DC-SIGN and mannosylated surface structures of Mycobacterium tuberculosis: a deceptive liaison. *Eur. J. Cell Biol.* **89**, 95-101, doi:10.1016/j.ejcb.2009.10.004 (2010).
240 Geijtenbeek, T. B. H. *et al.* Mycobacteria target DC-SIGN to suppress dendritic cell function. *J. Exp. Med.* **197**, 7-17, doi:10.1084/jem.20021229 (2003).
241 van Kooyk, Y. & Geijtenbeek, T. B. H. DC-SIGN: escape mechanism for pathogens. *Nat. Rev. Immunol.* **3**, 697-709, doi:10.1038/nri1182 (2003).
242 Majlessi, L., Prados-Rosales, R., Casadevall, A. & Brosch, R. Release of mycobacterial antigens. *Immunol. Rev.* **264**, 25-45, doi:10.1111/imr.12251 (2015).
243 Joller, N. *et al.* Antibodies protect against intracellular bacteria by Fc receptor-mediated lysosomal targeting. *Proceedings of the National Academy of Sciences* **107**, 20441-20446, doi:10.1073/pnas.1013827107 (2010).
244 Chen, T. *et al.* Association of Human Antibodies to Arabinomannan With Enhanced Mycobacterial Opsonophagocytosis and Intracellular Growth Reduction. *J. Infect. Dis.* **214**, 300-310, doi:10.1093/infdis/jiw141 (2016).
245 Zarember, K. A. & Godowski, P. J. Tissue expression of human Toll-like receptors and differential regulation of Toll-like receptor mRNAs in leukocytes in response to microbes, their products, and cytokines. *J. Immunol.* **168**, 554-561, doi:10.4049/jimmunol.168.2.554 (2002).
246 Gilleron, M., Nigou, J., Nicolle, D., Quesniaux, V. & Puzo, G. The Acylation State of Mycobacterial Lipomannans Modulates Innate Immunity Response through Toll-like Receptor 2. *Chemistry & Biology* **13**, 39-47, doi:10.1016/j.chembiol.2005.10.013 (2006).
247 Quesniaux, V. J. *et al.* Toll-like receptor 2 (TLR2)-dependent-positive and TLR2-independent-negative regulation of proinflammatory cytokines by mycobacterial lipomannans. *J. Immunol.* **172**, 4425-4434, doi:10.4049/jimmunol.172.7.4425 (2004).
248 Nigou, J. *et al.* Mycobacterial lipoarabinomannans: modulators of dendritic cell function and the apoptotic response. *Microbes Infect.* **4**, 945-953, doi:10.1016/s1286-4579(02)01621-0 (2002).
249 Nigou, J., Zelle-Rieser, C., Gilleron, M., Thurnher, M. & Puzo, G. Mannosylated lipoarabinomannans inhibit IL-12 production by human dendritic cells: evidence for a negative signal delivered through the mannose receptor. *J. Immunol.* **166**, 7477-7485, doi:10.4049/jimmunol.166.12.7477 (2001).
250 Johansson, U. Inhibition of IL-12 production in human dendritic cells matured in the presence of Bacillus Calmette–Guerin or lipoarabinomannan. *Immunology Letters* **77**, 63-66, doi:10.1016/s0165-2478(01)00190-0 (2001).
251 Reed, M. B., Gagneux, S., Deriemer, K., Small, P. M. & Barry, C. E., 3rd. The W-Beijing lineage of Mycobacterium tuberculosis overproduces triglycerides and has the DosR

dormancy regulon constitutively upregulated. *J. Bacteriol.* **189**, 2583-2589, doi:10.1128/JB.01670-06 (2007).
252 Huet, G. *et al.* A lipid profile typifies the Beijing strains of Mycobacterium tuberculosis: identification of a mutation responsible for a modification of the structures of phthiocerol dimycocerosates and phenolic glycolipids. *J. Biol. Chem.* **284**, 27101-27113, doi:10.1074/jbc.M109.041939 (2009).
253 Manca, C. *et al.* Hypervirulent M. tuberculosis W/Beijing strains upregulate type I IFNs and increase expression of negative regulators of the Jak-Stat pathway. *J. Interferon Cytokine Res.* **25**, 694-701, doi:10.1089/jir.2005.25.694 (2005).
254 Fäldt, J. *et al.* Activation of human neutrophils by mycobacterial phenolic glycolipids. *Clin. Exp. Immunol.* **118**, 253-260, doi:10.1046/j.1365-2249.1999.01040.x (1999).
255 Nabatov, A. A., Hatzis, P., Rouschop, K. M. A., van Diest, P. & Vooijs, M. Hypoxia inducible NOD2 interacts with 3-O-sulfogalactoceramide and regulates vesicular homeostasis. *Biochim. Biophys. Acta* **1830**, 5277-5286, doi:10.1016/j.bbagen.2013.07.017 (2013).
256 Brozna, J. P., Horan, M., Rademacher, J. M., Pabst, K. M. & Pabst, M. J. Monocyte responses to sulfatide from Mycobacterium tuberculosis: inhibition of priming for enhanced release of superoxide, associated with increased secretion of interleukin-1 and tumor necrosis factor alpha, and altered protein phosphorylation. *Infection and Immunity* **59**, 2542-2548, doi:10.1128/iai.59.8.2542-2548.1991 (1991).
257 Pabst, M. J., Gross, J. M., Brozna, J. P. & Goren, M. B. Inhibition of macrophage priming by sulfatide from Mycobacterium tuberculosis. *J. Immunol.* **140**, 634-640 (1988).
258 Zhang, L., English, D. & Andersen, B. R. Activation of human neutrophils by Mycobacterium tuberculosis-derived sulfolipid-1. *J. Immunol.* **146**, 2730-2736 (1991).
259 Zhang, L., Goren, M. B., Holzer, T. J. & Andersen, B. R. Effect of Mycobacterium tuberculosis-derived sulfolipid I on human phagocytic cells. *Infection and Immunity* **56**, 2876-2883, doi:10.1128/iai.56.11.2876-2883.1988 (1988).
260 Rousseau, C. *et al.* Production of phthiocerol dimycocerosates protects Mycobacterium tuberculosis from the cidal activity of reactive nitrogen intermediates produced by macrophages and modulates the early immune response to infection. *Cell. Microbiol.* **6**, 277-287, doi:10.1046/j.1462-5822.2004.00368.x (2004).
261 Arbues, A., Lugo-Villarino, G., Neyrolles, O., Guilhot, C. & Astarie-Dequeker, C. Playing hide-and-seek with host macrophages through the use of mycobacterial cell envelope phthiocerol dimycocerosates and phenolic glycolipids. *Front. Cell. Infect. Microbiol.* **4**, 173, doi:10.3389/fcimb.2014.00173 (2014).
262 Feinberg, H. *et al.* Mechanism for Recognition of an Unusual Mycobacterial Glycolipid by the Macrophage Receptor Mincle. *Journal of Biological Chemistry* **288**, 28457-28465, doi:10.1074/jbc.m113.497149 (2013).
263 Feinberg, H. *et al.* Binding Sites for Acylated Trehalose Analogs of Glycolipid Ligands on an Extended Carbohydrate Recognition Domain of the Macrophage Receptor Mincle. *J. Biol. Chem.* **291**, 21222-21233, doi:10.1074/jbc.M116.749515 (2016).
264 Decout, A. *et al.* Rational design of adjuvants targeting the C-type lectin Mincle. *Proc. Natl. Acad. Sci. U. S. A.* **114**, 2675-2680, doi:10.1073/pnas.1612421114 (2017).
265 Lee, K.-S. *et al.* Diacyltrehalose of Mycobacterium tuberculosis inhibits lipopolysaccharide- and mycobacteria-induced proinflammatory cytokine production in

human monocytic cells. *FEMS Microbiol. Lett.* **267**, 121-128, doi:10.1111/j.1574-6968.2006.00553.x (2007).
266 Saavedra, R., Segura, E., Leyva, R., Esparza, L. A. & López-Marín, L. M. Mycobacterial di-O-acyl-trehalose inhibits mitogen- and antigen-induced proliferation of murine T cells in vitro. *Clin. Diagn. Lab. Immunol.* **8**, 1081-1088, doi:10.1128/CDLI.8.6.1-91-1088.2001 (2001).
267 Aguilo, J. I. *et al.* ESX-1-induced apoptosis is involved in cell-to-cell spread of Mycobacterium tuberculosis. *Cell. Microbiol.* **15**, 1994-2005, doi:10.1111/cmi.12169 (2013).
268 Quigley, J. *et al.* The Cell Wall Lipid PDIM Contributes to Phagosomal Escape and Host Cell Exit of. *MBio* **8**, doi:10.1128/mBio.00148-17 (2017).
269 Fratti, R. A., Backer, J. M., Gruenberg, J., Corvera, S. & Deretic, V. Role of phosphatidylinositol 3-kinase and Rab5 effectors in phagosomal biogenesis and mycobacterial phagosome maturation arrest. *J. Cell Biol.* **154**, 631-644, doi:10.1083/jcb.200106049 (2001).
270 Fratti, R. A., Chua, J., Vergne, I. & Deretic, V. Mycobacterium tuberculosis glycosylated phosphatidylinositol causes phagosome maturation arrest. *Proc. Natl. Acad. Sci. U. S. A.* **100**, 5437-5442, doi:10.1073/pnas.0737613100 (2003).
271 Axelrod, S. *et al.* Delay of phagosome maturation by a mycobacterial lipid is reversed by nitric oxide. *Cell. Microbiol.* **10**, 1530-1545, doi:10.1111/j.1462-5822.2008.01147.x (2008).
272 Day, T. A. *et al.* Mycobacterium tuberculosis strains lacking surface lipid phthiocerol dimycocerosate are susceptible to killing by an early innate host response. *Infect. Immun.* **82**, 5214-5222, doi:10.1128/IAI.01340-13 (2014).
273 Vergne, I. *et al.* Mycobacterium tuberculosis phagosome maturation arrest: mycobacterial phosphatidylinositol analog phosphatidylinositol mannoside stimulates early endosomal fusion. *Mol. Biol. Cell* **15**, 751-760, doi:10.1091/mbc.e03-05-0307 (2004).
274 Goren, M. B., D'Arcy Hart, P., Young, M. R. & Armstrong, J. A. Prevention of phagosome-lysosome fusion in cultured macrophages by sulfatides of Mycobacterium tuberculosis. *Proceedings of the National Academy of Sciences* **73**, 2510-2514, doi:10.1073/pnas.73.7.2510 (1976).
275 Goren, M. B., Vatter, A. E. & Fiscus, J. Polyanionic agents as inhibitors of phagosome-lysosome fusion in cultured macrophages: evolution of an alternative interpretation. *J. Leukoc. Biol.* **41**, 111-121, doi:10.1002/jlb.41.2.111 (1987).
276 Brodin, P. *et al.* High content phenotypic cell-based visual screen identifies Mycobacterium tuberculosis acyltrehalose-containing glycolipids involved in phagosome remodeling. *PLoS Pathog.* **6**, e1001100, doi:10.1371/journal.ppat.1001100 (2010).
277 Kato, M. & Goren, M. B. Synergistic Action of Cord Factor and Mycobacterial Sulfatides on Mitochondria. *Infection and Immunity* **10**, 733-741, doi:10.1128/iai.10.4.733-741.1974 (1974).
278 Wadee, A. A., Kuschke, R. H. & Dooms, T. G. The inhibitory effects of Mycobacterium tuberculosis on MHC class II expression by monocytes activated with riminophenazines and phagocyte stimulants. *Clinical & Experimental Immunology* **100**, 434-439, doi:10.1111/j.1365-2249.1995.tb03718.x (2008).

279 Rocha-Ramírez, L. M. *et al.* Mycobacterium tuberculosis lipids regulate cytokines, TLR-2/4 and MHC class II expression in human macrophages. *Tuberculosis* **88**, 212-220, doi:10.1016/j.tube.2007.10.003 (2008).
280 Hava, D. L. *et al.* Evasion of peptide, but not lipid antigen presentation, through pathogen-induced dendritic cell maturation. *Proc. Natl. Acad. Sci. U. S. A.* **105**, 11281-11286, doi:10.1073/pnas.0804681105 (2008).
281 Harding, C. V. & Henry Boom, W. Regulation of antigen presentation by Mycobacterium tuberculosis: a role for Toll-like receptors. *Nat. Rev. Microbiol.* **8**, 296-307, doi:10.1038/nrmicro2321 (2010).
282 Torres, M. *et al.* Role of Phagosomes and Major Histocompatibility Complex Class II (MHC-II) Compartment in MHC-II Antigen Processing of Mycobacterium tuberculosis in Human Macrophages. *Infection and Immunity* **74**, 1621-1630, doi:10.1128/iai.74.3.1621-1630.2006 (2006).
283 Fulton, S. A. *et al.* Inhibition of major histocompatibility complex II expression and antigen processing in murine alveolar macrophages by Mycobacterium bovis BCG and the 19-kilodalton mycobacterial lipoprotein. *Infect. Immun.* **72**, 2101-2110, doi:10.1128/iai.72.4.2101-2110.2004 (2004).
284 Pinto, R. *et al.* Influence of phthiocerol dimycocerosate on CD4 T cell priming and persistence during Mycobacterium tuberculosis infection. *Tuberculosis* **99**, 25-30, doi:10.1016/j.tube.2016.04.001 (2016).
285 Garcia-Vilanova, A., Chan, J. & Torrelles, J. B. Underestimated Manipulative Roles of Mycobacterium tuberculosis Cell Envelope Glycolipids During Infection. *Frontiers in Immunology* **10**, doi:10.3389/fimmu.2019.02909 (2019).
286 Choreño-Parra, J. A. *et al.* Mycobacterium tuberculosis HN878 Infection Induces Human-Like B-Cell Follicles in Mice. *J. Infect. Dis.* **221**, 1636-1646, doi:10.1093/infdis/jiz663 (2020).
287 Jeyanathan, M., Yao, Y., Afkhami, S., Smaill, F. & Xing, Z. New Tuberculosis Vaccine Strategies: Taking Aim at Un-Natural Immunity. *Trends Immunol.* **39**, 419-433, doi:10.1016/j.it.2018.01.006 (2018).
288 Tian, G., Li, X., Li, H., Wang, X. & Cheng, B. Systematic meta-analysis of the association between monocyte chemoattractant protein-1 -2518A/G polymorphism and risk of tuberculosis. *Genet. Mol. Res.* **14**, 5501-5510, doi:10.4238/2015.May.25.1 (2015).
289 Gopal, R. *et al.* Unexpected role for IL-17 in protective immunity against hypervirulent Mycobacterium tuberculosis HN878 infection. *PLoS Pathog.* **10**, e1004099, doi:10.1371/journal.ppat.1004099 (2014).
290 Yona, S. *et al.* Fate mapping reveals origins and dynamics of monocytes and tissue macrophages under homeostasis. *Immunity* **38**, 79-91, doi:10.1016/j.immuni.2012.12.001 (2013).
291 Antonelli, L. R. V. *et al.* Intranasal Poly-IC treatment exacerbates tuberculosis in mice through the pulmonary recruitment of a pathogen-permissive monocyte/macrophage population. *Journal of Clinical Investigation* **120**, 1674-1682, doi:10.1172/jci40817 (2010).
292 Gagneux, S. & Small, P. M. Global phylogeography of Mycobacterium tuberculosis and implications for tuberculosis product development. *Lancet Infect. Dis.* **7**, 328-337, doi:10.1016/S1473-3099(07)70108-1 (2007).

293 Serbina, N. V., Shi, C. & Pamer, E. G. Monocyte-Mediated Immune Defense Against Murine Listeria monocytogenes Infection. *Immunity to Listeria Monocytogenes*, 119-134, doi:10.1016/b978-0-12-394590-7.00003-8 (2012).
294 Eruslanov, E. B. *et al.* Neutrophil Responses to Mycobacterium tuberculosis Infection in Genetically Susceptible and Resistant Mice. *Infection and Immunity* **73**, 1744-1753, doi:10.1128/iai.73.3.1744-1753.2005 (2005).
295 Lowe, D. M. *et al.* Neutrophilia independently predicts death in tuberculosis: Table 1–. *European Respiratory Journal* **42**, 1752-1757, doi:10.1183/09031936.00140913 (2013).
296 Lowe, D. M., Redford, P. S., Wilkinson, R. J., O'Garra, A. & Martineau, A. R. Neutrophils in tuberculosis: friend or foe? *Trends in Immunology* **33**, 14-25, doi:10.1016/j.it.2011.10.003 (2012).
297 Vásquez-Loarte, T., Trubnykova, M. & Guio, H. Genetic association meta-analysis: a new classification to assess ethnicity using the association of MCP-1 -2518 polymorphism and tuberculosis susceptibility as a model. *BMC Genet.* **16**, doi:10.1186/s12863-015-0280-2 (2015).
298 Pasparakis, M. *et al.* TNF-mediated inflammatory skin disease in mice with epidermis-specific deletion of IKK2. *Nature* **417**, 861-866, doi:10.1038/nature00820 (2002).
299 Wang, J., Gigliotti, F., Bhagwat, S. P., Maggirwar, S. B. & Wright, T. W. Pneumocystisstimulates MCP-1 production by alveolar epithelial cells through a JNK-dependent mechanism. *American Journal of Physiology-Lung Cellular and Molecular Physiology* **292**, L1495-L1505, doi:10.1152/ajplung.00452.2006 (2007).
300 Gautier, E. L. *et al.* Systemic Analysis of PPARγ in Mouse Macrophage Populations Reveals Marked Diversity in Expression with Critical Roles in Resolution of Inflammation and Airway Immunity. *The Journal of Immunology* **189**, 2614-2624, doi:10.4049/jimmunol.1200495 (2012).
301 Love, M. I., Huber, W. & Anders, S. Moderated estimation of fold change and dispersion for RNA-seq data with DESeq2. *Genome Biol.* **15**, 550, doi:10.1186/s13059-014-0550-8 (2014).
302 Roy, S. *et al.* Batf2/Irf1 Induces Inflammatory Responses in Classically Activated Macrophages, Lipopolysaccharides, and Mycobacterial Infection. *The Journal of Immunology* **194**, 6035-6044, doi:10.4049/jimmunol.1402521 (2015).
303 Xu, H. *et al.* Notch–RBP-J signaling regulates the transcription factor IRF8 to promote inflammatory macrophage polarization. *Nature Immunology* **13**, 642-650, doi:10.1038/ni.2304 (2012).
304 Mass, E. *et al.* Specification of tissue-resident macrophages during organogenesis. *Science* **353**, doi:10.1126/science.aaf4238 (2016).
305 Jager, S. C. A. d. *et al.* Growth differentiation factor 15 deficiency protects against atherosclerosis by attenuating CCR2-mediated macrophage chemotaxis. *The Journal of Experimental Medicine* **208**, 217-225, doi:10.1084/jem.20100370 (2011).
306 Hu, J. *et al.* Polo-Like Kinase 1 (PLK1) Is Involved in Toll-like Receptor (TLR)-Mediated TNF-α Production in Monocytic THP-1 Cells. *PLoS ONE* **8**, e78832, doi:10.1371/journal.pone.0078832 (2013).
307 Lyu, J. H., Huang, B., Park, D.-W. & Baek, S.-H. Regulation of PHLDA1 Expression by JAK2-ERK1/2-STAT3 Signaling Pathway. *Journal of Cellular Biochemistry* **117**, 483-490, doi:10.1002/jcb.25296 (2016).

308 Satpathy, A. T. *et al.* Notch2-dependent classical dendritic cells orchestrate intestinal immunity to attaching-and-effacing bacterial pathogens. *Nature Immunology* **14**, 937-948, doi:10.1038/ni.2679 (2013).
309 Lu, B. *et al.* Abnormalities in Monocyte Recruitment and Cytokine Expression in Monocyte Chemoattractant Protein 1–deficient Mice. *Journal of Experimental Medicine* **187**, 601-608, doi:10.1084/jem.187.4.601 (1998).
310 Khader, S. A. *et al.* IL-23 and IL-17 in the establishment of protective pulmonary CD4+ T cell responses after vaccination and during Mycobacterium tuberculosis challenge. *Nat. Immunol.* **8**, 369-377, doi:10.1038/ni1449 (2007).
311 Lin, Y. *et al.* Interleukin-17 Is Required for T Helper 1 Cell Immunity and Host Resistance to the Intracellular Pathogen Francisella tularensis. *Immunity* **31**, 799-810, doi:10.1016/j.immuni.2009.08.025 (2009).
312 Davies, L. C., Jenkins, S. J., Allen, J. E. & Taylor, P. R. Tissue-resident macrophages. *Nature Immunology* **14**, 986-995, doi:10.1038/ni.2705 (2013).
313 Desvignes, L., Wolf, A. J. & Ernst, J. D. Dynamic roles of type I and type II IFNs in early infection with Mycobacterium tuberculosis. *J. Immunol.* **188**, 6205-6215, doi:10.4049/jimmunol.1200255 (2012).
314 Bedoret, D. *et al.* Lung interstitial macrophages alter dendritic cell functions to prevent airway allergy in mice. *Journal of Clinical Investigation* **119**, 3723-3738, doi:10.1172/jci39717 (2009).
315 Jakubzick, C. *et al.* Minimal Differentiation of Classical Monocytes as They Survey Steady-State Tissues and Transport Antigen to Lymph Nodes. *Immunity* **39**, 599-610, doi:10.1016/j.immuni.2013.08.007 (2013).
316 Khader, S. A. *et al.* IL-23 compensates for the absence of IL-12p70 and is essential for the IL-17 response during tuberculosis but is dispensable for protection and antigen-specific IFN-gamma responses if IL-12p70 is available. *J. Immunol.* **175**, 788-795, doi:10.4049/jimmunol.175.2.788 (2005).
317 Kim, D., Langmead, B. & Salzberg, S. L. HISAT: a fast spliced aligner with low memory requirements. *Nature Methods* **12**, 357-360, doi:10.1038/nmeth.3317 (2015).
318 Kanehisa, M., Sato, Y., Kawashima, M., Furumichi, M. & Tanabe, M. KEGG as a reference resource for gene and protein annotation. *Nucleic Acids Research* **44**, D457-D462, doi:10.1093/nar/gkv1070 (2016).
319 Smith, C. L. & Eppig, J. T. The Mammalian Phenotype Ontology as a unifying standard for experimental and high-throughput phenotyping data. *Mammalian Genome* **23**, 653-668, doi:10.1007/s00335-012-9421-3 (2012).
320 Zhang, B., Kirov, S. & Snoddy, J. WebGestalt: an integrated system for exploring gene sets in various biological contexts. *Nucleic Acids Research* **33**, W741-W748, doi:10.1093/nar/gki475 (2005).
321 Schorey, J. S. & Schlesinger, L. S. Innate Immune Responses to Tuberculosis. *Microbiol Spectr* **4**, doi:10.1128/microbiolspec.TBTB2-0010-2016 (2016).
322 Dutta, N. K. *et al.* The stress-response factor SigH modulates the interaction between Mycobacterium tuberculosis and host phagocytes. *PLoS One* **7**, e28958, doi:10.1371/journal.pone.0028958 (2012).
323 Feng, W. X. *et al.* CCL2−2518 (A/G) polymorphisms and tuberculosis susceptibility: a meta-analysis. *Int. J. Tuberc. Lung Dis.* **16**, 150-156, doi:10.5588/ijtld.11.0205 (2012).

324 Flores-Villanueva, P. O. *et al.* A functional promoter polymorphism in monocyte chemoattractant protein-1 is associated with increased susceptibility to pulmonary tuberculosis. *J. Exp. Med.* **202**, 1649-1658, doi:10.1084/jem.20050126 (2005).
325 Brace, P. T. *et al.* Mycobacterium tuberculosis subverts negative regulatory pathways in human macrophages to drive immunopathology. *PLOS Pathogens* **13**, e1006367, doi:10.1371/journal.ppat.1006367 (2017).
326 Koo, M.-S., Subbian, S. & Kaplan, G. Strain specific transcriptional response in Mycobacterium tuberculosis infected macrophages. *Cell Commun. Signal.* **10**, 2, doi:10.1186/1478-811X-10-2 (2012).
327 Choreño-Parra, J. A., Weinstein, L. I., Yunis, E. J., Zúñiga, J. & Hernández-Pando, R. Thinking Outside the Box: Innate- and B Cell-Memory Responses as Novel Protective Mechanisms Against Tuberculosis. *Front. Immunol.* **11**, 226, doi:10.3389/fimmu.2020.00226 (2020).
328 Zembrzuski, V. M. *et al.* Cytokine genes are associated with tuberculin skin test response in a native Brazilian population. *Tuberculosis* **90**, 44-49, doi:10.1016/j.tube.2009.11.002 (2010).
329 Martinez, F. O., Helming, L. & Gordon, S. Alternative activation of macrophages: an immunologic functional perspective. *Annu. Rev. Immunol.* **27**, 451-483, doi:10.1146/annurev.immunol.021908.132532 (2009).
330 Labonte, A. C., Tosello-Trampont, A.-C. & Hahn, Y. S. The role of macrophage polarization in infectious and inflammatory diseases. *Mol. Cells* **37**, 275-285, doi:10.14348/molcells.2014.2374 (2014).
331 Todd, E. M. *et al.* Alveolar macrophage development in mice requires L-plastin for cellular localization in alveoli. *Blood* **128**, 2785-2796, doi:10.1182/blood-2016-03-705962 (2016).
332 Ginhoux, F. Fate PPAR-titioning: PPAR-γ 'instructs' alveolar macrophage development. *Nat. Immunol.* **15**, 1005-1007, doi:10.1038/ni.3011 (2014).
333 Wager, C. M. L., Leopold Wager, C. M., Arnett, E. & Schlesinger, L. S. Macrophage nuclear receptors: Emerging key players in infectious diseases. *PLOS Pathogens* **15**, e1007585, doi:10.1371/journal.ppat.1007585 (2019).
334 Lang, R., Patel, D., Morris, J. J., Rutschman, R. L. & Murray, P. J. Shaping gene expression in activated and resting primary macrophages by IL-10. *J. Immunol.* **169**, 2253-2263, doi:10.4049/jimmunol.169.5.2253 (2002).
335 Mills, C. M1 and M2 Macrophages: Oracles of Health and Disease. *Critical Reviews in Immunology* **32**, 463-488, doi:10.1615/critrevimmunol.v32.i6.10 (2012).
336 Mills, C. D., Lenz, L. L. & Ley, K. *M1/M2 Macrophages: The Arginine Fork in the Road to Health and Disease*. (Frontiers Media SA, 2015).
337 Hesse, M. *et al.* Differential regulation of nitric oxide synthase-2 and arginase-1 by type 1/type 2 cytokines in vivo: granulomatous pathology is shaped by the pattern of L-arginine metabolism. *J. Immunol.* **167**, 6533-6544, doi:10.4049/jimmunol.167.11.6533 (2001).
338 Verreck, F. A. W. *et al.* Human IL-23-producing type 1 macrophages promote but IL-10-producing type 2 macrophages subvert immunity to (myco)bacteria. *Proc. Natl. Acad. Sci. U. S. A.* **101**, 4560-4565, doi:10.1073/pnas.0400983101 (2004).
339 Verreck, F. A. W., de Boer, T., Langenberg, D. M. L., van der Zanden, L. & Ottenhoff, T. H. M. Phenotypic and functional profiling of human proinflammatory type-1 and anti-

inflammatory type-2 macrophages in response to microbial antigens and IFN-γ- and CD40L-mediated costimulation. *Journal of Leukocyte Biology* **79**, 285-293, doi:10.1189/jlb.0105015 (2006).

340 Baeuerle, P. A. & Henkel, T. Function and activation of NF-kappa B in the immune system. *Annu. Rev. Immunol.* **12**, 141-179, doi:10.1146/annurev.iy.12.040194.001041 (1994).

341 Stranges, P. B. *et al.* Elimination of antigen-presenting cells and autoreactive T cells by Fas contributes to prevention of autoimmunity. *Immunity* **26**, 629-641, doi:10.1016/j.immuni.2007.03.016 (2007).

342 Diamond, M. S. *et al.* Type I interferon is selectively required by dendritic cells for immune rejection of tumors. *J Exp Med* **208**, 1989-2003, doi:10.1084/jem.20101158 (2011).

343 Dong, Y. *et al.* Generation and Identification of GM-CSF Derived Alveolar-like Macrophages and Dendritic Cells From Mouse Bone Marrow. *J. Vis. Exp.*, doi:10.3791/54194 (2016).

344 Helft, J. *et al.* GM-CSF Mouse Bone Marrow Cultures Comprise a Heterogeneous Population of CD11c(+)MHCII(+) Macrophages and Dendritic Cells. *Immunity* **42**, 1197-1211, doi:10.1016/j.immuni.2015.05.018 (2015).

345 Na, Y. R., Jung, D., Gu, G. J. & Seok, S. H. GM-CSF Grown Bone Marrow Derived Cells Are Composed of Phenotypically Different Dendritic Cells and Macrophages. *Mol. Cells* **39**, 734-741, doi:10.14348/molcells.2016.0160 (2016).

346 Wu, M., Stockley, P. G. & Martin, W. J. An improved Western blotting technique effectively reduces background. *ELECTROPHORESIS* **23**, 2373-2376, doi:10.1002/1522-2683(200208)23:15<2373::aid-elps2373>3.0.co;2-w (2002).

347 Petruccioli, E. *et al.* Correlates of tuberculosis risk: predictive biomarkers for progression to active tuberculosis. *Eur. Respir. J.* **48**, 1751-1763, doi:10.1183/13993003.01012-2016 (2016).

348 Moreira-Teixeira, L. *et al.* T Cell–Derived IL-10 Impairs Host Resistance to Mycobacterium tuberculosis Infection. *The Journal of Immunology* **199**, 613-623, doi:10.4049/jimmunol.1601340 (2017).

349 Redford, P. S. *et al.* Enhanced protection to Mycobacterium tuberculosis infection in IL-10-deficient mice is accompanied by early and enhanced Th1 responses in the lung. *Eur. J. Immunol.* **40**, 2200-2210, doi:10.1002/eji.201040433 (2010).

350 Vossenkämper, A. *et al.* Inhibition of NF-κB signaling in human dendritic cells by the enteropathogenic Escherichia coli effector protein NleE. *Journal of immunology (Baltimore, Md. : 1950)* **185**, 4118-4127, doi:10.4049/jimmunol.1000500 (2010).

351 Ade, N. *et al.* NF-kappaB plays a major role in the maturation of human dendritic cells induced by NiSO(4) but not by DNCB. *Toxicological sciences : an official journal of the Society of Toxicology* **99**, 488-501, doi:10.1093/toxsci/kfm178 (2007).

352 LeibundGut-Landmann, S., Weidner, K., Hilbi, H. & Oxenius, A. Nonhematopoietic cells are key players in innate control of bacterial airway infection. *J. Immunol.* **186**, 3130-3137, doi:10.4049/jimmunol.1003565 (2011).

353 Mayer-Barber, K. D. & Barber, D. L. Innate and Adaptive Cellular Immune Responses to Mycobacterium tuberculosis Infection. *Cold Spring Harb. Perspect. Med.* **5**, doi:10.1101/cshperspect.a018424 (2015).

354 Lastrucci, C. *et al.* Tuberculosis is associated with expansion of a motile, permissive and immunomodulatory CD16(+) monocyte population via the IL-10/STAT3 axis. *Cell Res.* **25**, 1333-1351, doi:10.1038/cr.2015.123 (2015).
355 Kaushal, D., Mehra, S., Didier, P. J. & Lackner, A. A. The non-human primate model of tuberculosis. *J. Med. Primatol.* **41**, 191-201, doi:10.1111/j.1600-0684.2012.00536.x (2012).
356 Scanga, C. A. & Flynn, J. L. Modeling tuberculosis in nonhuman primates. *Cold Spring Harb. Perspect. Med.* **4**, a018564, doi:10.1101/cshperspect.a018564 (2014).
357 Flynn, J. L. *et al.* Non-human primates: a model for tuberculosis research. *Tuberculosis* **83**, 116-118, doi:10.1016/s1472-9792(02)00059-8 (2003).
358 Muñoz, M. *et al.* Occurrence of an antigenic triacyl trehalose in clinical isolates and reference strains of Mycobacterium tuberculosis. *FEMS Microbiol. Lett.* **157**, 251-259, doi:10.1111/j.1574-6968.1997.tb12781.x (1997).
359 Sassetti, C. M., Boyd, D. H. & Rubin, E. J. Comprehensive identification of conditionally essential genes in mycobacteria. *Proc. Natl. Acad. Sci. U. S. A.* **98**, 12712-12717, doi:10.1073/pnas.231275498 (2001).
360 Sassetti, C. M. & Rubin, E. J. Genetic requirements for mycobacterial survival during infection. *Proc. Natl. Acad. Sci. U. S. A.* **100**, 12989-12994, doi:10.1073/pnas.2134250100 (2003).
361 Ford, C. B. *et al.* Use of whole genome sequencing to estimate the mutation rate of Mycobacterium tuberculosis during latent infection. *Nat. Genet.* **43**, 482-486, doi:10.1038/ng.811 (2011).
362 Lin, P. L. *et al.* Sterilization of granulomas is common in active and latent tuberculosis despite within-host variability in bacterial killing. *Nat. Med.* **20**, 75-79, doi:10.1038/nm.3412 (2014).
363 Awasthy, D., Ambady, A., Narayana, A., Morayya, S. & Sharma, U. Roles of the two type II NADH dehydrogenases in the survival of Mycobacterium tuberculosis in vitro. *Gene* **550**, 110-116, doi:10.1016/j.gene.2014.08.024 (2014).
364 Bottai, D. *et al.* Disruption of the ESX-5 system of Mycobacterium tuberculosis causes loss of PPE protein secretion, reduction of cell wall integrity and strong attenuation. *Mol. Microbiol.* **83**, 1195-1209, doi:10.1111/j.1365-2958.2012.08001.x (2012).
365 Stewart, G. R. *et al.* Dissection of the heat-shock response in Mycobacterium tuberculosis using mutants and microarrays a aA list of the 100 ORFs most highly induced by heat shock is provided as supplementary data with the online version of this paper (http://mic.sgmjournals.org). *Microbiology* **148**, 3129-3138, doi:10.1099/00221287-148-10-3129 (2002).
366 Lee, S. *et al.* Protection Elicited by Two Glutamine Auxotrophs of Mycobacterium tuberculosis and In Vivo Growth Phenotypes of the Four Unique Glutamine Synthetase Mutants in a Murine Model. *Infection and Immunity* **74**, 6491-6495, doi:10.1128/iai.00531-06 (2006).
367 Cavet, J. S., Graham, A. I., Meng, W. & Robinson, N. J. A Cadmium-Lead-sensing ArsR-SmtB Repressor with Novel Sensory Sites. *Journal of Biological Chemistry* **278**, 44560-44566, doi:10.1074/jbc.m307877200 (2003).
368 Chauhan, S., Kumar, A., Singhal, A., Tyagi, J. S. & Krishna Prasad, H. CmtR, a cadmium-sensing ArsR-SmtB repressor, cooperatively interacts with multiple operator

sites to autorepress its transcription in Mycobacterium tuberculosis. *FEBS Journal* **276**, 3428-3439, doi:10.1111/j.1742-4658.2009.07066.x (2009).
369 Wu, J. *et al.* Multiple cytokine responses in discriminating between active tuberculosis and latent tuberculosis infection. *Tuberculosis* **102**, 68-75, doi:10.1016/j.tube.2016.06.001 (2017).
370 Berry, M. P. R. *et al.* An interferon-inducible neutrophil-driven blood transcriptional signature in human tuberculosis. *Nature* **466**, 973-977, doi:10.1038/nature09247 (2010).
371 Verbon *et al.* Serum concentrations of cytokines in patients with active tuberculosis (TB) and after treatment. *Clinical and Experimental Immunology* **115**, 110-113, doi:10.1046/j.1365-2249.1999.00783.x (1999).
372 Chandrashekara, S., Anupama, K. R., Sambarey, A. & Chandra, N. High IL-6 and low IL-15 levels mark the presence of TB infection: A preliminary study. *Cytokine* **81**, 57-62, doi:10.1016/j.cyto.2016.02.003 (2016).
373 Bermudez, L. E. & Goodman, J. Mycobacterium tuberculosis invades and replicates within type II alveolar cells. *Infect. Immun.* **64**, 1400-1406 (1996).
374 Jackson, M. The mycobacterial cell envelope-lipids. *Cold Spring Harb. Perspect. Med.* **4**, doi:10.1101/cshperspect.a021105 (2014).
375 Scordo, J. M. *et al.* Mycobacterium tuberculosis Cell Wall Fragments Released upon Bacterial Contact with the Human Lung Mucosa Alter the Neutrophil Response to Infection. *Frontiers in Immunology* **8**, doi:10.3389/fimmu.2017.00307 (2017).
376 Gautam, U. S. *et al.* In vivo inhibition of tryptophan catabolism reorganizes the tuberculoma and augments immune-mediated control of Mycobacterium tuberculosis. *Proceedings of the National Academy of Sciences* **115**, E62-E71, doi:10.1073/pnas.1711373114 (2018).
377 Mehra, S. *et al.* The DosR Regulon Modulates Adaptive Immunity and Is Essential for Mycobacterium tuberculosis Persistence. *Am. J. Respir. Crit. Care Med.* **191**, 1185-1196, doi:10.1164/rccm.201408-1502OC (2015).
378 Hudock, T. A. *et al.* Hypoxia Sensing and Persistence Genes Are Expressed during the Intragranulomatous Survival of Mycobacterium tuberculosis. *Am. J. Respir. Cell Mol. Biol.* **56**, 637-647, doi:10.1165/rcmb.2016-0239OC (2017).
379 Hudock, T. A., Lackner, A. A. & Kaushal, D. Microdissection approaches in tuberculosis research. *J. Med. Primatol.* **43**, 294-297, doi:10.1111/jmp.12141 (2014).
380 Dutta, N. K. *et al.* Genetic requirements for the survival of tubercle bacilli in primates. *J. Infect. Dis.* **201**, 1743-1752, doi:10.1086/652497 (2010).
381 Torrelles, J. B., Azad, A. K. & Schlesinger, L. S. Fine discrimination in the recognition of individual species of phosphatidyl-myo-inositol mannosides from Mycobacterium tuberculosis by C-type lectin pattern recognition receptors. *J. Immunol.* **177**, 1805-1816, doi:10.4049/jimmunol.177.3.1805 (2006).
382 Schnappinger, D. *et al.* Transcriptional Adaptation of Mycobacterium tuberculosis within Macrophages. *Journal of Experimental Medicine* **198**, 693-704, doi:10.1084/jem.20030846 (2003).
383 Sevalkar, R. R. *et al.* Functioning of Mycobacterial Heat Shock Repressors Requires the Master Virulence Regulator PhoP. *Journal of Bacteriology* **201**, doi:10.1128/jb.00013-19 (2019).

384 Wilkinson, K. A. *et al.* Infection Biology of a Novel α-Crystallin of Mycobacterium tuberculosis: Acr2. *The Journal of Immunology* **174**, 4237-4243, doi:10.4049/jimmunol.174.7.4237 (2005).
385 Vilchèze, C., Weinrick, B., Leung, L. W. & Jacobs, W. R. Plasticity of Mycobacterium tuberculosis NADH dehydrogenases and their role in virulence. *Proceedings of the National Academy of Sciences* **115**, 1599-1604, doi:10.1073/pnas.1721545115 (2018).
386 Tullius, M. V., Harth, G. & Horwitz, M. A. Glutamine Synthetase GlnA1 Is Essential for Growth of Mycobacterium tuberculosis in Human THP-1 Macrophages and Guinea Pigs. *Infection and Immunity* **71**, 3927-3936, doi:10.1128/iai.71.7.3927-3936.2003 (2003).
387 Botella, H. *et al.* Mycobacterial P1-Type ATPases Mediate Resistance to Zinc Poisoning in Human Macrophages. *Cell Host & Microbe* **10**, 248-259, doi:10.1016/j.chom.2011.08.006 (2011).
388 Domenech, P., Reed, M. B. & Barry, C. E. Contribution of the Mycobacterium tuberculosis MmpL Protein Family to Virulence and Drug Resistance. *Infection and Immunity* **73**, 3492-3501, doi:10.1128/iai.73.6.3492-3501.2005 (2005).
389 Melly, G. & Purdy, G. MmpL Proteins in Physiology and Pathogenesis of M. tuberculosis. *Microorganisms* **7**, 70, doi:10.3390/microorganisms7030070 (2019).
390 Rousseau, C. *et al.* Sulfolipid deficiency does not affect the virulence of Mycobacterium tuberculosis H37Rv in mice and guinea pigs. *Infect. Immun.* **71**, 4684-4690, doi:10.1128/iai.71.8.4684-4690.2003 (2003).
391 Tekaia, F. *et al.* Analysis of the proteome of Mycobacterium tuberculosis in silico. *Tubercle and Lung Disease* **79**, 329-342, doi:10.1054/tuld.1999.0220 (1999).
392 Minnikin, D. E., Kremer, L., Dover, L. G. & Besra, G. S. The Methyl-Branched Fortifications of Mycobacterium tuberculosis. *Chemistry & Biology* **9**, 545-553, doi:10.1016/s1074-5521(02)00142-4 (2002).
393 Blanc, L. *et al.* inhibits human innate immune responses via the production of TLR2 antagonist glycolipids. *Proc. Natl. Acad. Sci. U. S. A.* **114**, 11205-11210, doi:10.1073/pnas.1707840114 (2017).
394 Heitmann, L., Schoenen, H., Ehlers, S., Lang, R. & Hölscher, C. Mincle is not essential for controlling Mycobacterium tuberculosis infection. *Immunobiology* **218**, 506-516, doi:10.1016/j.imbio.2012.06.005 (2013).

Appendix

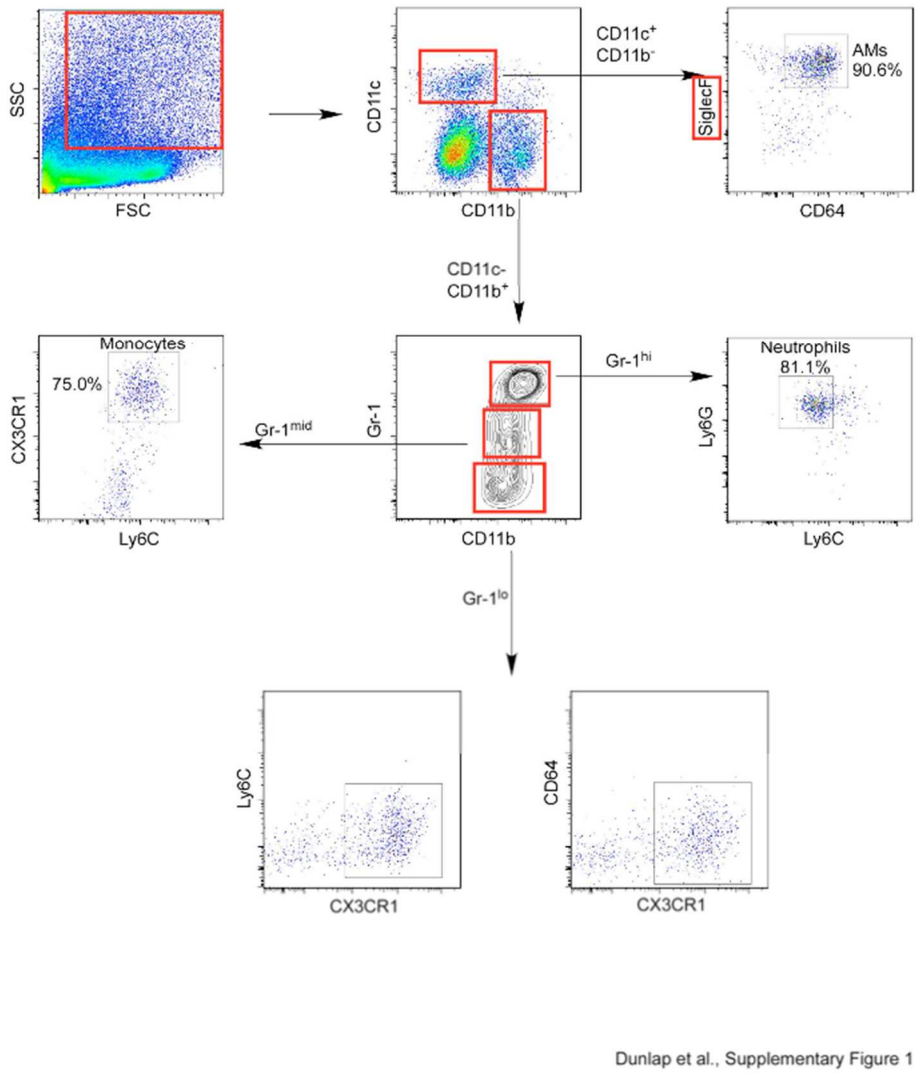

Supplementary Figure 1: The flow cytometry gating strategy for myeloid populations, validated with additional surface markers. (a) Briefly, AMs were defined as CD11b- CD11c+ Siglec F+ ; > 90% of these AMs also express CD64+ . Neutrophils were defined as CD11b+ CD11c-Gr-1hi cells; neutrophils also express Ly6G, but not Ly6C. Monocytes were defined as CD11b+ CD11c-Gr-1lo cells; the majority of them expressed Ly6C and CX3CR1. RMs were defined as CD11b+ CD11c-Gr-1- ; RMs also expressed CX3CR1, but not CD64 or Ly6C. Red boxes define the criteria used for gating subsets in all figures.

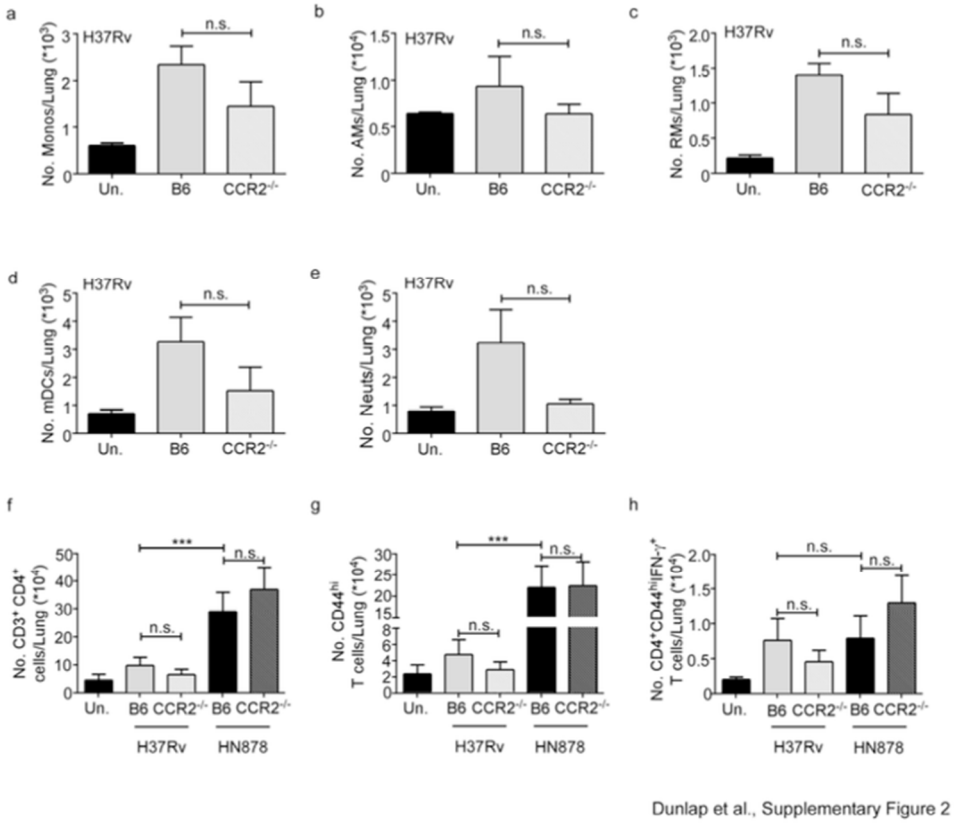

Supplementary Figure 2: Accumulation of lung innate and adaptive cell populations upon H37Rv or HN878 infection in B6 and CCR2$^{-/-}$ mice. (a-e) B6 and CCR2$^{-/-}$ mice (n=5) were aerosol-infected with 100 CFU of H37Rv and lung innate immune populations were determined at 30 d.p.i. by flow cytometry. (f-h) B6 and CCR2$^{-/-}$ mice were infected with H37Rv or HN878 and accumulation of total CD4^{+} T cells and CD44hi activated CD4^{+} T cells producing IFN-γ were determined using flow cytometry. Un.=uninfected, Monos=Monocytes, AMs=Alveolar Macrophages, RMs=Recruited Macrophages, mDCs=Myeloid Dendritic Cells, Neuts=Neutrophils. n=5, (a-h) 1-Way ANOVA with Tukey's post-test.

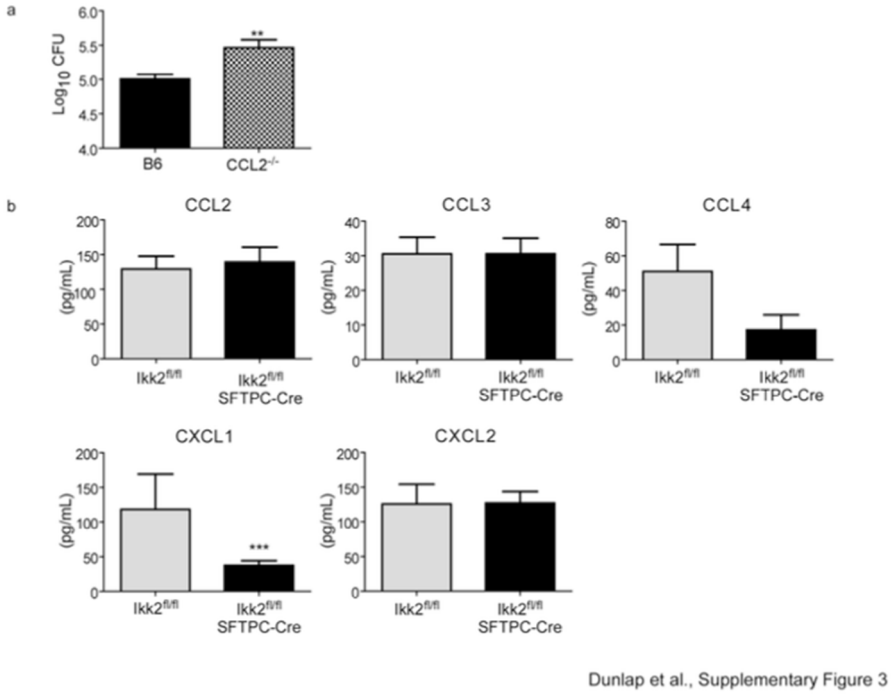

Supplementary Figure 3: CCL2 deficient mice are susceptible to HN878 infection. (a) B6 and CCL2$^{-/-}$ (n=5) were infected with HN878 and lung bacterial burden was analyzed at 30 d.p.i. (b) Chemokines protein levels were measured in lung homogenates of HN878 infected IKK2$^{fl/fl}$ Sftpc-Cre mice and littermate controls at 21 d.p.i. (a-b) Student's t-test.

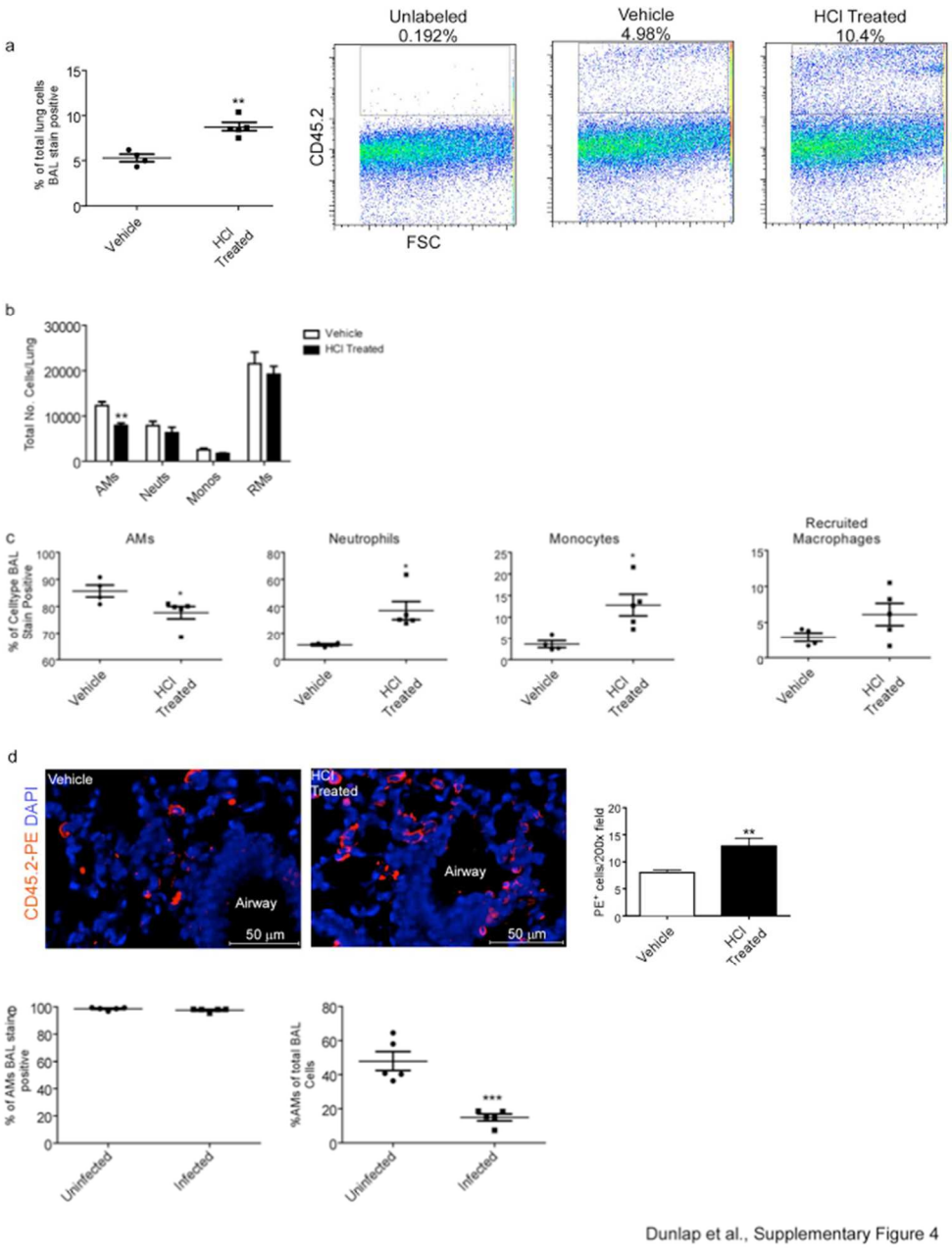

Dunlap et al., Supplementary Figure 4

Supplementary Figure 4: Validation of airway labeling technique using the HCl lung injury model. B6 mice were treated i.t. with 50 uL of sterile water (vehicle, n=4) or HCl (pH 1.5, n=5) and rested 24 hours prior to airway CD45.2 labelling and lung harvest. (a) The percentage of total lung cells stained with airway CD45.2 was determined by flow cytometry. (b) Total cell counts for lung myeloid populations were determined by flow cytometry. (c) The percentage of each myeloid cell type positive for airway labelled CD45.2 in vehicle and HCl treated mice is shown. (d) Airway label CD45.2 PE localization was by IHC in PBS treated and HCl treated mice. (e) BAL samples were collected ~10 min after airway labelling with CD45.2 Ab from uninfected and infected mice at 45 d.p.i. The proportion of AMs stained with airway CD45.2 (left panel, uninfected average= 98.6%, infected =97.5%) as well as the proportion of AMs of the total collected BAL sample (right panel, uninfected average= 48.6%, infected=15.3%). (a-d) Student's t-test was used to compare between groups separately for each myeloid cell type. (e) Student's t-test.

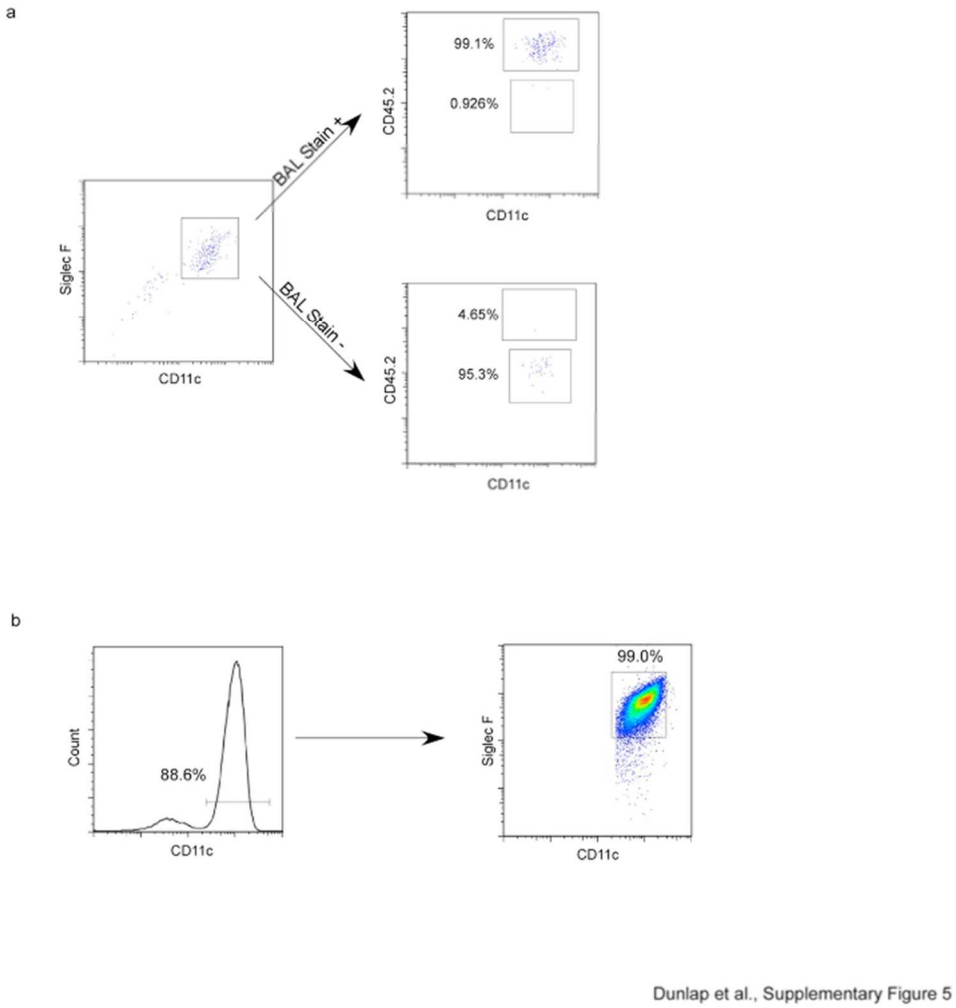

Supplementary Figure 5: Sorting strategy of airway AMs and non-airway AMs. Single cell lung suspensions from airway CD45.2 labelled, uninfected (n=4) and infected mice (n=4-5) were prepared and (a) the gating strategy for airway and non-airway AMs is shown. Briefly, $CD11c^+$ $SiglecF^+$ $CD45.2^+$ cells were gated as airway AMs, while $CD11c^+$ $SiglecF^+$ $CD45.2^-$ cells were gated as non-airway AMs. (b) Enrichment of AMs by CD11c magnetic bead sorting for adoptive transfer into mice was carried out using the Miltenyi $CD11c^+$ sorting kit. Expression of SiglecF and CD11c on sorted cells was determined by flow cytometry.

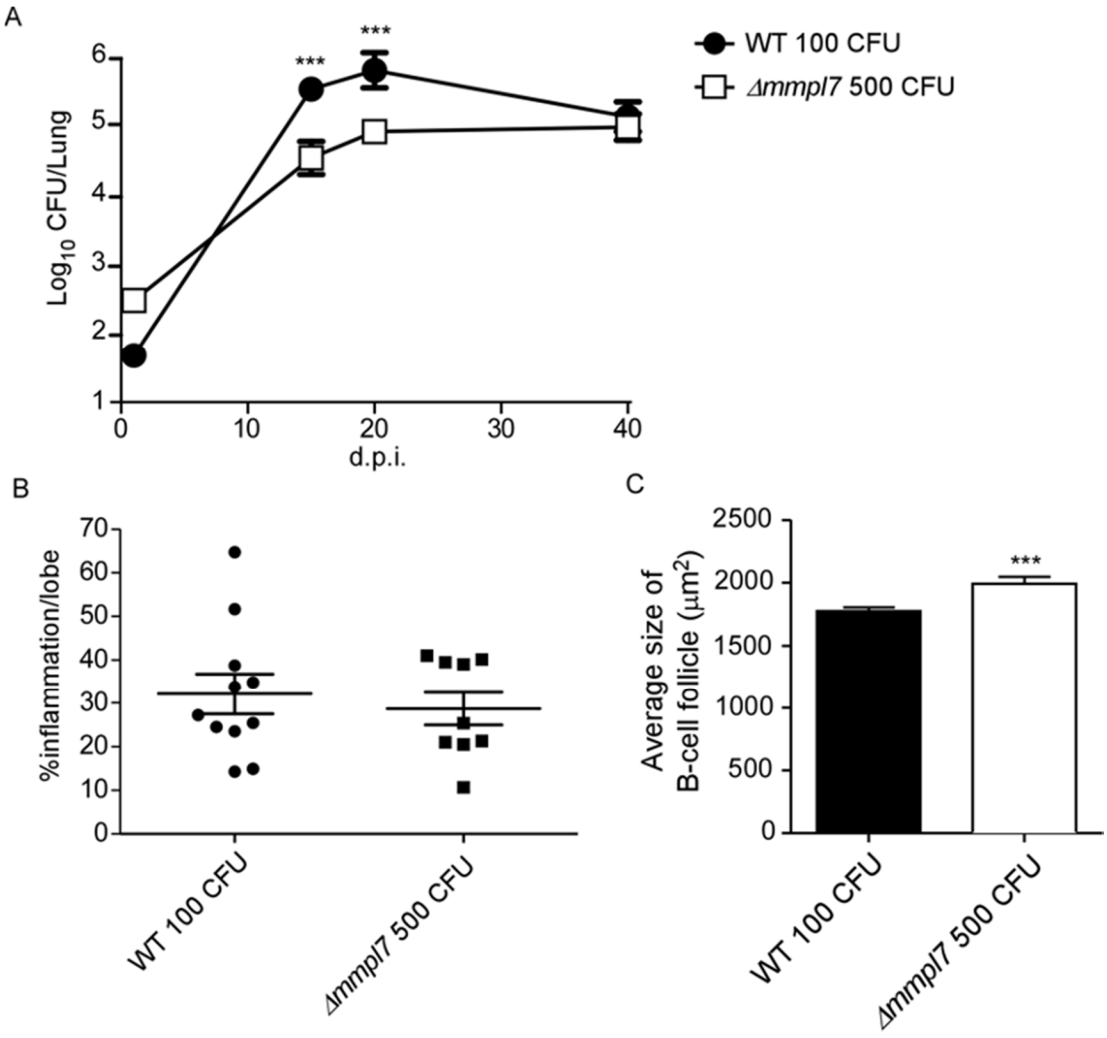

Supplemental Figure 6: *Δmmpl7* mutant drives *Mtb* enhanced B cell follicle formation in mouse model. Sex and age matched C57BL/6 mice were infected with 100 CFU of *Mtb* Erdman WT or 500 CFU *Δmmpl7*. A) Lung homogenates were taken and serially diluted to determine bacterial CFU counts at indicated time points. B) Lungs from *Mtb*-infected mice at 40 d.p.i. were formalin fixed, embedded in paraffin and used for H&E staining and inflammation was quantified by tracing areas. C) B-cell follicles present within lung sections were visualized by confocal microscopy. Slides were visualized and quantified by outlining the lesions using the automated tool of the Zeiss Axioplan 2 microscope. Infected groups (n≥5) comparing WT Erdman and *Δmmpl7 Mtb* strains at individual time points were compared using Student's t-test. Mean and standard deviation (SD) were plotted for each group at each indicated time point. *p<0.05, **p<0.01, ***p<0.001

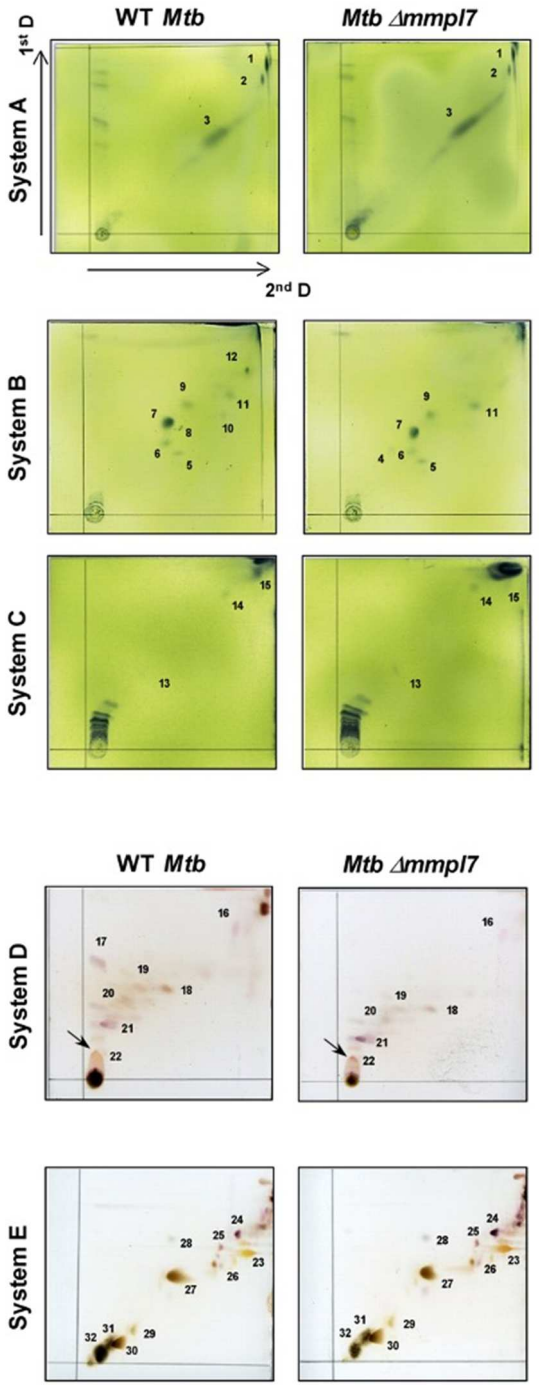

Supplemental Figure 7: *Δmmpl7* mutant *Mtb* overexpresses DATs. Two dimensional Thin Layer Chromatography was performed on total lipids from *Mtb* Erdman WT or *Δmmpl7* obtained as described in the main text and as resolved using the following solvent systems: System A: (1) petroleum ether (boiling point 60–80 °C)/ethyl acetate (98 : 2, three times); (2) petroleum ether/acetone (98 : 2). System B: (1) petroleum ether/acetone (92 : 8, three times); (2) toluene/acetone (95 : 5). System C: (1st D) chloroform/methanol (96 : 4); (2nd D) toluene/acetone (80 : 20). System D: (1) chloroform/methanol/water (100 : 14 : 0.8); (2) chloroform/acetone/methanol/water (50 : 60 : 2.5 : 3).System E: (1) chloroform/methanol/water (60 : 30 : 6); (2) chloroform/acetic acid/methanol/water (40 : 25 : 3 : 6). Identities of separated lipid moieties 1-2: Phthiocerol dimycocerosate (PDIM) family; 3: Triacylglycerides (TAG); 4-8: Mycolipenates of Trehalose; 9: Free fatty acid (FA); 10-12: Unknown (?); 13: Phenolic Glycolipid-I (PGL-I); 14-15:

Mixture of Free Fatty Acids (FA) and Diacyl glycerols (DAGs)*; 16: Sulfolipid-I (SL-I); 17: Unknown (?)**; 18: Glycolipid; 19-20: Sulfolipids (SL); 21: Trehalose Dimycolate (TDM); 22: Mixture of Diacyl trehaloses (DATs, black arrows) and Trehalose Monomycolate (MMT); 23: Diphosphatidyl-Glycerol (DPG); 24: Ac_2PIM_2; 25-26: Phospholipids (PC, PE, PS); 27: Ac_1PIM_2; 28: PI; 29: Ac_2PIM_6; 30: Ac_1PIM_6; 31-32: Lipooligosaccharides (LOSs).

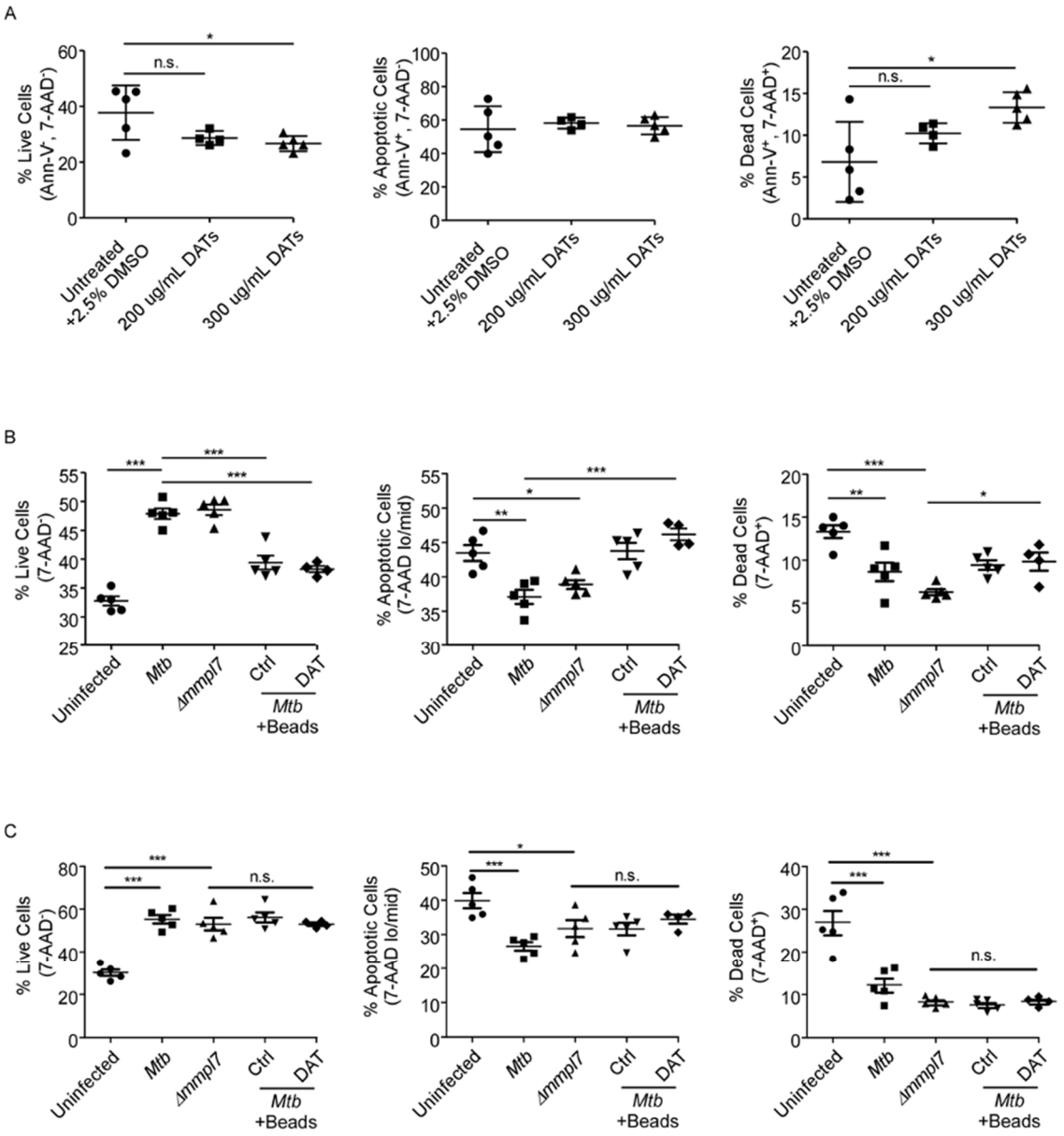

Supplemental Figure 8: DAT administration does not significantly alter apoptosis and cell death in epithelial cells, macrophages, or DCs. A) Mouse lung epithelial cells (n=5) were treated with either 2.5% DMSO or raw DATs in DMSO at indicated dosage for 6 days. B) Mouse bone marrow derived Macrophages (BMDMs) (n=5) or C) dendritic cells (BMDCs) (n=5) were infected with *Mtb* Erdman WT with or without the addition of BSA control or DAT coated agarose beads, or *Δmmpl7* for 3 days. The percentage of live (left panels; Annexin V^-, 7-AAD^-), apoptotic (middle panels; Annexin V^+, 7-AAD^-), and dead (right panels; Annexin V^+, 7-AAD^+) cells were quantified by flow cytometry utilizing Annexin V and 7-AAD staining as per manufacturer's suggested protocol. Multiple groups were compared by 1-way ANOVA with Tukey's post-tests. *$p<0.05$, **$p<0.01$, ***$p<0.001$. Mean and standard deviation (SD) were plotted for each group at each indicated time point.

Supplementary Table 1: Gene expression values of airway and non-airway AM transcriptional signatures from *Mtb*-infected mice.

Gene			Infected airway AMs					Infected non-airway AMs				Uninfected airway AMs			
ENSMUSG00000015947	Fcgr1	Fc receptor, IgG, high affinity I	1.8	1.7	1.7	1.7	1.8	1.8	1.8	1.8	1.9	1.5	1.5	1.5	1.3
ENSMUSG00000032440	Tgfbr2	transforming growth factor, beta receptor II	1.2	1.1	1.0	1.0	1.0	1.2	1.0	1.0	1.0	1.5	1.4	1.5	1.4
ENSMUSG00000014361	Mertk	c-mer proto-oncogene tyrosine kinase	1.4	1.4	1.4	1.3	1.4	1.4	1.4	1.4	1.2	1.8	1.8	1.8	1.8
ENSMUSG00000000440	Pparg	peroxisome proliferator activated receptor gamma	2.0	1.8	1.8	1.7	1.9	1.9	1.8	1.8	1.8	1.9	2.0	1.8	1.7
ENSMUSG00000030789	Itgax	integrin alpha X	1.7	1.7	1.7	1.7	1.8	1.8	1.7	1.7	1.8	2.1	2.1	2.1	2.0
ENSMUSG00000039013	Siglecf	sialic acid binding Ig-like lectin F	2.1	1.9	1.9	1.8	2.0	2.1	2.0	1.9	2.0	2.2	2.3	2.2	2.1
ENSMUSG00000069516	Lyz2	lysozyme 2	4.8	4.8	4.8	4.8	4.8	4.8	4.9	4.8	4.9	4.6	4.7	4.5	4.3
ENSMUSG00000071714	Csf2rb2	colony stimulating factor 2 receptor, beta 2	1.0	1.0	1.0	1.0	1.2	1.1	1.0	1.1	1.3	1.6	1.4	1.6	1.5
ENSMUSG00000059326	Csf2ra	colony stimulating factor 2 receptor, alpha	2.4	2.4	2.4	2.4	2.5	2.4	2.4	2.3	2.4	2.4	2.4	2.3	2.1
ENSMUSG00000008845	Cd163	CD163 antigen	0.0	0.2	0.0	0.0	0.0	0.1	0.0	0.1	0.0	0.2	0.3	0.3	1.9
ENSMUSG00000030786	Itgam	integrin alpha M	0.3	0.4	0.4	0.6	0.3	0.6	0.6	0.6	0.8	-0.5	-0.4	0.0	0.1
ENSMUSG00000079018	Ly6c1	lymphocyte antigen 6 complex, locus C1	0.4	0.6	0.2	0.5	0.1	0.5	0.2	0.6	0.5	0.6	0.4	0.6	0.9

Supplementary Table 1: Gene expression values of airway and non-airway AM transcriptional signatures from *Mtb*-infected mice. RNA sequencing datasets of populations of sorted airway ($CD45.2^+$ $CD11c^+$ $SiglecF^+$) and non-airway AMs ($CD45.2^-$ $CD11c^+$ $SiglecF^+$) from infected (n=4-5, 100 CFU HN878, 30 d.p.i.) and uninfected mice (n=4) were analyzed for expression (Log FPKM) of the common AM gene signature (Gautier et al 2012, Misharin et al 2017) (i.e. Siglecf, Pparg, Tgfbr2, Csf2r, Mertk, Itgax, Lyz2, Sftpc,, and Fcgr1) and genes associated with monocyte-derived interstitial or recruited macrophages (i.e. Ly6c1, Itgam, Cx3cr1, and CD163).

Supplementary Table 2a: Pearson correlation of gene expression levels between sorted airway and non-airway AMs from infected mice, based on the gene expression levels of all genes.

	Infected Airway AMs					Infected non-airway AMs				Uninfected Airway AMs			
Infected Airway AMs		0.9965	0.9960	0.9773	0.9940	0.9976	0.9866	0.9923	0.9796	0.9067	0.9465	0.8924	0.8575
	0.9965		0.9991	0.9801	0.9966	0.9957	0.9885	0.9971	0.9856	0.9106	0.9468	0.8996	0.8652
	0.9960	0.9991		0.9849	0.9974	0.9952	0.9875	0.9967	0.9863	0.9124	0.9452	0.9014	0.8669
	0.9773	0.9801	0.9849		0.9818	0.9833	0.9820	0.9841	0.9890	0.8719	0.9108	0.8547	0.8206
	0.9940	0.9966	0.9974	0.9818		0.9938	0.9878	0.9962	0.9863	0.9238	0.9502	0.9125	0.8763
Infected non-airway AMs	0.9976	0.9957	0.9952	0.9833	0.9938		0.9939	0.9958	0.9889	0.9016	0.9447	0.8846	0.8463
	0.9866	0.9885	0.9875	0.9820	0.9878	0.9939		0.9918	0.9923	0.9068	0.9530	0.8866	0.8421
	0.9923	0.9971	0.9967	0.9841	0.9962	0.9958	0.9918		0.9934	0.9044	0.9394	0.8917	0.8534
	0.9796	0.9856	0.9863	0.9890	0.9863	0.9889	0.9923	0.9934		0.8856	0.9249	0.8680	0.8262
Uninfected Airway AMs	0.9067	0.9106	0.9124	0.8719	0.9238	0.9016	0.9068	0.9044	0.8856		0.9820	0.9964	0.9596
	0.9465	0.9468	0.9452	0.9108	0.9502	0.9447	0.9530	0.9394	0.9249	0.9820		0.9692	0.9277
	0.8924	0.8996	0.9014	0.8547	0.9125	0.8846	0.8866	0.8917	0.8680	0.9964	0.9692		0.9700
	0.8575	0.8652	0.8669	0.8206	0.8763	0.8463	0.8421	0.8534	0.8262	0.9596	0.9277	0.9700	

Supplementary Table 2b: Pearson correlation of gene expression levels between sorted airway and non-airway AMs from infected mice, based on the gene expression levels of the 12 AM signature genes.

	Infected Airway AMs					Infected non-airway AMs				Uninfected Airway AMs			
Infected Airway AMs		0.9999987	0.9999994	0.9999978	0.9999984	0.9999991	0.9999991	0.9999989	0.9999987	0.9999600	0.9999914	0.9999008	0.9999474
	0.9999987		0.9999997	0.9999995	0.9999990	0.9999998	0.9999989	0.9999987	0.9999987	0.9999680	0.9999938	0.9999148	0.9999559
	0.9999994	0.9999997		0.9999988	0.9999984	0.9999995	0.9999997	0.9999996	0.9999996	0.9999617	0.9999915	0.9999043	0.9999491
	0.9999978	0.9999995	0.9999988		0.9999996	0.9999994	0.9999973	0.9999971	0.9999971	0.9999717	0.9999942	0.9999214	0.9999594
	0.9999984	0.9999990	0.9999984	0.9999996		0.9999994	0.9999969	0.9999965	0.9999965	0.9999719	0.9999948	0.9999210	0.9999598
Infected non-airway AMs	0.9999991	0.9999998	0.9999995	0.9999994	0.9999994		0.9999986	0.9999983	0.9999982	0.9999696	0.9999949	0.9999168	0.9999580
	0.9999991	0.9999989	0.9999997	0.9999973	0.9999969	0.9999986		1.0000000	0.9999999	0.9999564	0.9999893	0.9998960	0.9999435
	0.9999989	0.9999987	0.9999996	0.9999971	0.9999965	0.9999983	1.0000000		1.0000000	0.9999545	0.9999882	0.9998931	0.9999413
	0.9999987	0.9999987	0.9999996	0.9999971	0.9999965	0.9999982	0.9999999	1.0000000		0.9999546	0.9999880	0.9998935	0.9999415
Uninfected Airway AMs	0.9999600	0.9999680	0.9999617	0.9999717	0.9999719	0.9999696	0.9999564	0.9999545	0.9999546		0.9999871	0.9999865	0.9999974
	0.9999914	0.9999938	0.9999915	0.9999942	0.9999948	0.9999949	0.9999893	0.9999882	0.9999880	0.9999871		0.9999473	0.9999804
	0.9999008	0.9999148	0.9999043	0.9999214	0.9999210	0.9999168	0.9998960	0.9998931	0.9998935	0.9999865	0.9999473		0.9999881
	0.9999474	0.9999559	0.9999491	0.9999594	0.9999598	0.9999580	0.9999435	0.9999413	0.9999415	0.9999974	0.9999804	0.9999881	

Supplementary Table 2: Pearson correlation of gene expression levels between sorted airway and non-airway AMs from infected mice. RNA sequencing datasets of populations of sorted airway ($CD45.2^+$ $CD11c^+$ $SiglecF^+$) and non-airway AMs ($CD45.2^-$ $CD11c^+$ $SiglecF^+$) from infected (n=4-5, 100 CFU HN878, 30 d.p.i.) and uninfected mice (n=4) were compared by Pearson correlation for expression of all genes (a) and the AM signature genes (b).

Supplementary Table 4: KEGG pathways significantly enriched among the 116 genes overexpressed in non-airway AMs compared to airway AMs during infection.

KEGG ID		# genes in pathway	# genes in test set	Expected # genes	Enrichment Ratio	Adjusted P value
mmu05150	Staphylococcus aureus infection	52	7	0.42	16.63	4.9E-05
mmu05133	Pertussis	75	7	0.61	11.53	3.2E-04
mmu04610	Complement and coagulation cascades	87	7	0.70	9.94	5.8E-04
mmu04514	Cell adhesion molecules (CAMs)	169	8	1.37	5.85	4.5E-03
mmu05230	Central carbon metabolism in cancer	66	5	0.53	9.36	1.1E-02
mmu05144	Malaria	49	4	0.40	10.09	2.9E-02
mmu04145	Phagosome	184	7	1.49	4.70	2.9E-02

Supplementary Table 4: KEGG pathways significantly enriched among the 116 genes overexpressed in non-airway AMs compared to airway AMs during infection. Differentially expressed genes overexpressed in non-airway samples were tested for significant enrichment among KEGG pathways using WebGestalt (default settings, adjusted P = 0.05 threshold for enrichment).

Supplementary Table 5: Descriptions of the 12 genes significantly overexpressed in airway AMs compared to non-airway AMs in HN878-infected mice.

Gene ID	Gene short name	Gene Name	Average expression level (FPKM)		Adjusted P value
			Airway	Non-airway	
ENSMUSG00000028680	Plk3	Polo-like kinase 3	41.95	24.46	3.0E-04
ENSMUSG00000038508	Gdf15	Growth differentiation factor 15	31.3	14.4	3.3E-03
ENSMUSG00000052512	Nav2	Neuron navigator 2	0.7	0.3	4.5E-03
ENSMUSG00000041268	Dmxl2	Dmx-like 2	6.3	4.0	1.8E-02
ENSMUSG00000033705	Stard9	START domain containing 9	0.5	0.3	1.8E-02
ENSMUSG00000037279	Ovol2	Ovo like zinc finger 2	5.0	2.6	2.4E-02
ENSMUSG00000020205	Phlda1	Pleckstrin homology like domain, family A, member 1	26.8	14.3	2.5E-02
ENSMUSG00000038352	Arl5c	ADP-ribosylation factor-like 5C	73.4	33.2	3.1E-02
ENSMUSG00000042745	Id1	Inhibitor of DNA binding 1	33.9	18.9	3.5E-02
ENSMUSG00000033004	Mycbp2	MYC binding protein 2	3.2	1.9	4.1E-02
ENSMUSG00000056708	Ier5	Immediate early response 5	32.3	19.2	4.1E-02
ENSMUSG00000025893	Kbtbd3	Kelch repeat and BTB (POZ) domain containing 3	6.3	4.0	4.9E-02

Supplementary Table 5: Descriptions of the 12 genes significantly overexpressed in airway AMs compared to non-airway AMs in HN878-infected mice. RNA-sequencing of sorted airway AMs ($CD45.2^+$ $CD11c^+SiglecF^+$) and non-airway AMs ($CD45.2^-$ $CD11c^+$ $SiglecF^+$) from HN878 infected B6 mice (n=4-5) at 30 d.p.i. DESeq2 was used to determine overexpressed genes compared to non-airway samples. FPKM average expression levels and adjusted p values displayed for each.

Supplementary Tables 3, 6, 7: See Dunlap et al, 2018 for large data sets